UNIVERSITAT POLITÈCNICA DE CATALUNYA BARCELONATECH

Improved condition monitoring of hydraulic turbines based on artificial intelligence techniques

Weiqiang Zhao

Improved condition monitoring of hydraulic turbines based on artificial intelligence techniques

Article-Based Thesis
Doctor by the Universitat Politècnica de Catalunya

Presented to the Department of Fluid Mechanics of the Universitat Politècnica de Catalunya (UPC) by

Weiqiang ZHAO

Under the supervision of
Professor Dr. Eng. Eduard Egusquiza i Estevez
and **Dr. Eng. Alexandre Presas Batlló**

Barcelona, July 2021

ACKNOWLEDGEMENT

First of all, I would like to express my deepest gratitude to my thesis supervisor, Prof. Dr. Eng. Eduard Egusquiza and tutor Dr. Eng. Alexandre Presas, for their time, support and advices throughout all the work and cooperation during my thesis duration in UPC. This work would not be possible without their support.

Special thanks to Dr. Eng. Carme Valero Ferrando for her kind help as my tutor at the start of my Ph.D. time.

Thanks to Professor Dr. Eng. Lingjiu Zhou for her recommendation.

I would like to thank to Dr. Eng. Mònica Egusquiza, Dr. Eng. David Valentín for their help in my works. Their experiment, numerical simulation results have made possible to realize my idea. I also would like to thank to my other colleagues of CDIF for their kind treatment with me: Dr. Eng. Alfredo Guardo, Dr. Eng. Ming Zhang, Dr. Eng. Matias Bossio, Dr. Eng. Linlin Geng, Mr. Jian Chen and Mr. Greco Alonso.

Moreover, I want to acknowledge also to my economical supporter: China Scholarship Council for granting me a competitive Ph.D. Scholarship (CSC201706350258).

Finally, I want to thanks to Shan Zhang for giving me her continuous support and love during these years. Without this would not be possible. Special thanks also to my family and friends who have been always together with me and giving me courage.

Barcelona, July 2021 **Weiqiang ZHAO**

ABSTRACT

As a type of renewable energy that can provide rapid response to the requirement of the power grid, hydropower plays a fairly important position in the energy market. In recent years, with the enormous entrance of new renewable energies (NREs) such as wind energy and solar energy, the stability of the power grid has been challenged: the intermittent power supply from the NREs requires the hydraulic turbines to work more in off-design conditions and regulate the output much more frequently than they did before. In this new scenario, several problems have appeared in hydraulic turbine units. In order to reduce the maintaining periods and critical damages on the unit, condition monitoring techniques have been proved to be a useful tool for operators. However, these techniques shall be improved and updated in order to consider this new situation for hydropower.

At present, hydraulic turbines have been monitored by different types of sensors. However, new data analysis technologies such as artificial intelligence haven't been implemented in the systematical analyses of the prototypes. These techniques could improve the actual condition monitoring systems and could help to improve the diagnosis capacity for some critical problems, where classical analysis may fail.

In this study, existing monitoring and field test data from various types of turbines (Pump turbine, Francis turbine and Pelton turbine) has been used and several artificial intelligence (AI) techniques and data-driven methods have been applied in order to improve the existing condition monitoring techniques.

Firstly, for the pump turbine analyzed, artificial neural network (ANN) have been used to generate vibration hill charts based on the indicators used for condition monitoring. This has helped to analyze abnormal behaviors of the machine and to propose a better condition monitoring based on the generated maps. This can provide effective guidance for the operation plan of the unit.

Secondly, the limits of operation of a large Francis turbine due to overload instability have been analyzed. AI techniques have been applied on existing data to analyze the feasibility to detect the overload instability several seconds before it occurs. It is shown that by implementing these techniques in the existing condition monitoring system, the operating range of the unit could be safely increased.

Finally, for a failure that occurred in a Pelton turbine (broken bucket), artificial neural networks combined with dimension reduction techniques have been used to build up a model that can accurately predict the damage, which is helpful for the scheduled maintenance.

This is an Article-Based Thesis, so it is based on three Journal Papers that have been published during the thesis duration. These three Journal papers are about the improved hydro turbine condition monitoring and fault diagnosis based on AI techniques, and they are attached and commented though the whole document of this thesis.

RESUM

Com tipus d'energia renovable que pot proporcionar una resposta ràpida als requisits de la xarxa elèctrica, l'energia hidroelèctrica ocupa un lloc fonamental al mercat energètic. En els últims anys, amb l'enorme entrada de noves energies renovables (NRE) com l'eòlica i la solar, l'estabilitat de la xarxa elèctrica s'ha vist compromesa: el subministrament d'energia intermitent de les NRE obliga a que les turbines hidràuliques funcionin més freqüentment en condicions fora de disseny i regular la seva potència amb molta més freqüència que abans. En aquests nous escenaris, han aparegut diversos problemes en les turbines hidràuliques. Amb el fi de reduir els períodes de manteniment i els danys crítics en els prototips, les tècniques de "condition monitoring" han demostrat ser una eina útil per als operadors. Aquestes tècniques, però, han de ser millorades i actualitzades per considerar aquesta nova situació de l'energia hidroelèctrica.

En l'actualitat, les turbines hidràuliques han estat monitoritzades per diferents tipus de sensors. No obstant això, no s'han implementat noves tecnologies d'anàlisi de dades com la intel·ligència artificial (IA) en els anàlisis sistemàtics dels prototips. Aquestes tècniques podrien millorar els sistemes de "condition monitoring" reals i podríem ajudar a millorar la capacitat de diagnòstic per a alguns problemes crítics, on l'anàlisi clàssic no és suficient.

En aquest estudi, s'han utilitzat dades de diferents tipus de turbines prototips (turbina-bomba, turbina Francis i turbina Pelton) i s'han aplicat diverses tècniques d'intel·ligència artificial per millorar la seva monitorització.

En primer lloc, per a una turbina-bomba analitzada, s'ha utilitzat xarxes neuronals (ANN) per generar nous mapes de monitorització ("vibration hill charts") basats en els indicadors utilitzats

per a la monitorització de la màquina. Això ha ajudat a analitzar els comportaments anormals de la màquina i a un proponent una millor monitorització basada en els mapes generats. Això pot servir de referència per a una operació més eficaç de la màquina.

En segon lloc, s'han analitzat els límits de funcionament d'una turbina Francis causa de la inestabilitat en sobrecàrrega (overload instability). S'han aplicat tècniques d'IA en dades existents per analitzar la viabilitat de detectar la inestabilitat de sobrecàrrega diversos segons abans que passi. Es mostra que, a l'implementar aquestes tècniques en el sistema de monitorització existent, el rang d'operació de la màquina podria incrementar-se de manera segura.

Finalment, per a un dany ocorregut en una turbina Pelton, s'han utilitzat xarxes neuronals combinades amb tècniques de reducció dimensional per construir un model que pot predir amb precisió el dany, la qual cosa també és útil per al manteniment predictiu de la màquina.

Aquesta és una tesi basada en articles, pel que es basa en tres articles de revista que s'han publicat durant l'execució de la tesi. Aquests tres articles tracten sobre la millora de sistemes de "condition monitoring" i el diagnòstic de danys basat en tècniques d'intel·ligència artificial. Aquests articles s'adjunten i comenten en tot el document d'aquesta tesi.

RESUMEN

Como tipo de energía renovable que puede proporcionar una respuesta rápida a los requisitos de la red eléctrica, la energía hidroeléctrica ocupa un lugar fundamental en el mercado energético. En los últimos años, con la enorme entrada de nuevas energías renovables (NRE) como la eólica y la solar, la estabilidad de la red eléctrica se ha visto comprometida: el suministro de energía intermitente de las NRE obliga a que las turbinas hidráulicas funcionen más frecuentemente en condiciones fuera de diseño y regular su potencia con mucha más frecuencia que antes. En estos nuevos escenarios, han aparecido varios problemas en las turbinas hidráulicas. Con el fin de reducir los períodos de mantenimiento y los daños críticos en los prototipos, las técnicas de "condition monitoring" han demostrado ser una herramienta útil para los operadores. Sin embargo, estas técnicas deben ser mejoradas y actualizadas para considerar esta nueva situación de la energía hidroeléctrica.

En la actualidad, las turbinas hidráulicas han sido monitoreadas por diferentes tipos de sensores. Sin embargo, no se han implementado nuevas tecnologías de análisis de datos como la inteligencia artificial (IA) en los análisis sistemáticos de los prototipos. Estas técnicas podrían mejorar los sistemas de "condition monitoring" reales y podrían ayudar a mejorar la capacidad de diagnóstico para algunos problemas críticos, donde el análisis clásico no es suficiente.

En este estudio, se han utilizado datos de diferentes tipos de turbinas prototipos (turbina-bomba, turbina Francis y turbina Pelton) y se han aplicado varias técnicas de inteligencia artificial para mejorar su monitorización.

En primer lugar, para una turbina-bomba analizada, se han utilizado redes neuronales (ANN)

para generar nuevos mapas de monitorització (“vibration hill charts”) basados en los indicadores utilizados para la monitorización de la máquina. Esto ha ayudado a analizar los comportamientos anormales de la máquina y a proponer una mejor monitorización basada en los mapas generados. Esto puede servir de referencia para una operación más eficaz de la máquina.

En segundo lugar, se han analizado los límites de funcionamiento de una turbina Francis debido a la inestabilidad en sobrecarga (overload instability). Se han aplicado técnicas de IA en datos existentes para analizar la viabilidad de detectar la inestabilidad de sobrecarga varios segundos antes de que ocurra. Se muestra que, al implementar estas técnicas en el sistema de monitorización existente, el rango de operación de la máquina podría incrementarse de manera segura.

Finalmente, para un daño ocurrido en una turbina Pelton, se han utilizado redes neuronales combinadas con técnicas de reducción dimensional para construir un modelo que puede predecir con precisión el daño, lo cual también es útil para el mantenimiento programado de la máquina.

Esta es una tesis basada en artículos, por lo que se basa en tres artículos de revista que se han publicado durante la ejecución de la tesis. Estos tres artículos tratan sobre la mejoría de sistemas de “condition monitoring” y el diagnóstico de daños basado en técnicas de inteligencia artificial. Estos artículos se adjuntan y comentan en todo el documento de esta tesis.

CONTENTS

CAPTIONS

LIST OF FIGURES

LIST OF TABLES

NOMENCLATURE

f_f	Rotational frequency [Hz]
f_b	Blade passing frequency [Hz]
z_b	Number of blades
H	Head [m]

Acronyms	
NRE	New Renewable Energy
AI	Artificial Intelligence
ANN	Artificial Neural Network
MLP	Multi-Layer Perceptron
BP	Back Propagation
SOM	Self-Organizing Map
FFT	Fast Fourier Transform
FRF	Frequency Response Function
PCA	Principal Component Analysis
FA	Factor Analysis
WGO	Wicket Gate Opening
RSI	Rotor-Stator Interaction
RMSE	Root Mean Square Error

1

INTRODUCTION

The main purpose of this chapter is to explain the background and motivation of the thesis. First it shows why the topic of the thesis is important to be studied. Then, the state of the art in condition monitoring and fault diagnosis of hydraulic turbines and the development of artificial intelligence is presented. Moreover, it is also included what has been studied in the past by the research group and its research line. Finally, the outline of the present thesis is presented in a schematic way.

1.1 Background and interest of the topic

Hydroelectricity is one of the most important power resources in the world. In 2020, the generated hydropower is 4273.03 TW·h, accounting for 16 % of the global energy generation [1]. In recent years, with more and more countries having introduced targets to achieve net-zero emissions by midcentury, an acceleration in structural changes to the global energy generation and consumption is undergoing. Low-cost resources, low emissions and diversification are becoming the strategy for many companies and countries [2]. Due to their sustainable and environmentally friendly characteristics, new renewable energies (NREs) have been widely introduced into the energy market. The NREs includes solar energy (consists of solar photovoltaic, concentrated solar power), wind energy (consists of on-shore and off-shore wind energies), geothermal energy biomass energy (consists of solid biofuels and renewable waste, bagasse, renewable municipal waste, liquid biofuels and biogas) and other energies. Figure 1-1 shows the global generation shared by different energy sources from the year of 1985 to 2020. It can be found that from 2005, the proportion of NREs has been increasing significantly. What's more, it is estimated that 21 % of global electricity production is projected to come from variable renewables by 2040, up from 12 % in 2020 [2].

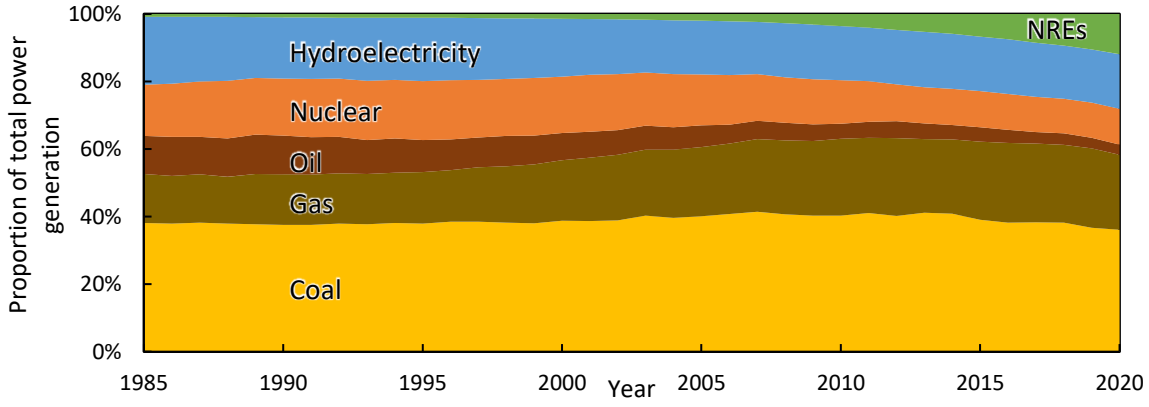

Figure 1-1 Global generation shares from varies of sources, 1985-2020. Sources from BP Energy [3].

The growth of NREs can be seen more clearly from the structural change of the renewable

energy itself in Figure 1-2. In the recent 20 years, the worlds' installed capacity proportion of wind and solar energy has increased from 2.06 % to 26.17 % and from 0.15 % to 25.51 % respectively, totally accounting for more than half of the renewable energy capacity. Although hydropower remains the largest renewable source of electricity, solar is the main driver of growth as it sets new records for deployment each year, followed by wind [4].

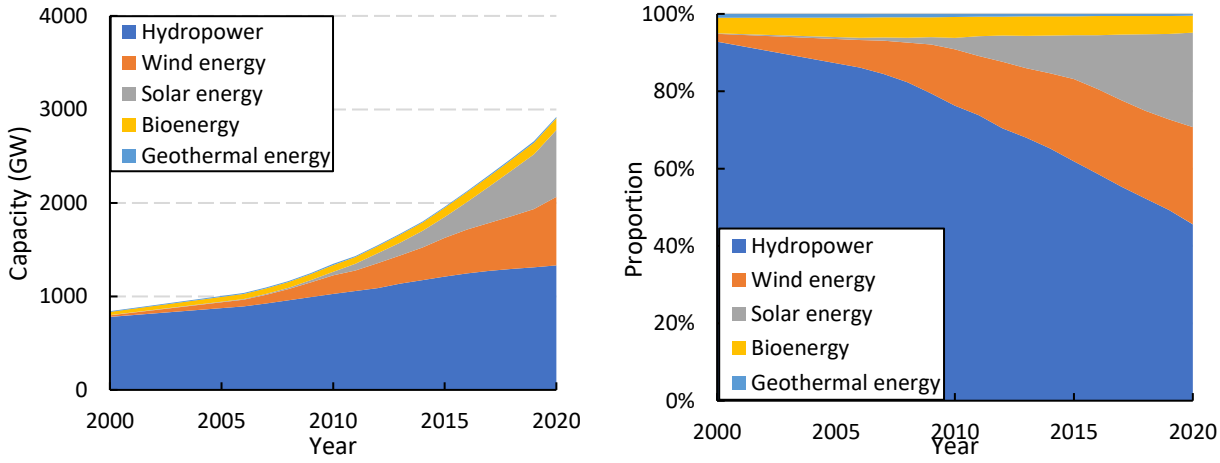

Figure 1-2 Left: Global installed renewable energy capacity, 2000-2020; Right: Global installed renewable energy capacity shares from varies of sources, 2000-2020. Sources from International Energy Agency (IEA) statistics [5].

However, the disadvantages of NREs are emerging: the output of the NREs, especially by wind and solar power, strongly depend on meteorological factors. Thus, their supply to the power grid is intermittent and hard to be regulated and this will inevitably lead to particular challenges to operating power systems. A particular example of this is highlighted in the so-called duck curve, made famous by the California Independent System Operator (California ISO). Figure 1-3 shows the impact of increasing NREs installed capacity on the demand for grid electricity. The lines in this figure show the energy generation in California without considering the NRE's. With the increasing installed capacity of NREs, and especially solar power which works during the central hours of the day, the demand difference for grid electricity between afternoon and evening keep growing from 2014 to 2020 [6]. This new scenario requires more regulation, flexibility and fast

response of the power grid in order to satisfy the energy demand.

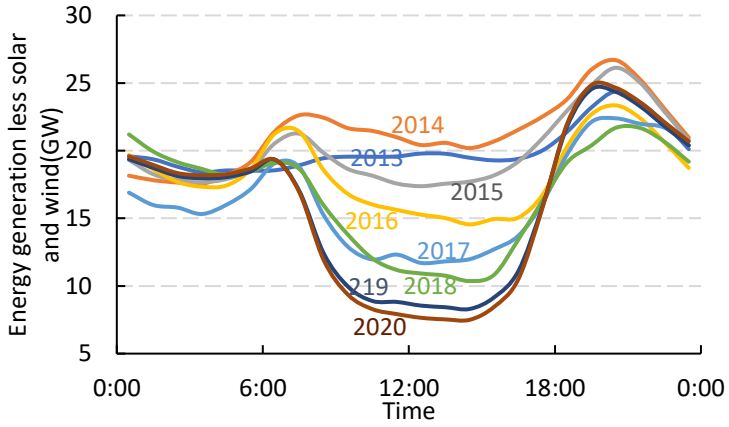

Figure 1-3 The California Duck Curve. Data taken from [6].

On one hand, the flexibility of grid is needed. On the other hand, power plant operators can have higher benefits if their machines operate in an extended operating range or if these units can be used to provide auxiliary services, such as frequency regulation or reactive power compensation. The electricity price in the energy market varies with the supply and demand. For example, as shown in Figure 1-4, the price variates dramatically with the change of the supply of NREs (when the participation of wind is reduced the price is increased) [7]. This frequent changes on the prices, can imply significant benefits for hydraulic power plants if they can respond quickly. In addition, the price difference means great income for the pump-storage plants, which is able to consume an excess of electricity buying the energy at a very low cost and generate power when the price of the energy is very high.

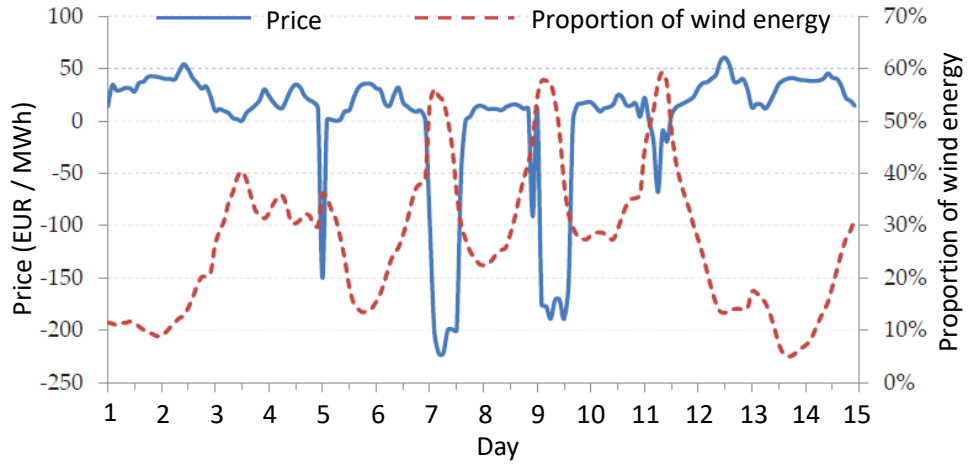

Figure 1-4 Electricity price variation caused by the NREs [8]

However, the extension of operating range of hydraulic turbines has caused new challenges to the power plants. With the extension of operating range, hydraulic turbines have to work more in off-design conditions and regulate the output much more frequently than they did before (Figure 1-5).

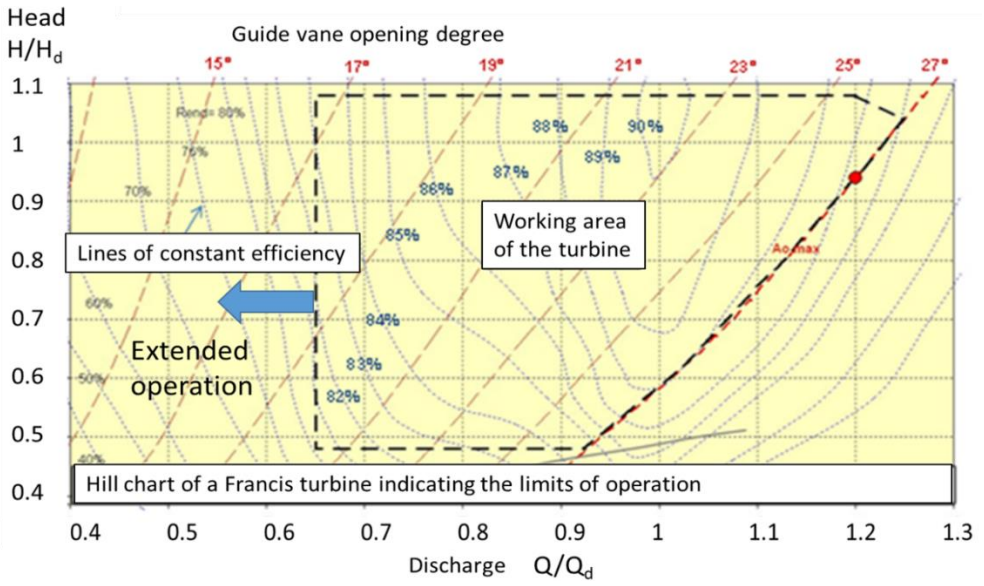

Figure 1-5 Hydraulic turbines have to operate in extended range

Under such situation, several types of dangerous phenomena occur, which have caused more damages and failures in the critical components of the machine. These phenomena are mainly:

- Erosive cavitation in some off-design conditions;
- Accelerated wear and tear of critical components;
- Cracks and fractures due to High Cycle Fatigue;
- Premature failures due to excessive stresses and structural resonances (low cycle fatigue);
- Power swings due to hydraulic resonances and self-excited phenomena.

Figure 1-6 shows examples of erosive cavitation damage in a turbine blade and a fracture on a pump turbine runner.

Figure 1-6 Left: Cavitation damage in a turbine blade [9]; Right: Cracks in a runner generated by excessive rotor-stator interaction (RSI) [10]

In summary, on one side, hydropower provides flexibility to the grid which is absolutely necessary nowadays and on the other side, to operate hydropower units in an extended operating range and with multiple transients will accelerate the degradation of the machine and increase the maintenance costs. As represented in Figure 1-7, if a hydraulic turbine provides more flexibility services, the estimated useful life of the unit will be shortened. However, the income of the plant per unit time will be increased. A more conservative operation will represent less benefit per hour of operation but a longer useful life. Therefore, the main question for hydropower in terms of sustainability and economic viability is: is it worth to provide flexibility

at a cost of sacrificing useful life of the machine?

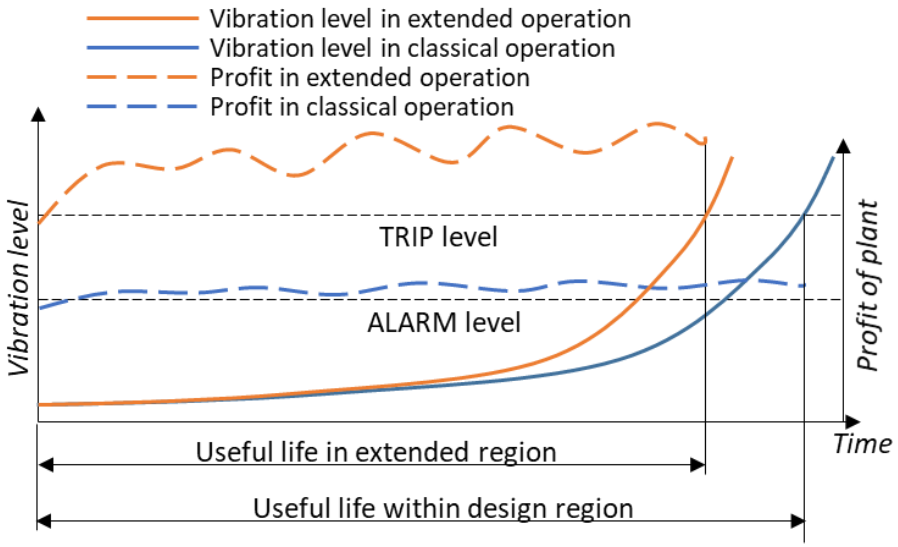

Figure 1-7 The extension of regulation capacity decreases the useful life while increases revenue for power plants

Condition monitoring of hydraulic turbines certainly help powerplant operators to reduce maintenance costs and also to quantify them. Some of the existing techniques have been proved to be feasible to detect many types of problems in different types of units [11–13]. Nevertheless, these techniques may not be feasible to address all of the aforementioned problems. Therefore, the work in this thesis proposes to improve existing condition monitoring techniques in hydropower by applying different artificial intelligence techniques, which have been shown promising results when they have been applied for condition monitoring and diagnosis in other engineering fields.

1.2 State of the art

The state of the art related to the topic of study has been separated in two different sections. The first one is the state of the art of the condition monitoring and diagnosis of hydraulic turbines

and the second one of the development and latest applications of AI on structural condition monitoring and diagnosis.

1.2.1 Condition monitoring and diagnosis of hydraulic turbines

Condition monitoring is the term used to describe a combination of techniques for implementing a condition-based maintenance strategy on industrial machinery. Data such as vibration levels, temperature, oil analysis etc., are acquired from plant, and analyzed to determine the condition of that plant at the time of measurement [14]. As the theoretical basis of condition monitoring and diagnosis, the dynamic behavior of hydraulic turbines has been studied extensively in the last years [15–19]. The effect and symptoms of different types of damage and fault on hydraulic turbines have been analyzed by many researches [20–24]. As a direct and fast technique, vibration-based condition monitoring has been applied on hydraulic turbine units since the end of last century [13]. Vibration sensors including accelerometers and proximity probes are installed in the bearings (turbine bearing, generator bearing, thrust bearing), spiral casing and draft tube. At the beginning, signals from accelerometers and pressure sensors were recorded and saved in the power plant, as well as the parameters related to the operating conditions of the machine. Then some limited processing of the data was performed. This was known as off-line monitoring. With the development of sensors and communication technology, new on-line monitoring system were installed in the turbine units and the signals were acquired and sent to diagnosis centers which are far from the power plants [11,25,26]. The vibration signal can be initially processed by the acquisition system to extract different spectral band values [12].

Traditionally, a hydraulic turbine operates near to its best efficiency point (BEP), where the hydraulic excitation forces are in a relatively low level. Nevertheless, far away from the BEP, vibration levels and pressure pulsations will increase. International standards define a series of levels for different positions of different types of turbine units [27]. Once the monitored vibration

values reach the defined ALARM or TRIP level, corresponding actions need to be taken in order to protect the machine. However, these recommendations are more suitable for machines working around the BEP. For units working with an extended operating range, these standards have some limitations:

- Levels are generally defined as global levels (overall rms, overall peak-peak), neglecting the detailed change in the vibration signal which can be related to incipient damages, erosive cavitation, etc.
- The constant value of action limits is not very suitable for a machine which is withstanding very different operating conditions.

With the extension of the operating condition, the hydraulic turbines are facing many new complex operating conditions such as:

1) Multiple transient conditions such as start-up, coast down and load change;

2) Operation in different head and load;

3) In new pump-turbines, fast transitions from pump to turbine mode without stopping the unit;

4) Some Hydraulic units provide auxiliary services to the grid, such as frequency regulation or reactive power compensation.

Classical condition monitoring techniques and standards may not be able to consider all this variety of situations that can occur in the actual operation of hydraulic turbines. Therefore, it is worth to implement new condition monitoring and diagnosis techniques for hydraulic turbines, more adapted to these new scenarios.

1.2.2 Application of AI techniques on condition monitoring and diagnosis

Artificial intelligence (AI) is a branch of computer science concerned with algorithms capable of performing tasks that typically require human intelligence. In 1956, the term “artificial intelligence” was firstly introduced by John McCarthy [28] in Dartmouth workshop, which is credited as the event that initiated AI as a research discipline. The next year, Frank Rosenblatt [29] invented perceptron algorithm and by the early 1960s a special-purpose hardware "Mark 1 perceptron" was built by him for alphabet recognition. His theory had firstly proposed the information was saved in the weights between the perceptrons and the learning process was “self-organized” [30]. In 1960, Bernard Widrow and Marcian Hoff [31] proposed “Adaline” (adaptive linear element) model, in which the weights can be adjusted according to the error in the output end. By “Adaline”, the structure of the perceptrons can be configured by “training” without manual intervention. In 1969, Marvin Minsky and Seymour Papert [32] published the famous book *Perceptrons* which pointed out multi-layer perceptrons (MLP) were capable of learning and XOR function, which was the weakness of single-layer perceptron. However, the misinterpretation of this book had dragged the neural computing research into a low tide of more than ten years [33]. In 1972, Teuvo Kohonen proposed self-organizing map (SOM). Being different from MLP, the training process was unsupervised, which is suitable for classification without knowing the classification types [32]. In 1974, the American machine learning pioneer Paul Werbos [34] introduced backpropagation (BP) into NN’s training, which is one of the most important contribution for NNs in the history of AI. In 1980s, after John Hopfield [35] invented Hopfield network, AI was valued by researchers again. In the book *Parallel Distributed Processing* written by David Rumelhart et.al., the three main characteristics of NNs were defined: structure, activation function and training method [36]. The recent 30 years are the golden age for AI, many new types of NNs have been invented such as RNN (recurrent neural network) [37], LSTM (long short-term memory) [37], CNN (convolutional neural network) [38], GAN (generative adversarial network) [39]. At present, AI is experiencing booming growth with the development of computer technology and wide application of GPU [40]. AI is creating a paradigm shift in virtually every sector of the tech industry.

As a typical kind of engineering problem, condition monitoring and diagnosis often deal with incomplete and noisy data which is one area where NNs are most applicable [41]. In 1991, BP-MLP was firstly used to identify damage in a plate stiffened with a 4 x 4 array of bays. The result showed that the neural network was able to predict the location of the damaged bay [42]. Over the next several years, many efforts had been made in application of NNs on numerical simulation result for structural damage detection in which different kind of inputs (damage indicators) were tried, such as lines of Fast Fourier Transform (FFT) spectrum [43], modal frequencies [44], frequency response function (FRF) [45], characteristics of time signal [44]. These initial attempts convinced that it was feasible to apply AI on structural health monitoring and damage identification. In 1997, George P. Succi and Harrison Chin [46] applied both NN and SOM on the vibration measurement of a pump with different flow rate and mechanical conditions. The energy of the shaft order frequency and its harmonics were used as the input of the networks. The results showed AI provided fairly good results on the classification for different conditions of hydraulic machines. In 2006, Mari Cruz Garcia et al. [47] introduced MLP into condition monitoring of a wind turbine gearbox. Indicators such as the bearing and oil temperature, generate power and fan speed were used as the inputs of the model. This study concludes that AI modelling techniques are adequate for health condition monitoring of wind turbines. In 2011, Meik Schlechtingen and Ilmar Ferreira Santos [48] compared the capabilities of ANN and autoregressive models on the wind turbine fault identification. The temperatures of critical components in the generator and gearbox and shaft speed were used as the input. The AI technique showed easier abnormal behavior identification than the regressive model. AI techniques have also been applied on related research of hydraulic turbines, such as blade design [49], diffuser shape optimization [50], characteristic curve mapping [51], stress and strain prediction [52,53], etc. Although AI has been proven to be an effective tool for vibration-based mechanical damage diagnosis in several studies, there remains a very common hurdle in most of the studies: the size of the input data, which is determined by the resolution of the spectrum. A higher resolution provides more details about the dynamic response of the structure but the

number of inputs is too large for the neural networks' applications on engineering problems. A general way to deal with this problem is to use Principal Component Analysis (PCA) to reduce the size of the input pattern [54]. In 2013, R.A. Saeed et al. [55] used PCA to extract features from the FRF obtained from the simulation of a hydro turbine runner. The FRF features were used for training ANN in order to predict the crack length on the blade. However, the calculation of one principal component (PC) depends on every input variable, which means the PCs will change with the increase of the samples. In addition, there is no real meaning in the extracted principal components [56]. To address this problem, Factor Analysis (FA) is proposed. It describes variables in terms of a lower number of factors that have different loading values regarding the input variables and also tries to find out one or more latent variables (factors) that exert causal influence (loadings) on these observed variables [57]. FA has been applied for solving several engineering problems [58,59]. The dimension reduction techniques like PCA and FA are useful tool for improving the performance of AI on condition monitoring and diagnosis.

1.3 Methodology

The presented thesis involves three sets of existing monitoring data from different hydraulic turbine units: a reversible pump turbine, a Francis turbine and a Pelton turbine. For the pump turbine, the data are taken from on-line monitoring system over one month; for the Francis turbine, the data were measured by field test while for the Pelton turbine, the data from an off-line monitoring system were used. On one hand, the units are facing some problem: high vibration levels due to the extension of operating range, limited operating range at high loads due to overload instability and a damage on the runner. On the other hand, these problems cannot be properly addressed with classical condition monitoring techniques:

- Some abnormal behaviors in part load conditions cannot be monitored conveniently with traditional action limits based on the standard levels;
- The onset of the overload instability cannot be easily predicted;
- An incipient damage on the runner may not be detected until the crack is very large or even when the fracture already occurred (Remaining Useful Life prediction).

Taking the existing data and indicators that have been used for the condition monitoring of the aforementioned prototypes, the main contribution of this thesis has been to apply artificial intelligence techniques and dimension reduction methods in order to improve the existing condition monitoring techniques. In particular, the application of these techniques in the existing condition monitoring data has permitted to accomplish the following objectives defined at the beginning of the thesis.

1.4 Objectives

Taking into account the analyzed prototypes and the data available for each of these units, the objectives of the thesis were defined as:

1. To identify the abnormal behavior region for hydro turbines that are operating in extended range based on vibration hill charts mapped by AI techniques. Especially for part load conditions, to improve the condition monitoring based on the vibration hill charts;

2. For Francis turbines working in high load conditions, to use AI techniques for an early detection of the overload instability;

3. To predict the remaining useful life of critical components of hydraulic turbines, such as the runner, by means of AI techniques.

1.5 Outline of the thesis

1.5.1 Preliminary work

The first period of the thesis was dedicated to perform a preliminary work on the state of the art. During this period the author had a specific training in background knowledge of vibration, behavior of hydraulic turbine, modal analysis and experimentation.

1.5.2 Abnormal behavior analysis for turbine units in extended range

The author had a literature review on the latest application of artificial intelligence algorithms and tried to apply artificial neural networks on the existing monitoring data of a Reversible Pump Turbine. This turbine was operating in an extended range in which it was withstanding different types of excitations which may decrease the remaining useful life of the machine. As a contribution of this period, the author published one Journal Paper [9] and one conference paper [60] as first author. This section corresponds to Chapter 2 of the thesis.

1.5.3 Overload instability detection

This period was dedicated to investigate the overload instability in a Francis Turbine, which occurs suddenly and hence limits the operating range in high load. In order to analyze the feasibility of extending the operating range, several AI methods had been used on the on-site measurement data for an early detection the overload instability. As a contribution of this period, the author published one Journal Paper [61] as first author. This section corresponds to Chapter 3 of the thesis.

1.5.4 Damage prediction by AI and data-driven methods

In this period, a Pelton turbine that suffered from a fatigue damage was investigated. The

most significant indicators were selected from the long-term monitoring vibration data and used as the input of ANN to predict the damage. As a result of this period of investigation, the author published one Journal Paper [61] as a first author and collaborated in another Journal Paper [52]. This section corresponds to Chapter 4 of the thesis.

1.5.5 Research line and main contribution of the thesis

The research line of this thesis is shown in Figure 1-8 and the main scientific contributions of this work (Journal Papers in the Q1 of the Journal Citation Reports and international conference papers) are summarized in Table 1-1.

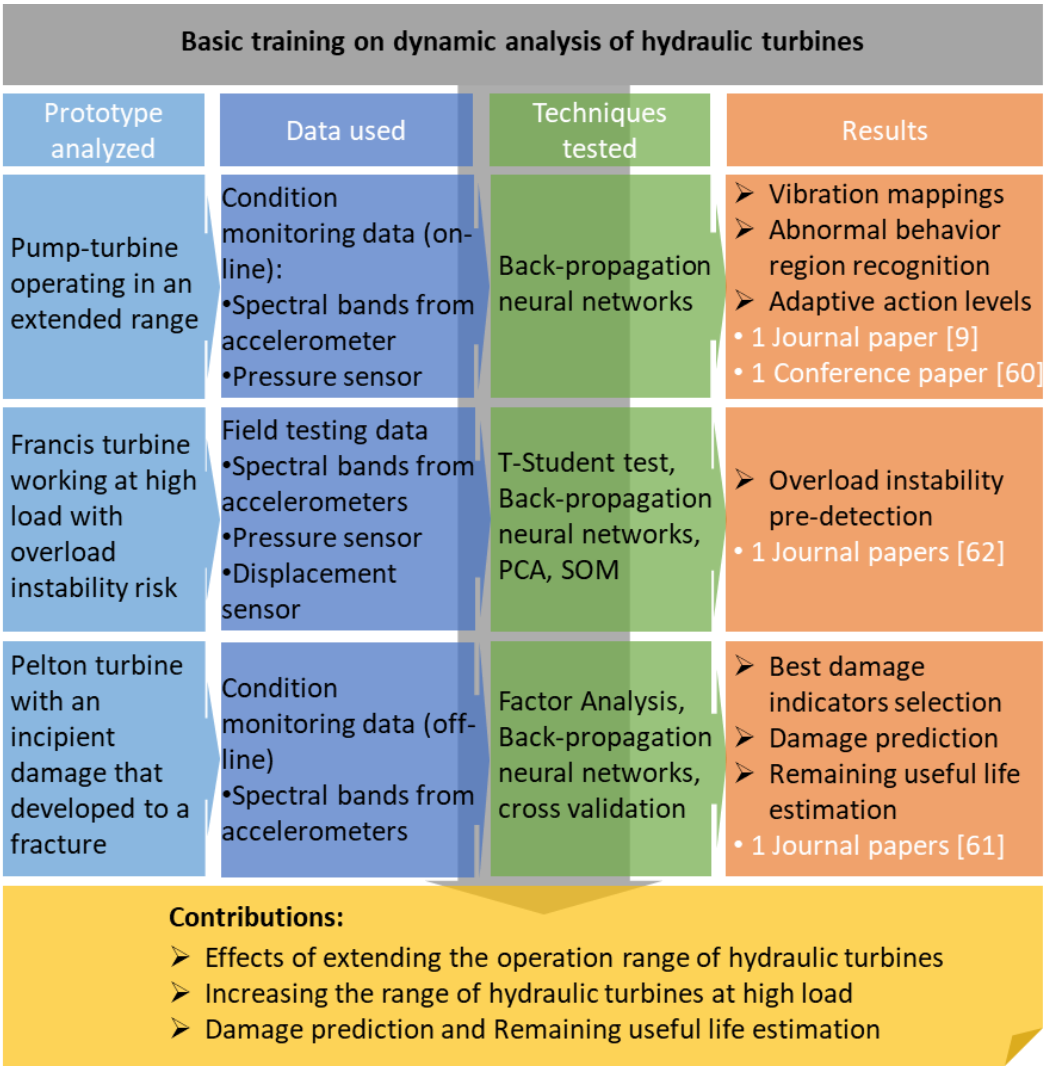

Figure 1-8 Schematic view of the outline of the thesis

Table 1-1 Paper Publications

Journal Paper Publications
First Author
[9] W. Zhao, M. Egusquiza, C. Valero, D. Valentín, A. Presas, E. Egusquiza, On the Use of Artificial Neural Networks for Condition Monitoring of Pump-Turbines with Extended Operation, Measurement. 163 (2020) 107952. doi: 10.1016/j.measurement.2020.107952.
[61] W. Zhao, M. Egusquiza, A. Estevez, A. Presas, C. Valero, D. Valentín, E. Egusquiza, Improved damage detection in Pelton turbines using optimized condition indicators and data-driven techniques, Struct. Heal. Monit. (2021) 147592172098183. doi: 10.1177/1475921720981839.
[62] W. Zhao, A. Presas, M. Egusquiza, D. Valentín, C. Valero, E. Egusquiza, Increasing the Operating Range and Energy Production in Francis Turbines by An Early Detection of the Overload Instability, Measurement. 181 (2021) 109580. doi: j.measurement.2021.109580.
Collaborations
[63] M. Zhang, D. Valentin, C. Valero, M. Egusquiza, W. Zhao, Numerical Study on the Dynamic Behavior of a Francis Turbine Runner Model with a Crack, Energies. 11 (2018) 1630. doi: 10.3390/en11071630.
[52] A. Presas, D. Valentin, W. Zhao, M. Egusquiza, C. Valero, E. Egusquiza, On the use of neural networks for dynamic stress prediction in Francis turbines by means of stationary sensors, Renew. Energy. 170 (2021) 652–660. doi: 10.1016/j.renene.2021.02.013.
Conferences Papers
[60] W. Zhao, E. Egusquiza, C. Valero, M. Egusquiza, D. Valentín, A. Presas, A Novel Condition Monitoring Methodology Based on Neural Network of Pump-Turbines with Extended Operating Range, in: 16th IMEKO TC10 Conf., Berlin, 2019: p. 4. https://www.imeko.org/publications/tc10-2019/IMEKO-TC10-2019-024.pdf.

Collaborations

[53] A. Presas, D. Valentin, W. Zhao, C. Valero, M. Egusquiza Montagut, E. Egusquiza, Strain prediction in Francis runners by means of stationary sensors, in: 30th Symp. Hydraul. Mach. Syst., Lausanne, 2020: p. 4.

2

EFFECTS OF EXTENDING THE OPERATING RANGE OF HYDRAULIC TURBINES OF PART LOAD

In this chapter, an improved condition monitoring and diagnosis methodology for hydraulic turbines is proposed and discussed. A set of vibration indicators previously defined have been used. Then, each indicator is mapped using artificial neural networks (vibration hill-chart). Finally, by tracking the evolution of the hill chart mappings in different historical time periods, the possibility of damage diagnostic is discussed.

2.1 Vibration monitoring data description

As shown in Figure 2-1, the researched turbine unit is a vertical pump turbine (PT) unit with a maximum capacity of 85 MW and rated rotating speed of 500 rpm. The number of the blades in the runner is 7 and there are 16 guide vanes in the distributor. An ICP Piezoelectric ceramic/ shear accelerometer was installed on the turbine bearing in radial direction. The radial acceleration on the turbine bearing and operating parameter (head *H* and wicket gate opening *WGO*) were collected and sent to the remote diagnosis center by internet.

During monitoring, the machine operation was in regulation mode, varying the load to match the changing demand from the power grid. Therefore, both *H* and *WGO* changed in a wide range. In the same day, the *WGO* of the machine variated frequently from 20 % to 100 % power in order to adjust the output in the shortest possible time while the *H* increased continually with pump operation and decreased in turbine operation but at a much slower pace. Finally, there were 614 sets of signals (vibration signal, *H* and *WGO*) obtained within one month.

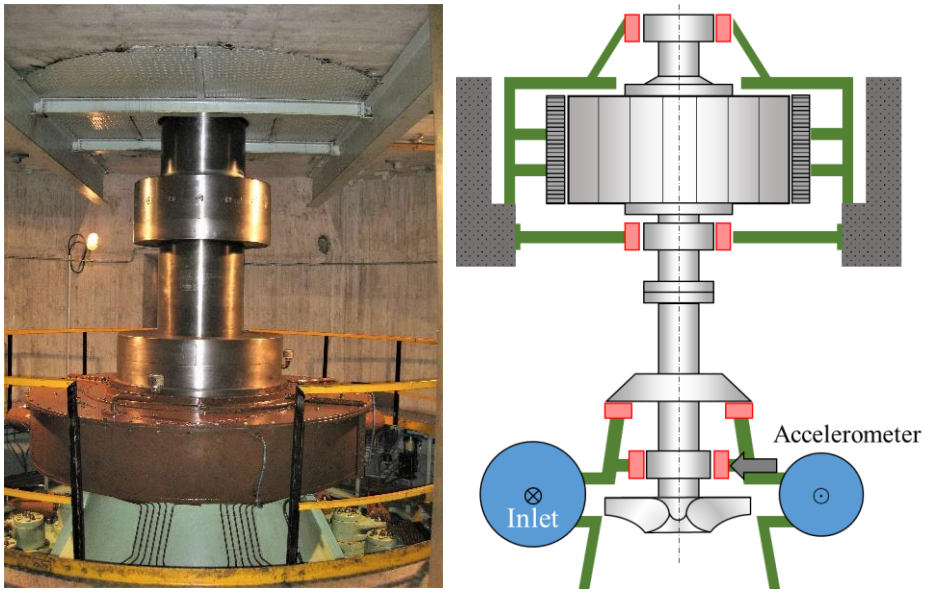

Figure 2-1 Prototype of the measured pump-turbine unit and sketch map of the turbine unit

2.2 Vibration hill chart mapping

A multi-dimensional vibration hill chart is proposed to improve the condition monitoring and diagnosis of hydraulic turbine units. The general flow diagram of the multi-dimensional vibration hill chart is shown in Figure 2-2.

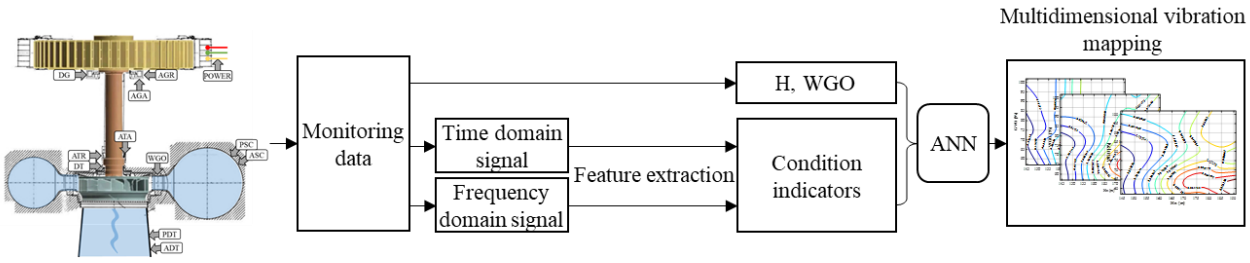

Figure 2-2 Multidimensional vibration mapping fitting process

2.2.1 Condition indicators extraction

The condition monitoring indicators in the researched unit were previously defined according to the following excitations:

- Unbalance
- RSI
- Cavitation vortex rope
- Turbulence

The band values of the spectrums from the system are used as the monitoring indicators and they are calculated according to Equation 2-1:

$$B = \sqrt{\sum \left(X_i \frac{c_E}{c_A} \right)^2} = 0.8165 \sum {X_i}^2 \qquad (2\text{-}1)$$

where B is the RMS value of the frequency band; X_i is the amplitude of each line in the

spectrum band (usually the spectral band width is around 1 Hz); c_E and c_A are energy and amplitude correction factors of the window function respectively.

2.2.2 Vibration hill chart by ANN

An artificial neural network with two layers is used for fitting each condition indicator within the operating range. It has been proven that a neural network with one hidden layer is able to fit any continuous function [64]. The data are divided into three groups: training set, validation set and testing set, which account for 70 %, 15 % and 15 % of the whole samples respectively. The normalized *H* and *WGO* are input into the ANN and each condition indicator is used as the output. Levenberg-Marquardt (LM) backpropagation function is chosen as the training algorithm. This training method has a faster convergence speed on training process of middle-sized feedforward networks [60].

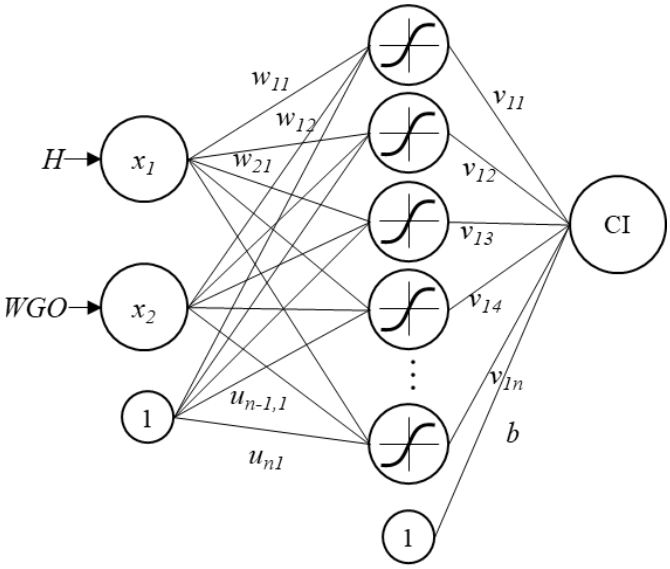

Figure 2-3 Architecture of the 2-layers fitting ANN

2.3 Result

The first indicator was defined to detect the vortex rope. The vortex rope generates large pressure pulsations that can damage the machine and produce power swing. Operation with a strong vortex rope can be considered abnormal because it can impair the operation of the turbine. Although the vibration levels generated by this phenomenon in the bearing are not large, the effects have to be checked with other parameters, like the pressure pulsation and the power swing. The feature selected for the identification of the vortex rope is a frequency band around the precession frequency of 0.25-0.35 f_f. In the mapping, the zone between 35-45 % of the WGO stands out and shows the maximum amplitude at the highest head. Under these conditions, the power swing is excessive.

Another typical problem is cavitation erosion, which increases maintenance works. Erosive cavitation generates high-frequency vibration that is transmitted to the bearings. For its detection, a high-frequency vibration band was selected as an indicator. The operating conditions where erosion occurs are 30-40 % WGO and at the lowest head.

Finally, the hill chart of RSI excitation is analyzed. In PTs the strong RSI excitation leads to large vibrations in the runner and, therefore, to fatigue problems. In this case, the chosen indicator was the RSI amplitude. The mapping of the RSI excitation shows that the maximum vibration occurs at maximum load and at the highest heads.

Regarding all this information, the worst operating conditions take place at the minimum head with loads of 30-40 % and at the maximum head with loads 30-40 % and 90-100 %. The operation of the machine should be restricted although the effects on the RUL have to be calculated.

About damage detection, the condition monitoring can be improved with the vibration hill charts. Fatigue damage in the runner can produce destruction of one part of the runner what generates an increase in the unbalance force that can be small. Therefore, rapid detection of an increase in f_f and f_b can avoid catastrophic damage. Finally, damage can produce a change in

amplitude of the natural frequencies of the rotor, therefore the mapping of them is also convenient.

The content in this chapter reproduces the paper entitled “On the Use of Artificial Neural Networks for Condition Monitoring of Pump-Turbines with Extended Operation” published in 2020 in the journal “Measurement” with an Impact Factor of 3.364 (Q1) [9] which can be found in Chapter 6 of this thesis report.

3

INCREASING THE OPERATING RANGE OF HYDRAULIC TURBINES AT HIGH LOADS BY AN EARLY DETECION OF THE OVERLOAD INSTABILITY

In this chapter a Francis turbine with a limited operating range due to a huge overload instability is analyzed. AI techniques have been applied to detect and quantify the proximity of the overload instability when the unit is working at high loads.

3.1 Overload instability description and data acquisition

When a Francis turbine operates at loads higher than design, the cavitating vortex rope that is generated in the draft tube may become unstable, producing huge pressure fluctuations, vibrations and power swing, referred as overload instability [65]. The overload instability is a problem that is dangerous for the turbine unit. This phenomenon was firstly documented in 1940 [66] but it is still one of the main concerns in current operating units [67]. It is known that such phenomenon starts with a stable cavitating vortex rope in the draft tube. Such rope is generally a vertical cavitation column centered in the runner cone [68]. In this situation, the overload instability emerges abruptly (see Figure 3. of [62] or Chapter 6).

The analyzed turbine unit is a large medium-head Francis turbine located in a hydro power plant in Canada, with a rated power of 444 MW. It presents a clear part load instability [5] and under some circumstances an overload instability with high power fluctuations. Later, some works measured and confirmed the existence of power swing in both in real prototype and model experiment [65,67–70]. Accelerometers and pressure sensors have been installed on different positions of the machine (see Figure 4. of [62] or Chapter 6). The data from the sensors and operating parameters (*H* and *WGO*) have already been obtained by previous researches [71,72]. Different time signals measured are windowed with a 4s-window and 0.25 s shift and a set of indicators is obtained. Two main types of indicators have been obtained for every window. The first type of indicators is calculated in the time domain. These are the RMS value, the mean value and the peak-peak value of the signal part. The second type of indicators corresponds to frequency bands obtained after performing the FFT. The main spectral bands have been selected according to the excitation forces in Table 3 of [62]. Finally, 32 indicators are extracted for the following analysis.

3.2 Data analysis by different methods

Although the unit was able to produce around 490 MW (*WGO* of the regulation system at 100 %) the operators limited the power of the machine to approximately 440 MW in order to reduce the risk of an overload instability. With an appropriate monitoring system, the operating range of the machine could be safely increased. It is roughly estimated in Figure 3-1 that the amount of energy contained in this increased range area (energy that could have been produced with an extended range) is 160 GWh per year. The data described in section 3.1 are analyzed by 1-D, 3-D and high-dimensional methods.

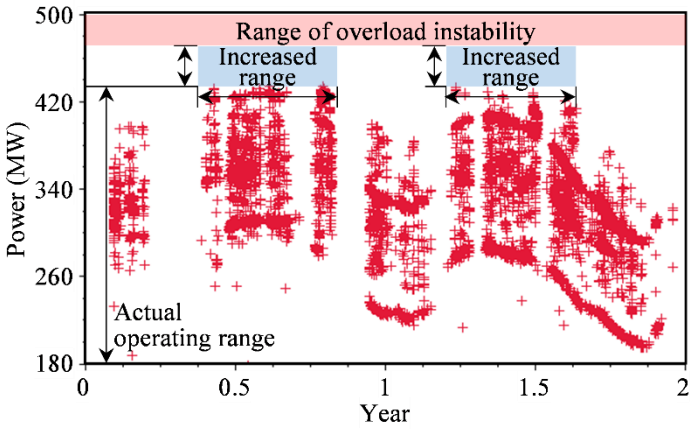

Figure 3-1 Actual operating range based on real monitoring data. Estimated possible increased range below the overload instability area.

3.2.1 One-dimensional analysis (t-Student test)

The result of the analysis shows that there is no indicator which behaves as desired (see Table 5 and Table 6. of [62] or Chapter 6). Therefore, we conclude that for an early detection of the instability, the trend of a single indicator is not significant enough and that more refined techniques are necessary.

3.2.2 *Three-dimensional analysis (PCA)*

The PCA result is able to distinguish the conditions that developed into overload instability (*S-U*) from those didn't (*S-S*). However, PCA is not able to detect any intrinsic change in the signal before the onset of instabilities, which is important for the instability prediction.

3.2.3 *High-dimensional analysis (SOM)*

In this section, two sets of data are compared by SOM: data far away from the instability and data close to the instability. The SOM neighbor distances of *S-S* condition and *S-U* condition are shown in Figure 3-2. There are 100 nodes connected in hexagonal topology in each map. The color between two adjacent nodes represents the distance between them. Apparently, the distances map of *S-S* condition and *S-U* condition are quite different. The colors in *S-S* map are uniform, indicating that the distances between different nodes are similar. This means it is difficult to find any clear trend among all of the samples in this data set. For the *S-U* condition, the color distribution is completely different: a line of dark points splits the color map into two parts or clusters. In one cluster, all nodes are closely connected with the adjacent nodes (light color). The dark color in the maps, indicates that a long distance between the two clusters exists.

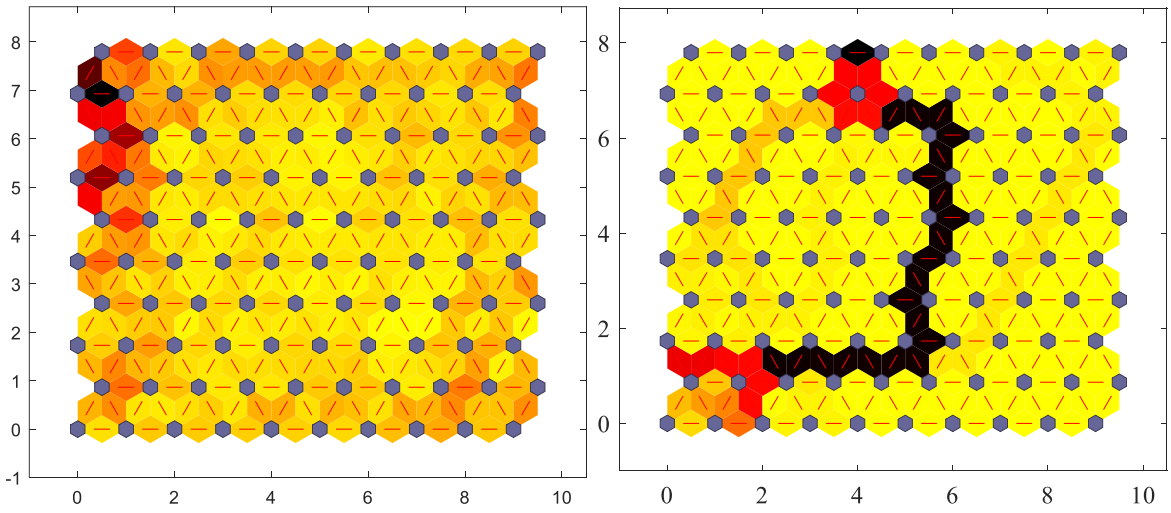

Figure 3-2 SOM neighbor distances for *S-S* condition (left) and *S-U* (right)

3.3 Instability pre-detection

According to the result obtained in Section 3.2, ANN is used to predict the onset of overload instability. The 32 indicators are used as the input of the ANN and the output the artificial unstable index (*AUI*).

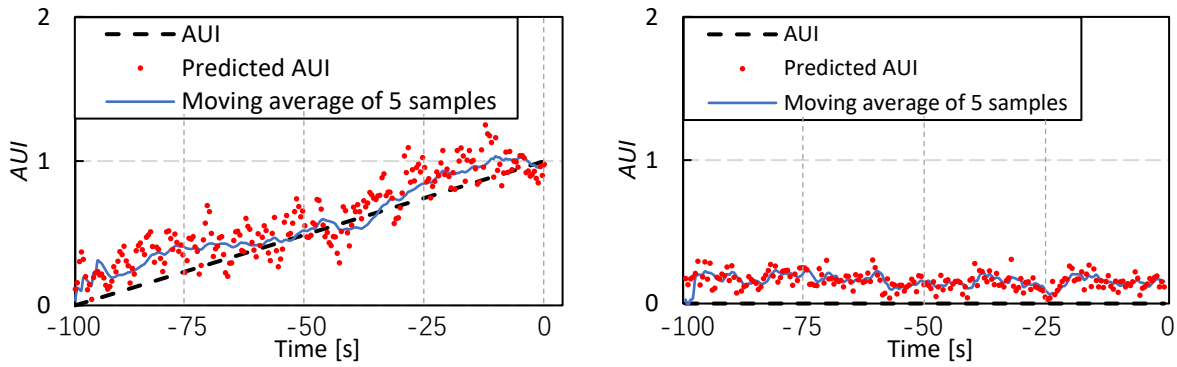

Figure 3-3 *AUI* prediction result by ANN of *S-U* (left) and *S-S*2 (right)

From Figure 3-3 it can be seen that the *AUI* for condition *S-U* (left) increases from 0 to 1 in a relatively smooth way before the instability appears. For the stable condition *S-S*2 (right), the *AUI* shows a constant trend near zero. These results show that the trained ANN is capable to correctly predict the trend and classifying an *S-U* and *S-S* condition.

The content in this chapter reproduces the paper entitled “Increasing the operating range and energy production in Francis turbines by an early detection of the overload instability” published in 2021 in the journal “Measurement” with an Impact Factor of 3.364 (Q1) [62] which can be found in Chapter 6 of this thesis report.

4

INCIPIENT DAMAGE DIAGNOSIS AND REMAINING USEFUL LIFE ESTIMATION BASED ON AI METHOD

In this chapter, the feasibility of performing incipient damage diagnosis and remaining useful life calculation with AI techniques is discussed. The prototype selected is a Pelton turbine with an incipient damage that led to a fracture on the runner (broken bucket). From all the data set, the most relevant indicators are extracted by using factor analysis (FA). Then ANN have been used to predict the remaining useful life.

4.1 Case description

The researched machine is a Pelton turbine with a maximum power of 34 MW. The machine suffered a failure in which one of the buckets broke off during operation. The inspection of the machine later revealed the failure was due to a deviated jet, which caused several cracks to appear and propagate on different buckets [21].

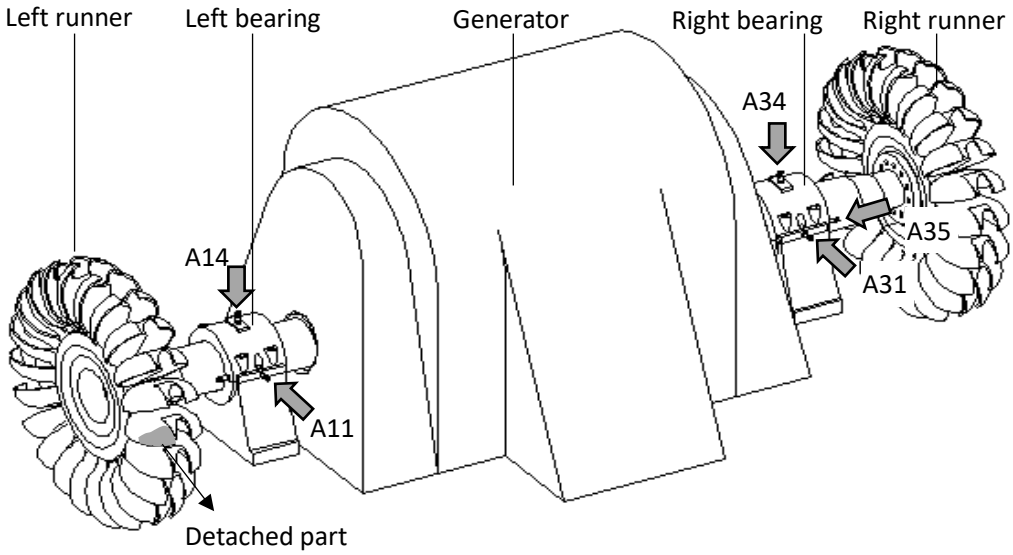

Figure 4-1 Sketch of the Pelton turbine and layout of the vibration sensors

In order to analyze the evolution of the damage, the monitoring data over 13 years are used. A total of 5 accelerometers were installed on both bearings in the radial and axial directions, as seen in Figure 4-1. Accelerometers A11 and A31 were installed horizontally in the same direction in which the jet impinges the runner. A14, A34 and A35 were installed in the vertical and axial directions, respectively.

4.2 New monitoring method by new indicators and factor analysis

4.2.1 New condition indicators

In order to implement the new condition indicators on the monitoring system, the natural frequencies are obtained from previous studies [13,73,74]. The frequency bands are divided into two main groups, the ones corresponding to the rotor's natural frequencies and the ones belonging to the runner. These investigations provided a deeper understanding of the operation of the Pelton turbine and allowed defining new frequency bands related to the most excitable modes of the critical components. Besides the typical synchronous bands for unbalance, misalignment and bucket passing frequencies were devised.

4.2.2 Factor analysis

After extracting the condition monitoring indicators based on the dynamics of the turbine, FA technique is used to reduce the dimension of the database and select the most relevant indicators. FA is preferred over PCA for dimension reduction as the physical meaning of the indicators is retained.

4.2.2.1 Number of common factors determination

The relative eigenvalues, as well as their cumulative percentages, are displayed in Figure 4-2. From the scree plot it can be seen that the inflection point is the third one, which indicates that three common factors are sufficient for retaining most of the information of the indicator matrix.

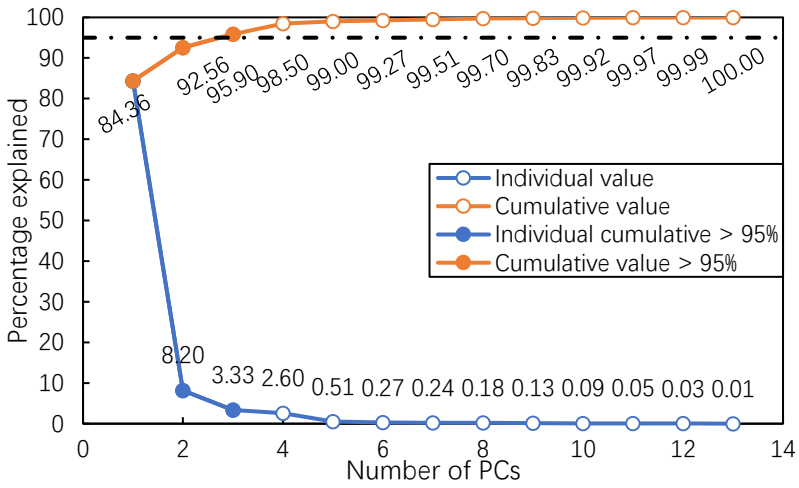

Figure 4-2 Scree plot of the eigenvalues

4.2.2.2 Loading factor calculation

After the retained number has been determined, FA is conducted on the indicator matrix and the loading matrix is calculated. The loadings of each indicator on the 3 common factors are listed in Table 4-1, as well as the module of each indicator, which is the Euclidean norm of the loadings.

Table 4-1 Loading factor of each damage indicator of point A34-10

Indicator	Factor1	Factor2	Factor3	Module
f_f	-0.4337	0.1769	0.3147	0.5643
2*f_f	0.0387	-0.0440	-0.8386	0.8406
3*f_f	-0.3144	0.8485	0.3779	0.9806
Rotor mode 1	-0.2751	0.9032	0.3218	0.9975
Rotor mode 2	0.0368	0.4883	0.0200	0.4901
Rotor mode 3	-0.4351	0.2472	0.3843	0.6310
f_b	-0.0392	0.1362	0.2187	0.2606
2*f_b	-0.4199	0.5066	0.7337	0.9855
3*f_b	0.9085	0.0224	-0.0414	0.9097
Runner mode 1	-0.4024	0.6606	0.5677	0.9595
Runner mode 2	0.8938	-0.1856	-0.2492	0.9463
Runner mode 3	0.8416	-0.1578	-0.0389	0.8571

Taking advantage of 3 loading factors, the loading matrix of point A34-10 can be represented

in a 3D plot, which is helpful for visualizing and comparing the loadings of the indicators. The loading vectors are shown in Figure 4-3. Thus, the direction and length (module) of each vector indicate its relevancy with the common factors. For example, there are 4 indicators with negative loadings on the first common factor and 7 with positive loadings. The indicator $3*f_b$ has the smallest angle with the axis and largest loading value, which indicates $3*f_b$ has the greatest dependency with the first common factor. On the contrary, the length of vector f_b is 0.2606, which is too small to represent any common factor.

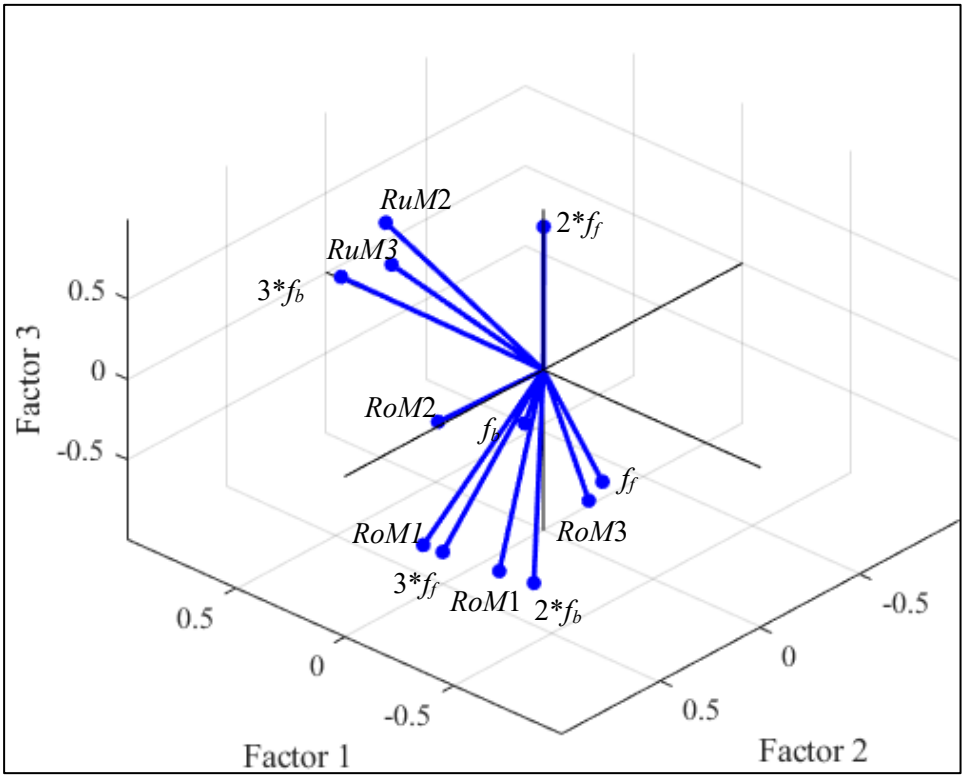

Figure 4-3 Loading factors of each new indicator on the three common factors

4.2.2.3 ANN training

The common factors are also extracted from the other sensors by the same process of Section 4.2.2.2. After obtaining all of the common factors, ANN is used for learning the evolution of the damage. An Artificial Damage Index (*ADI*) is defined based on the typical crack propagation behavior. These have been used in an ANN model in order to predict the *ADI* until failure occurs.

The same process has been followed for the typical condition indicators (spectrum level and harmonic level) used normally in condition monitoring of Pelton turbines in order to compare the results with the new method.

4.3 Result

It can be observed from Figure 4-4 that the prediction result of the “spectrum level” set has the largest error in every point and the new condition indicators has the lowest error in most of the measurement points. The mean RMSE in the rightmost item in the chart indicates that the proposed condition indicators have the lowest error among the three data sets. Compared to the “spectrum level” and “harmonic level” indicators, the prediction error of new condition indicators has been decreased by 23.62 % and 10.88 % respectively. The most accurate point for the damage detection is the vertical position when the machine is working at 100 % load (A34-10) and when the data set containing the new condition indicators is used. It can be concluded that the new condition indicators have a better correlation with the *ADI* for almost all the sensors analyzed (minimum RMSE). The reason lies in the characteristics of the especially selected spectral bands in the proposed set of indicators, which are more correlated to both the dynamic response of the structure and excitation forces. Thus, these indicators are more sensitive to detect the onset of an incipient damage.

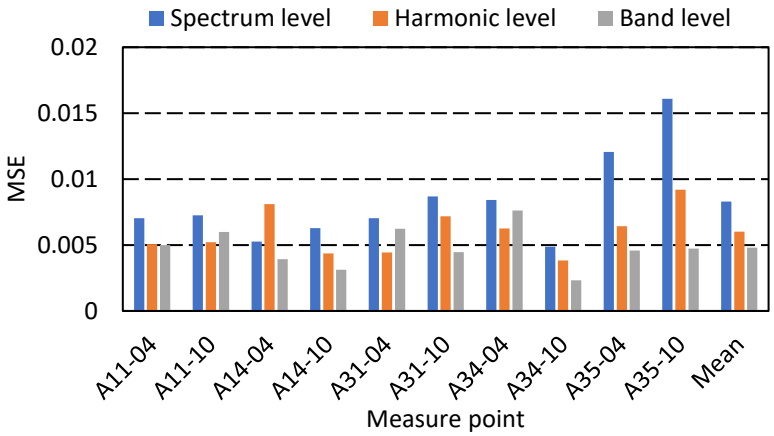

Figure 4-4 RMSE of the three indicators' sets for each measurement point and averaged performance

The complete content of this chapter can be found in the paper entitled "Improved damage detection in Pelton turbines using optimized condition indicators and data-driven techniques" published in 2020 in the journal "Structural Health Monitoring" with an Impact Factor of 4.870 (Q1) [61] which can be found in Chapter 6 of this thesis report.

5

CONCLUSIONS

In this chapter the major conclusions of this thesis are summarized. First, the main conclusions of the studies on multi-dimensional vibration hill chart are presented. Then the conclusions of instability prediction are pointed out. Finally, the conclusions obtained regarding incipient damage diagnosis are included.

The present investigation aimed to improve the condition monitoring and diagnosis of hydraulic turbine units by AI techniques in order to increase the regulation capacity of hydro power plants and extending the remaining useful life of the units. Summing up all the investigations conducted in this thesis, the following conclusions have been obtained:

- Regarding the effects of extending the **operating range of hydraulic turbines of part load**, artificial neural network (ANN) has been applied to map the condition indicators (vibration hill charts). The proposed vibration hill charts take the head and load into account, which is important for hydraulic turbines that operating in an extended range. The new condition monitoring based on vibration mappings decrease both false positive and false negative alarm rates. The mappings provide more detailed information of the behavior of the machine, which increases the sensitivity of damage detection. The region of strong vortex rope and erosive cavitation have been identified, which provide guidance to the operators of the plant.

- Regarding the **operating range of hydraulic turbines working at high loads**, it has been concluded, that with a condition monitoring system with a properly trained NN, the operating range could be increased. Different data-driven methods have been tried. Statistical hypothesis testing of the indicators during the stable conditions preceding the instability have demonstrated that there is not a single indicator that can clearly predict the onset of the instability. With principal component analysis (PCA) the data of the stable conditions preceding the instability can be clearly clustered. The stable operating conditions that finally lead to an overload instability can be classified and separated from those which did not. The self-organizing map (SOM) has been used as an alternative method for clustering. It has been shown that SOM is able to detect changes in the data set before the instability occurs while the PCA did not. Nevertheless, this method is not able to quantify the proximity of the instability onset. It has been proved that the trained ANN is able to quantify the risk of instability several seconds beforehand

and, therefore, that an early detection of the overload instability is possible.

- Regarding to the **incipient damage diagnosis and remaining useful life prediction** of turbine units, a new method involving factor analysis (FA) and ANN has been presented. By FA, the indicators related to the rotor modes, runner modes, bucket passing frequency and rotating frequency have been determined to be the most important indicators for predicting the damage on the runner, which justify the proposed new condition indicators adopted in this paper. In conclusion, the final set of proposed indicators contains more relevant information and has a smaller dimension compared to the previous ones.

6

COPY OF THE JOURNAL PAPERS

In this chapter the copy of the three Journal Papers that are part of the present Article- Based thesis is included. The first paper is entitled *"On the Use of Artificial Neural Networks for Condition Monitoring of Pump-Turbines with Extended Operation"* and it is published in the Journal of *Measurement* (Q1, 2020, Impact Factor 3.364). The second one is *"Increasing the Operating Range and Energy Production in Francis Turbines by An Early Detection of the Overload Instability"* published also in the Journal of *Measurement* (Q1, 2021, Impact Factor 3.364). The third Journal Paper is *"Improved damage detection in Pelton turbines using optimized condition indicators and data-driven techniques"* published in the Journal of *Structural Health Monitoring* (Q1, 2021, Impact Factor 4.870).

The paper related to Chapter 2 and the paper related to Chapter 4 are non-open access paper and therefore only the accepted manuscript is included (journal pre-proof). The paper related to Chapter 3 is an open access paper and the published version has been included in this document. The published papers should be consulted on the web page of the respective editors:

https://www.sciencedirect.com/science/article/pii/S0263224120304905

https://www.sciencedirect.com/science/article/pii/S0263224121005558

https://journals.sagepub.com/doi/abs/10.1177/1475921720981839

6.1 Journal paper 1

- W. Zhao, M. Egusquiza, C. Valero, D. Valentín, A. Presas, E. Egusquiza, On the Use of Artificial Neural Networks for Condition Monitoring of Pump-Turbines with Extended Operation, Measurement. 163 (2020) 107952. doi: 10.1016/j.measurement.2020.107952.

Measurement xxx (xxxx) xxx

Contents lists available at ScienceDirect

Measurement

journal homepage: www.elsevier.com/locate/measurement

On the use of artificial neural networks for condition monitoring of pump-turbines with extended operation

Weiqiang Zhao, Mònica Egusquiza, Carme Valero, David Valentín, Alexandre Presas, Eduard Egusquiza

Center for Industrial Diagnostics (CDIF), Polytechnic University of Catalonia (UPC), Barcelona, Spain

ARTICLE INFO

Article history:
Received 20 January 2020
Received in revised form 23 March 2020
Accepted 11 May 2020
Available online xxxx

Keywords:
Condition monitoring
Pump-turbine
Artificial neural networks
Extended operation

ABSTRACT

Because of the addition of stochastic supply to the power grid introduced by new renewable energies, hydropower is required to respond rapidly to the fluctuation between power demand and supply. Consequently, hydropower units must work under extreme off-design conditions, where the machines are more prone to suffer from damages and shorter useful lives. Novel supervision and monitoring techniques which are able to compare the revenues with the remaining useful life of the turbine unit are required to cope with these new scenarios.

In this paper, the upgrading of an existing monitoring system to deal with the extended operating range of a pump-turbine is discussed. Previously, the machine operating range was from 50% to 100% power and now it is from 20% to 100% power. For that purpose, the vibration signals collected from the current monitoring system have been used.

First, the autoregressive mapping of the overall levels measured in the machine for all the extended operating conditions has been carried out. Back-propagation neural network was applied for the mapping.

Second, the complex hydraulic phenomena that may occur in the extended operating range that can produce accelerated wear and tear have been studied. Typical phenomena are excessive turbulence, draft tube vortex rope, cavitation erosion, excessive vibration and excessive stresses in the runner.

For each of these abnormal operating conditions, several features (condition indicators) were selected and mapped on the operation hill-chart using neural networks. The consequences of each abnormal operation have been analyzed with physics-based models. With the mapping, the zones where operation is not recommended can be identified and the effects estimated.

1. Introduction

These years, new renewable energies (NREs) have been widely introduced into the energy grid due to their environmentally friendly and sustainable characteristics. However, with the entrance of NREs, the supply to the power grid has become random and hard to be regulated. As the only power system that can store a huge amount of energy [1], pump-turbines have to work in a wider range and switch the operation mode more frequently to respond to the demand from the grid. Both of these would cause the unit to operate far from the best efficient point (BEP).

In Fig. 1, the operating range of a turbine has been represented. In the working area, the efficiency is high and the operation is smooth. The energy generated depends on the head (H) and on the discharge, which depends on the guide vane opening (GVO). In extended operation, when the machine is working at extreme off-design conditions, the efficiency is reduced and strong excitation forces are generated. High levels of turbulence, cavitation and other phenomena may appear at some operating points. Damage would be induced by stress and great vibration when there's pressure pulsation and excessive turbulence on the machine [2–4]. Another typical phenomenon is a match between the pressure pulsations generated by cavitating vortex rope and one of the eigen frequencies of the hydraulic circuit, referred to as the hydraulic resonance. This might be detrimental to the stability of the power grid due to the hydraulic instability and power swing [5–9]. Although negative effect may be raised by the extended operation, utilities are demanding larger regulation capacity because this can always be translated into more revenues. A kind of advanced hydraulic turbine monitoring methodology needs to be developed so that the operation of the unit can be increased while being aware of the consequences on the machine (see Fig. 2).

Condition monitoring has already been applied for hydraulic machine protection for decades [1,10]. They are the foundation of

E-mail address: weiqiang.zhao@upc.edu (W. Zhao)

https://doi.org/10.1016/j.measurement.2020.107952
0263-2241/

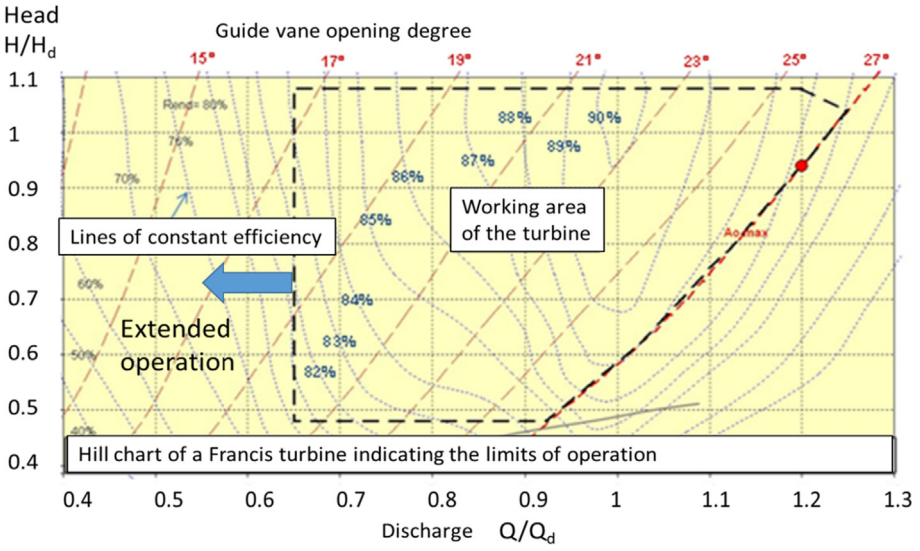

Fig. 1. Hill chart of a Francis turbine showing the working area and the extended operation zone.

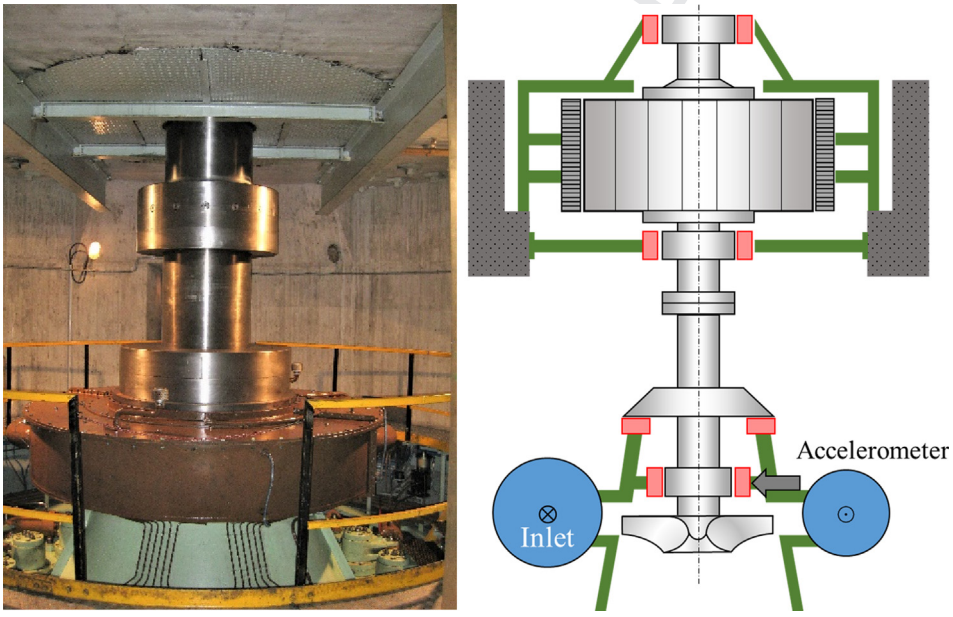

Fig. 2. Prototype of the measured pump-turbine unit and sketch map of the turbine unit.

remaining useful life prediction and programmed regulation of a pump-turbine unit. The signal feature extraction is critical to a monitoring system. In 2015, the PTs monitoring indicators' selection has been summarized by Egusquiza et al. [1] based on 15 years of monitoring several power plants. The type of the signal and measurement location also have great influence on the detection of different phenomena in a hydraulic turbine. In 2017, Presas et al. [11] introduced an optimized strategy for monitoring cavitation, RSI, etc. based on field test result with many sensors. In 2018, Egusquiza et al. [10] researched 28 different Pelton turbines before and after maintenance to detect the symptoms of damage and a theoretical model was built up to estimate the remaining life of the turbine. However, the methods above rely on expertise knowledge on the hydro turbine unit to a large extent and well-trained experts are required to be on the scene to carry out the analysis. It is imperative to develop an automatic recognition methodology to realize the self-diagnosis of the hydraulic turbine units.

Artificial intelligence (AI) is one of the most prevalent field and has been applied in condition monitoring. Schlenchtingen et al. [12] proposed an adaptive neuro-fuzzy-interference system model considering both wind speed and ambient inputs for power curve monitoring. Schlechtingen and Santos [13] compared the nonlinear neural network approaches and full signal reconstruction neural network with regression-based model approach for fault detection. Meik Schlechtingena, Ilmar Ferreira Santosb and Sofiane Achiche have developed normal behavior models of wind turbine monitoring system based on ANFIS model and predicted the error of wind turbine by fuzzy interference systems (FIS) [14,15]. While comparing with wind turbines, hydraulic turbines have lots of difference such as the structure, dynamic characteristic, excitation forces, etc. The abnormal condition in pump-turbines may come from hydraulic excitation forces, which would never happen on wind turbines. Hydraulic forces have to be considered in the hydraulic turbine monitoring and diagnosis. Saeed et al. [16] combined

Please cite this article as: W. Zhao, M. Egusquiza, C. Valero et al., On the use of artificial neural networks for condition monitoring of pump-turbines with extended operation, Measurement, https://doi.org/10.1016/j.measurement.2020.107952

numerical simulation and artificial neural networks to improve condition monitoring and fault diagnosis in Francis turbine. The recent research shows that neural networks have a better fault visibility and longer remaining operational period. However, current artificial intelligent monitoring and diagnosis on hydraulic turbines usually works well for a machine that always operates around BEP without generally considering the operating conditions. In an extended range, changes in vibration levels may be larger than the ones produced by damage which may induce misinformation. In [17] the same authors propose the preliminary ideas for a neural network-based monitoring method for pump-turbines that work in an extended range. As shown in that study, considering the influence of operating parameters on the vibration of the machine could improve the accuracy of condition monitoring. A deeper application of this methodology will be introduced in the present paper. Based on the vibration data acquired in the machine, several monitoring indicators related to different type of abnormal conditions and damage were selected from the expertise and physics-based models. First, mapping between operational conditions and condition indicators were learned by means of BP neural networks. Then the mappings in accordance with typical phenomena and different damage types are analyzed in detail. In the end, damage identification models considering the extended operating conditions are proposed.

2. System description

The existing monitoring system is mounted in a vertical PT unit with a maximum capacity of 85 MW and rated rotating speed of 500 rpm. The number of the blades in the runner is 7 and there are16 guide vanes in the distributor.

Radial acceleration on the turbine bearing, pressure in the draft tube and operating parameter (head and guide vane opening) are collected and sent to the remote diagnosis center by internet. The parameters of the accelerometer are listed in Table 1. The researched database includes 614 sets of signals with different working parameters within one month. The machine changed from pump to turbine operation and vice-versa over this period of time. In Fig. 3, the changes in the head and GVO of the turbine have been represented. In the same day, the head increased continually with pump operation and decreased in turbine operation and the GVO of the machine variated frequently from 20% to 100% power in order to adjust the output in the shortest possible time. It is important to be noticed that the machine operation was in regulation mode, varying the load to match the changing demand from the power grid. Head was also continually changing but at a much slower pace.

3. Vibration behavior analysis

It is known that the structure vibration is decided by the structure response and excitation forces. The change in the vibration is usually related with the variation of the excitation force or structure response which may be induced by damage on the component. This characteristic can be utilized for condition estimation on pump-turbines. By following the vibration indicators, the machine can be monitored and diagnosed. The indicators can be selected by analyzing the vibratory behavior of the turbine unit. Generally, the excitation forces of hydraulic turbine units are come from hydraulic, mechanical and electromagnetic origin [18].The mechanical origin excitation is mainly raised by the unbalance mass of the rotating structure. In our case, the frequency is $f_f = N/60 = 8.33$ Hz (N is the rotating speed in rpm). While the most important excitation in PTs is of hydraulic origin, generated by the rotor–stator interaction (RSI)[8]. RSI produces strong pressure pulsations that act on the periphery of the runner and increase with load. The frequencies of RSI equal to the blade passing frequency and its harmonics, determined by the number of blades z_b and rotating frequency f_f:

$$nf_b = n \cdot z_b \cdot f_f \tag{1}$$

In our case frequency excited by RSI are 58.33 Hz and its harmonics. Because of the fewer blades and higher rotating speed, PTs are suffering from more failure damage caused by RSI. Within part load, deep-part load and overload conditions, flow instabilities like vortex rope and turbulence can appear producing large vibration levels that may reach alarm or even trip thresholds, even though the machine has no damage. Cavitation vortex rope occurs when the turbine is at part load, generating strong pressure pulsations, shaft vibrations and torque fluctuation that can produce power swing. Another important excitation is produced by turbulence. Turbulence is generated in the runner and draft tube especially when the turbine is operating at deep part-load. This random excitation can produce large vibrations in all the machines. The rotor and runner natural frequencies are then excited generating strong vibrations. Erosive cavitation is another possible problem that may arise at some operating conditions, reducing the remaining useful life of the machine and have to be identified, as well as its effects on the machine components. For a PT unit which is operating in the extended condition, the intensity of excitations introduced above may increase significantly and cause failure damage on the structure.

A properly specified spectral alarm band is a critical tool to detect potentially serious problems in hydraulic turbines [1]. The band values of the spectrums from the system are used as the monitoring indicators and they are calculated according to Equation (2):

$$B = \sqrt{\sum \left(X_i \frac{c_E}{c_A}\right)^2} = 0.8165 \sum X_i^2 \tag{2}$$

where B is the RMS value of the frequency band; X_i is the amplitude of each line in the spectrum band; c_E and c_A are energy and amplitude correction factors of the window function respectively. In our

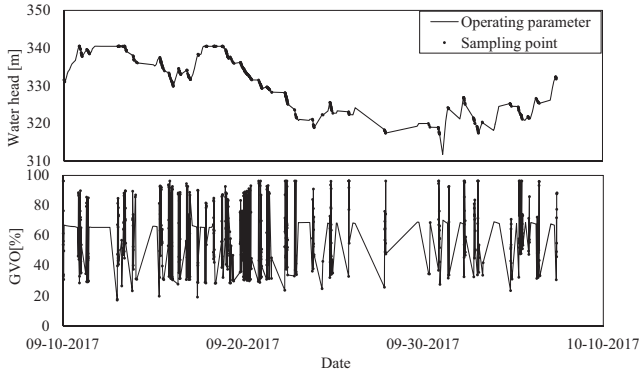

Fig. 3. Operating parameters of each sampling point.

Table 1
Characteristics of the accelerometer.

Specification	Value
Accelerometer type.	ICP Piezoelectric ceramic/ shear
Frequency range	1 Hz ~ 9 kHz
Sensitivity	100 mV/g ± 5%
Transverse sensitivity	<5%

Please cite this article as: W. Zhao, M. Egusquiza, C. Valero et al., On the use of artificial neural networks for condition monitoring of pump-turbines with extended operation, Measurement, https://doi.org/10.1016/j.measurement.2020.107952

case, Hann window is used as the window function so that c_E and c_A are 1.633 and 2.000 respectively.

4. Condition monitoring with ANN

According to previous studies, the variation of operating parameters such as head, guide vane opening and so on will modify the excitations like RSI, vortex rope, turbulence, etc. on the machine, changing the vibration level on the structure [19]. Artificial neural networks (ANN) were developed for machine learning by treating the computational parameters in a learning model with a manner similar to nervous system of human-beings. It hadn't attracted so much attention for decades until the turn of the century when big data has become available and computational power increased [20]. In these years, ANN has been reborn with a new label of "deep learning". Compared to linear regression models, NN based models have better performance on non-linear fitting, which would be suitable for feature learning for PTs because of the nonlinear relationships between the vibration characteristic and operating parameters of the machine. To evaluate and compare the vibration prediction performance of ANN and traditional fitting method, including scattered data interpolation, multivariate linear regression (MLR), local linear regression (LOWESS), 10-fold cross validation and predicted determination coefficient preR^2 are applied on each model. In the cross validation, all of the observations are divided into 10 parts. Each part in turn is removed and the model is refitted using the remaining observations. The process is repeated again and again until every observation is predicted and predicted only once. The preR^2 is determined by the mean squared error of each process:

$$preR^2 = \frac{PRESS}{SST} = \frac{\sum\left[\left(\hat{y}-\bar{y}\right)^2\right]}{\sum\left[\left(y-\bar{y}\right)^2\right]} \tag{3}$$

here y is the observation, $\hat{y}$ is the predicted value and $\bar{y}$ is the mean value of y. The $preR^2$ of one of the band values, the vortex rope band (B_v), are listed in Table 2 and it can be found that ANN model has the obviously highest prediction accuracy. The prediction result of each model is also shown in Fig. 4.

Neural networks will be used to improve the existing monitoring system of the power plant. With the data acquired, the NN will map the whole operating range of the machine with the overall vibration levels and with selected condition indicators able to identify abnormal operating conditions. The building-up process of the behavior model is described below.

4.1. Training data pre-processing

Before training the neural networks, the raw data has to be pre-processed like validity check, normalization, etc. One of the conditions for validity check is the data range checking. The samples whose head and GVO is out of the range introduced in Chapter 2 has to be removed. In addition, the consistency between input and output patterns has also been checked [13,21]. After the validity check, the outliners that have unexpected gradient or values were eliminated and finally 521 sets of raw monitoring data have been retained. 10% of the samples were selected as testing set to verify the effectiveness and accuracy of the neural network. While 10% of the data are used for improving the performance of the training by stopping the training process when the error begins to increase which indicates the network becomes overfitted. The remaining 80% of the data are used for training the networks. Each group of the input data is normalized into −1 to 1 before input into the networks, referred as data scaling. By data scaling the convergence speed of networks training would be raised because [-1, 1] is the most sensitive range for the sigmoid functions to the variables [21].

Table 2
Predicted determination coefficient of different models.

Model	$preR^2$
Scattered data interpolation	0.7755
MLR	0.4180
LOWESS	0.8063
ANN	0.8445

4.2. Parameters configuration for NNs

4.2.1. Network structure

The multi-layer perceptron (MLP) is selected as the topology structure of the model. As shown in Fig. 5, the typical structure of the MLP includes input layer, output layer and hidden layers. Theoretically, neural networks with one hidden layer are able of learning any mathematical function with sufficient training data [22]. However, there is no generally accepted equation to calculate the number of the layers and of neurons in the layers, which depend largely on the complexity of the functions. Optimum parameters of the neural networks have been obtained after performing several trials where the number of the layers and neurons are changed [23]. In each trial, the mean squared error (MSE) of the testing set was calculated by 10-fold cross validation. The MSE of vibration overall level predicted by different training parameters has been displayed in Fig. 6. Lower MSE indicates better performance of the NNs. Meanwhile, for the similar performance, fewer neurons and layers are preferred since too many neurons or layers may induce overfitting and require more time for computation [24]. For example, the single layer networks with 8 neurons has the best performance for the prediction of the vibration overall level on radial direction of the turbine bearing. The same process has been applied on all of the other vibration indicators.

4.2.2. Network initialization

The first step for any training runs of an MLP with the error back-propagation algorithm is the weight initialization. All of the weights in each layer have to be set to a small random number in the range of −0.01 to + 0.01[23]. It is important to perform multiple training runs with different random initializations in order to decrease the local minima effect of weight space. After several trials, the optimal network can be selected.

4.2.3. Training method

There are two types of learning method of neural networks, sequential learning (or "online learning", "online training") and batch learning (or "epoch learning", "epoch training"). In on-line training, weights and bias values are adjusted for every training sample based on the difference between computed outputs and the training data target outputs. While batch training the errors are accumulated over all training samples to give an aggregate set of deltas, and then applied to each weight and bias. In our case, batch learning is performed for the beginning to accelerate the training speed.

For the training algorithm, Levenberg-Marquardt (LM) back-propagation function is applied. This training method has a fast speed on the middle-sized feedforward neural networks' learning. While its weakness is it requires more computation space than the other algorithms. In LM algorithm, a damping factor λ has been added into the Gauss–Newton algorithm:

$$x_{k+1} = x_k + \left[J^T J + \lambda I\right]^{-1} J^T e \tag{4}$$

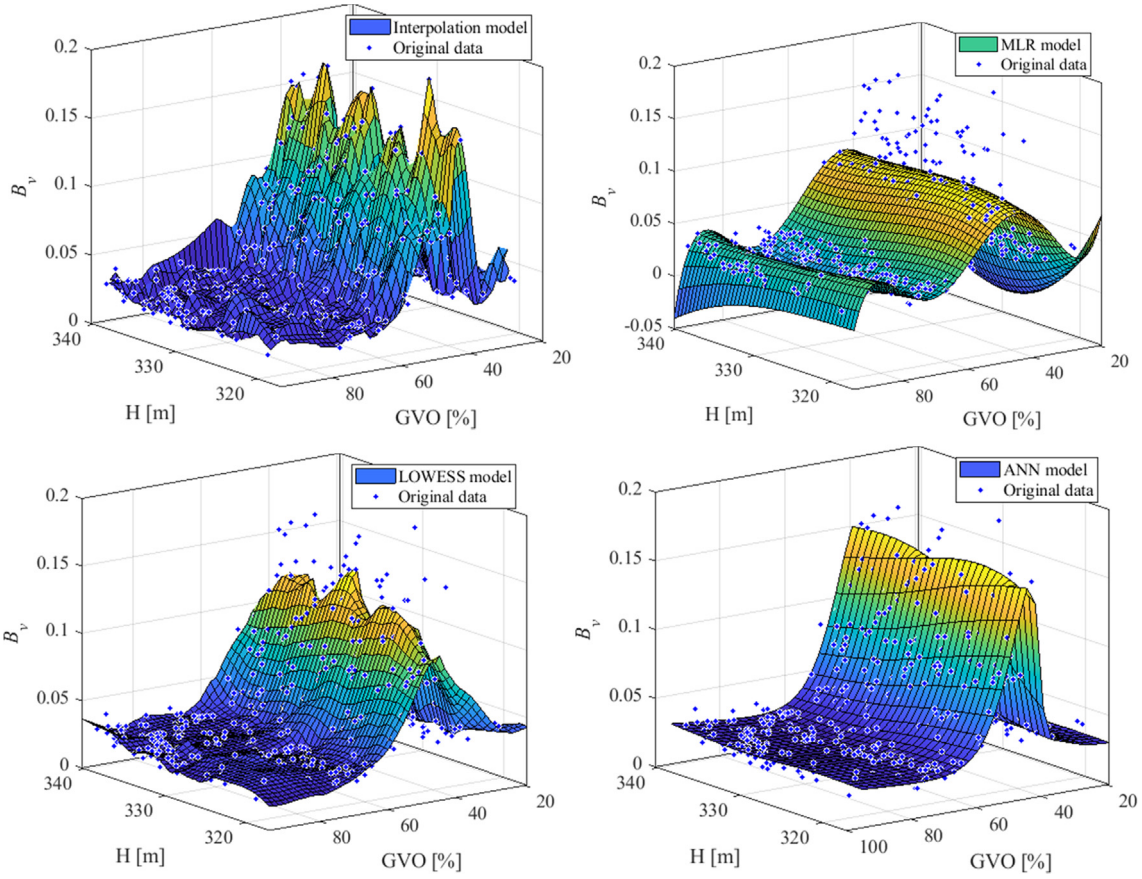

Fig. 4. Vibration prediction result of (a) LOWESS model, (b) MLR model, (c) Interpolation model and (d) ANN model.

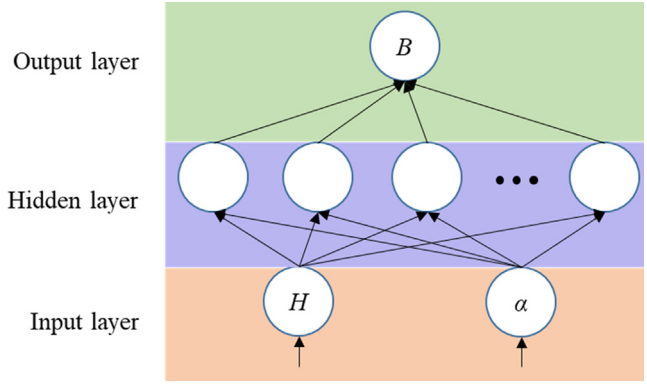

Fig. 5. Feed-forward network architecture.

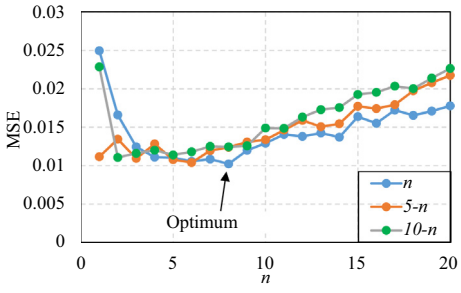

Fig. 6. MSE of indicator predicted by neural networks with different parameters (the format of the legend is the number of neurons in each layer. For example, the "5-n" means the number of neurons in the first and second layer are 5 and n respectively. The configuration with the best performance is marked with a triangle). The overall level is used as an example, the networks for the other indicators are modified with the same process.

where, J represents a Jacobian matrix which contains first derivatives of the output errors with respect to the weights and biases of the network, I represents the identity matrix and e denotes a vector of output errors. The outstand feature of this algorithm is the coefficient λ is able to adjust itself: with the learning proceed, λ decreases, which makes the algorithm closer to Gauss–Newton algorithm which has a higher accuracy on approximation [17,25].

5. Result and discussion

In Fig. 7, the overall vibration levels B_{OL} measured in turbine bearing are represented for all the extended operating conditions in terms of head and GVO (power). This figure shows the PT normal behavior model in terms of B_{OL}. Table 3 shows the main parameter of the networks for B_{OL} and its prediction performance. The accelerators of the standard monitoring system are robust enough so that the system is conceivable in the long term without calibration. The normal behavior model of the PT reflects the characteristics of the turbine unit. Once the normal behavior models have been determined, it would change only if damage takes place in the machine. Therefore, the models can be used for the abnormal condition detection. What's more, the change on different normal behavior model implies different types of damage, which can be used for the damage diagnosis.

It is interesting to see that the maximum vibration levels have an important increase when the turbine is operating in the

Please cite this article as: W. Zhao, M. Egusquiza, C. Valero et al., On the use of artificial neural networks for condition monitoring of pump-turbines with extended operation, Measurement, https://doi.org/10.1016/j.measurement.2020.107952

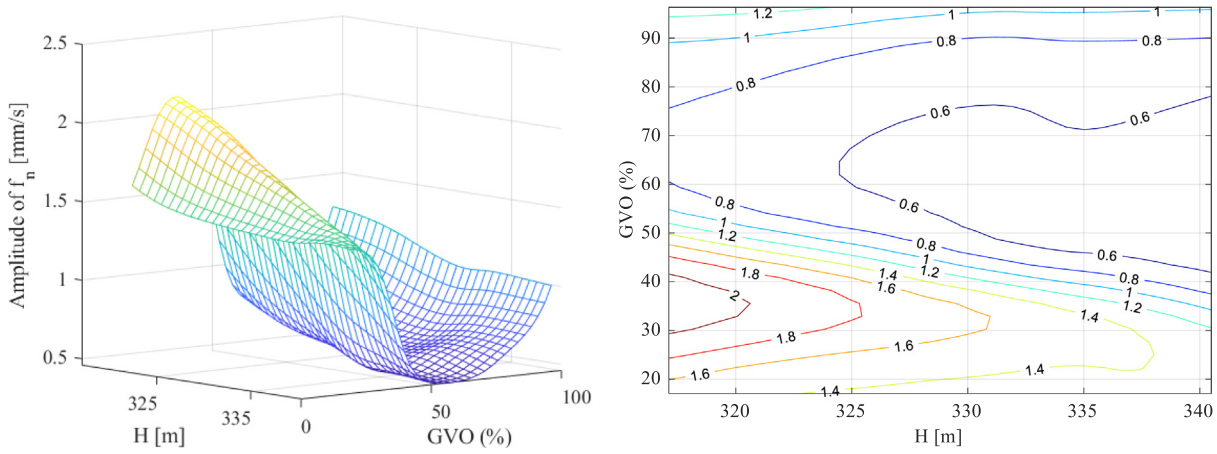

Fig. 7. Overall level B_{OL} changing with operating parameters [17].

Table 3
Configuration and performance of the B_{OL} NN model.

Parameters/ performance	B_{OL}
Number of neurons in the hidden layer	8
Learning rate	0.00005
Number of training epochs	69
predR^2	0.9632

extended operating range. The increase is maximum at the lowest head with a GVO of 30–40%, with higher values than the recommended by Standards for continuous operation. This information can be used for selecting an alarm threshold adapted to this variation and to identify the conditions that produce the maximum vibration levels. Anyway, abnormal operation and incipient damage may not produce important changes on the overall levels and remain hidden until large damage occurs [26]. In an abnormal behavior condition, the pump-turbine can operate over a certain period of time without any damage while it is suffering from strong excitation forces which make it more prone to have damages or affect the stability of the supply to the power grid. Therefore, an accurate identification of the abnormal behavior is essential for the generation stability and plant safety.

5.1. Identification of vortex rope

Part load vortex rope is one of the most studied dynamic problems in hydro turbines. A vortex rope is formed by a helical cavitation core in the draft tube with a precession frequency of about 0.25–0.35 times the rotating speed of the runner (Fig. 8 left). The vortex rope may induce strong pressure fluctuations at the rope precession frequency, which can be decomposed into two components: a rotating one under the runner and an axial one [27]. When there is a resonance with the hydraulic system, the amplitude of the pressure pulsation is amplified, affecting the stability of the machine operation. Large pressure pulsations may affect the dynamic behavior of the runner and the mechanical torque of the shaft, causing important power swing to the output of the hydraulic unit. Power swing is dangerous for the stability of the power grid and it has to be avoided during turbine mode operation.

As shown in Fig. 8 right, the root mean square (RMS) value of frequency band $0.25 \sim 0.35 f_f$ is selected as the condition indicator of vortex rope.

The network for vortex rope (B_v) has been built according to Table 4. The band values map of B_v of all of the operating conditions is shown in Fig. 9 (left). According to the figure, the highest value of the band appears at $35 \sim 45\%$ guide vane opening, which indicates there is a cavitation vortex rope in this area. From the contour map it can be seen that the peak value appears at lower guide vane openings with the increase of the head. The resonance between pressure pulsation and natural frequencies of the hydrau-

Table 4
Configuration and performance of the B_v NN model.

Parameters/performance	B_v
Number of neurons in the hidden layer	5
Learning rate	0.00005
Number of training epochs	78
predR^2	0.9721

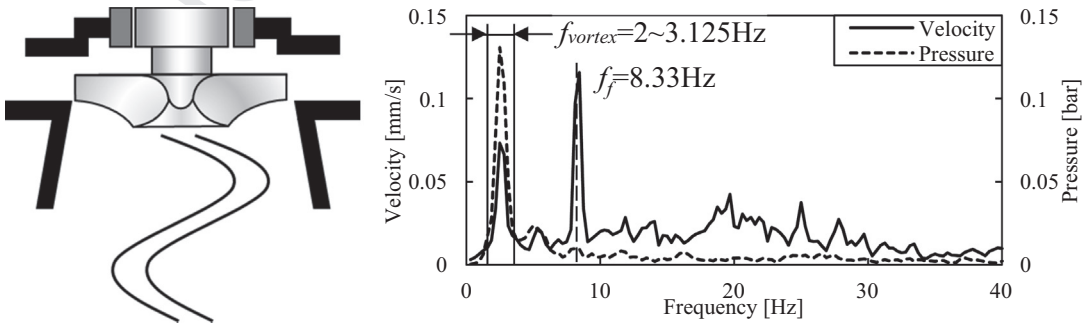

Fig. 8. Left: Vortex rope in the draft tube; Right: Pressure pulsation in the draft tube (denoted in dotted line) and vibration in turbine bearing (in solid line) under vortex rope excitation and spectral band selection for vortex rope.

Please cite this article as: W. Zhao, M. Egusquiza, C. Valero et al., On the use of artificial neural networks for condition monitoring of pump-turbines with extended operation, Measurement, https://doi.org/10.1016/j.measurement.2020.107952

lic circuit may lead to Part Load Instability like power swing [28], so it has to be avoided during operation. Training the NNs on the variation trend of the vortex rope, the abnormal behavior region can be identified systematically. From the figure it can be seen that around BEP, the vortex rope maintains a fairly low level of 0.25 mm/s. Because of the vortex break-down, the strength of vortex is also low (about 0.3 mm/s) under deep low load condition. The vortex level indicator shows a clear peak at high level (see Fig. 10 and Table 5).

Once the zone with vortex rope is detected, the next step is to determine the effect on the machine components. The rotating pressure field under the runner increases the turbine bearing vibration, thus reducing its useful life. The axial pressure fluctuations that propagate through the hydraulic system affect the piping and generate power swing and high vibration levels in the turbine and axial thrust bearing. In Fig. 8, the pressure fluctuation in the draft tube is shown, as well as the turbine bearing vibration. The band levels of vortex rope and pressure pulsation B_p of both vibration and pressure pulsation have been calculated according to Equation (4) and compared in Fig. 11. It can be found that B_p has a positive correlation with vibration level in the whole operating range and the correlation coefficient between them is 0.87, which implies that the turbine bearing is an ideal position for vortex rope monitoring. With this information the severity of operation under the cavitation vortex rope can be assessed and the threshold level selected.

Table 5
Configuration and performance of the B_c NN model.

Parameters/ performance	B_c
Number of neurons in the hidden layer	12
Learning rate	0.00005
Number of training epochs	54
$predR^2$	0.9636

5.2. Identification of erosive cavitation

Another important abnormal behavior in hydraulic turbines is erosive cavitation, which erodes the unit components, increases maintenance costs and reduces the remaining useful life of the runner severely. In Fig. 12, a picture of the eroded area provoked by cavitation is shown. The cavitation damage is repaired by welding and takes some time, reducing the operating time of the units. Although many techniques for detecting cavitation already exist [29], the effective detection in prototypes is a very complex problem. According to relevant literature, the best type of sensor to detect erosive cavitation should be an acoustic emission sensor located on the rotating shaft [30]. However, in the monitoring system installed on the turbine unit, only accelerometers located in the stationary parts are available. For the detection of erosive cavitation, the high-frequency vibrations produced by the impact of the cavitation bubbles on the runner surfaces have to be identified.

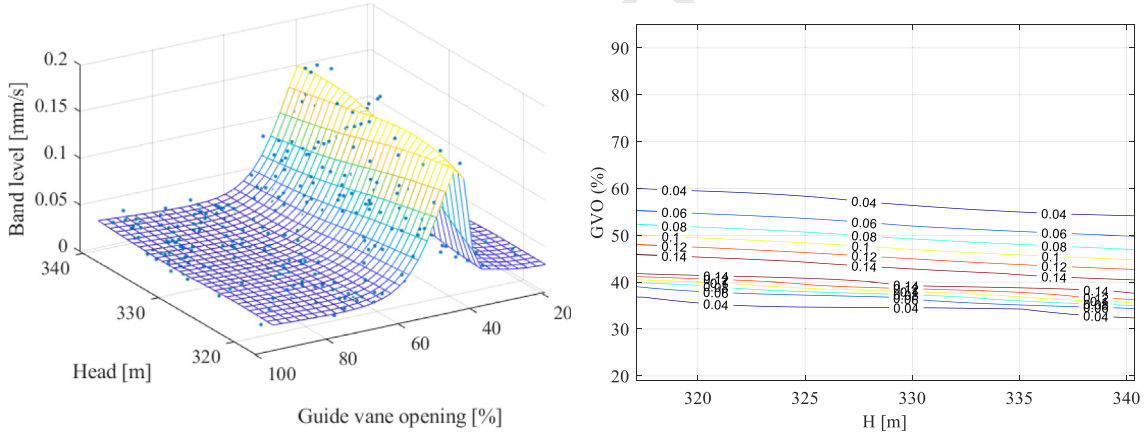

Fig. 9. Left: B_v under different operating parameters (head and GVO). The variation of band value is fitted by a 3-layer BP-neural network with 6 perceptrons in the hidden layer. Right: contour map of B_v.

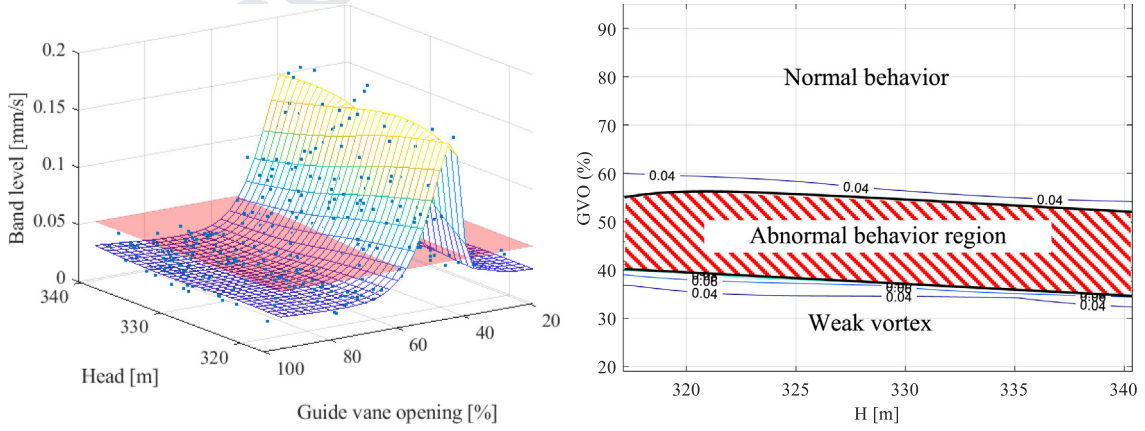

Fig. 10. Identification of vortex rope.

Please cite this article as: W. Zhao, M. Egusquiza, C. Valero et al., On the use of artificial neural networks for condition monitoring of pump-turbines with extended operation, Measurement, https://doi.org/10.1016/j.measurement.2020.107952

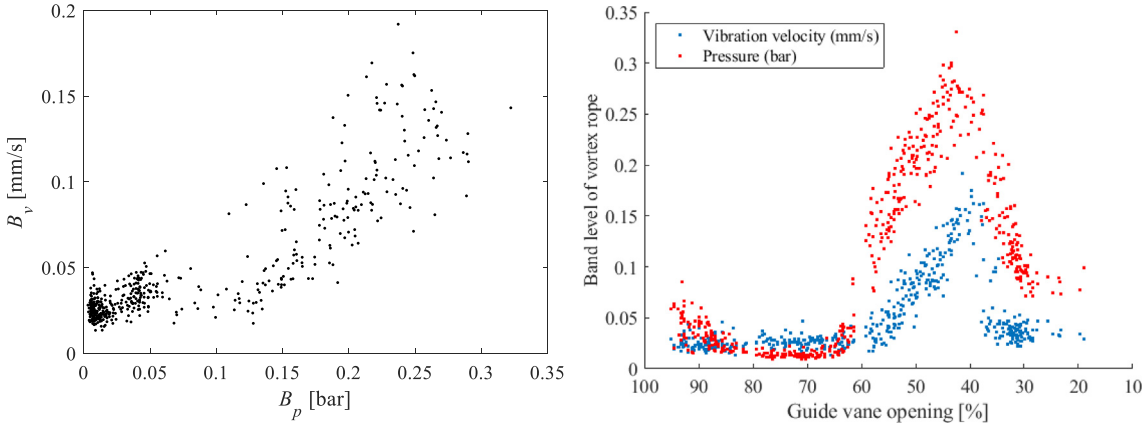

Fig. 11. Left: Variation of B_p versus B_v; Right Variation of B_p and B_v versus guide vane opening.

Fig. 12. Cavitation damage in a turbine blade.

The high-frequency acceleration signal from the turbine bearing was used for detecting the erosive cavitation in the runner.

Although there is not an exact rule for the accurate definition of the cavitation band, the high-frequency band is considered the main indicator for cavitation [31]. Transmissibility tests of high-frequency vibration from eroded areas to the measuring position are able to determine the best band for the cavitation control.

A spectrum comparison between high head and low head is shown in Fig. 13, where the high-frequency band (800–1000 Hz) shows a large difference between both operating conditions. The band has a higher amplitude when the draft tube pressure decreases and this occurs when the head increases. The RMS value of the band 800–1000 Hz is selected as the erosive cavitation indicator. The indicator values of high-frequency band (B_c) of all of the operating conditions are shown in Fig. 14. According to the figure, the band value goes up with the increase of the head. The highest value appears at high head, middle load, which indicates there might be strong cavitation in this area. From the contour map it can be found that for the same guide vane opening, the cavitation strength is stronger at high head. While for the same head, the peak value appears at middle-low load and the lowest level appears at high load. The change of the band level B_c maybe is caused by turbulence, which also has the same trend. To identify the abnormal behavior region systematically, a threshold of 0.15 mm/s is set as shown in Fig. 14. Within the abnormal region,

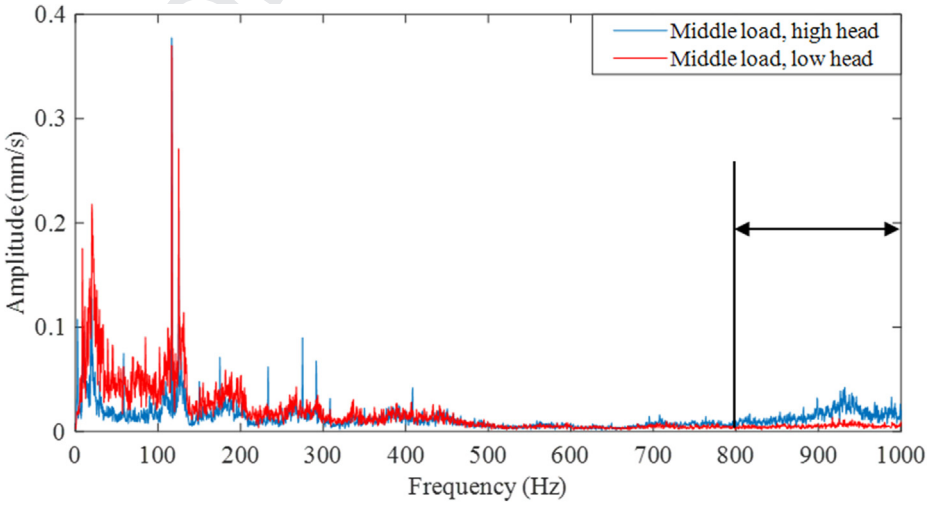

Fig. 13. Frequency spectrum comparison between high head and low head.

Please cite this article as: W. Zhao, M. Egusquiza, C. Valero et al., On the use of artificial neural networks for condition monitoring of pump-turbines with extended operation, Measurement, https://doi.org/10.1016/j.measurement.2020.107952

the runner is suffering cavitation erosion and the operation time has to be decided according to the balance between revenues and maintenance costs.

5.3. Damage and failure identification

5.3.1. Monitoring of excessive vibration on the runner

Another situation to be avoided in PT is the breakage of the runner by fatigue. Because of the special design, the pressure fluctuation induced by RSI in PTs is very strong [2–4]. The interference between the moving blades and the stationary wicket gates generates a periodic pressure fluctuation along the periphery of the runner. The frequencies of RSI depend on the rotating speed and the number of blades and vanes, while its amplitudes are determined by the operating parameters and the design of the machine. RSI is the main excitation for PT runners and high head Francis turbines working at high loads and close to the BEP [32] and therefore has to be considered for fatigue analysis. Fig. 15 and Table 6 show the mapping of the band level of RSI (B_{RSI}) for the analyzed runner and its configuration. The worst conditions can be seen in this figure. For the exact evaluation of the effects of the RSI on the runner, generally a stress calculation combined with fatigue analysis has to be performed [32–34] (see Table 7).

Fig. 16 left shows the typical peripheric deformations of the runner caused by the RSI excitation. Such deformations have associated high stress concentration and therefore some cracks have been found in the past in these areas as shown in Fig. 16 right. Similar cracks and failures in PT runners caused by RSI have been reported [8].

Many times, these cracks remain unnoticed before the runner has a critical failure causing important economic consequences [26,35]. As stated by the Paris Law [36], the growth of the crack is very slow for most of its growing life and only after the onset of the high cycle fatigue [26] the growth rate of the crack dramatically increases as seen in Fig. 17. Because of this growth behavior, the detection of cracks before the onset of high cycle fatigue is a critical and also a challenging task.

Table 6
Configuration and performance of the B_{RSI} NN model.

Parameters/performance	B_{RSI}
Number of neurons in the hidden layer	6
Learning rate	0.00005
Number of training epochs	106
$predR^2$	0.9400

Table 7
Configuration and performance of the B_f and B_n NN model.

Parameters/performance	B_f	B_n
Number of neurons in the hidden layer	6	8
Learning rate	0.00005	0.00005
Number of training epochs	58	68
$predR^2$	0.9744	0.9651

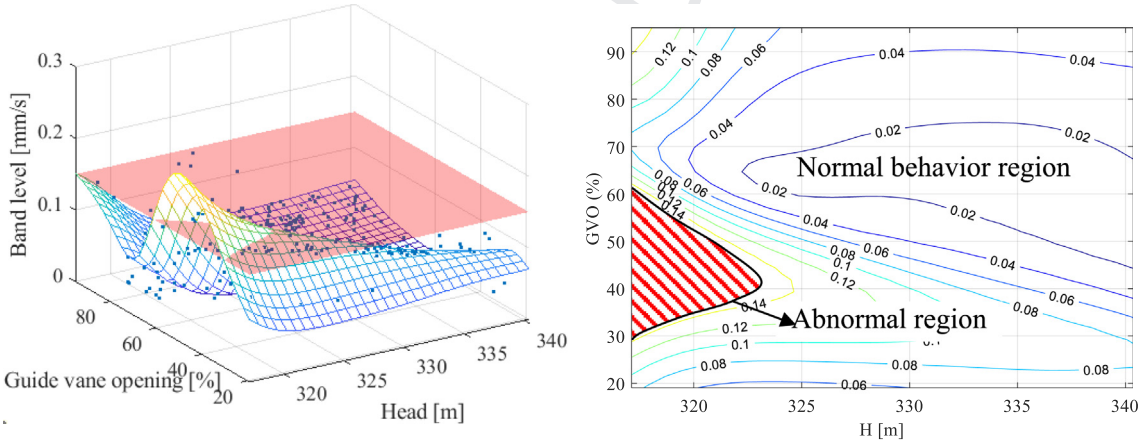

Fig. 14. Cavitation threshold setting and the abnormal behavior region.

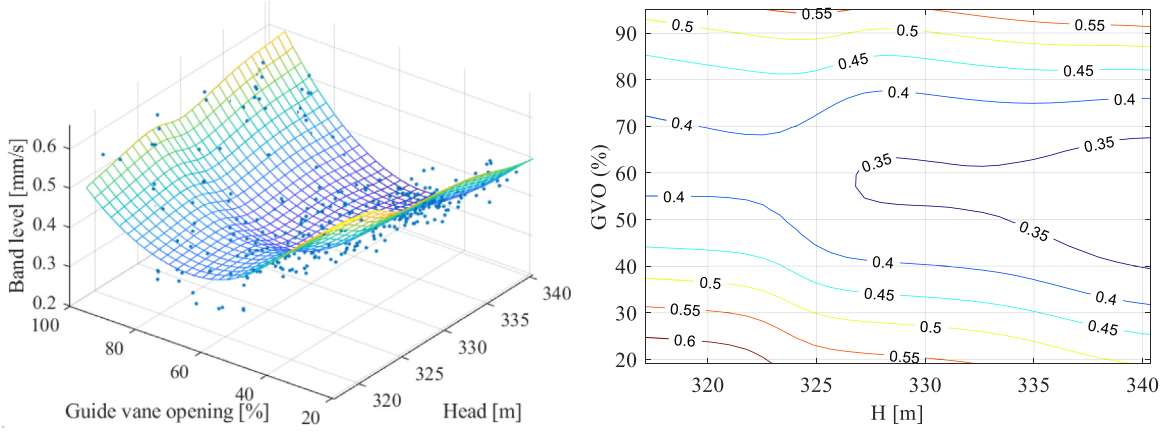

Fig. 15. Mapping of the B_{RSI} (Spectral band of twice blade passing frequency).

Please cite this article as: W. Zhao, M. Egusquiza, C. Valero et al., On the use of artificial neural networks for condition monitoring of pump-turbines with extended operation, Measurement, https://doi.org/10.1016/j.measurement.2020.107952

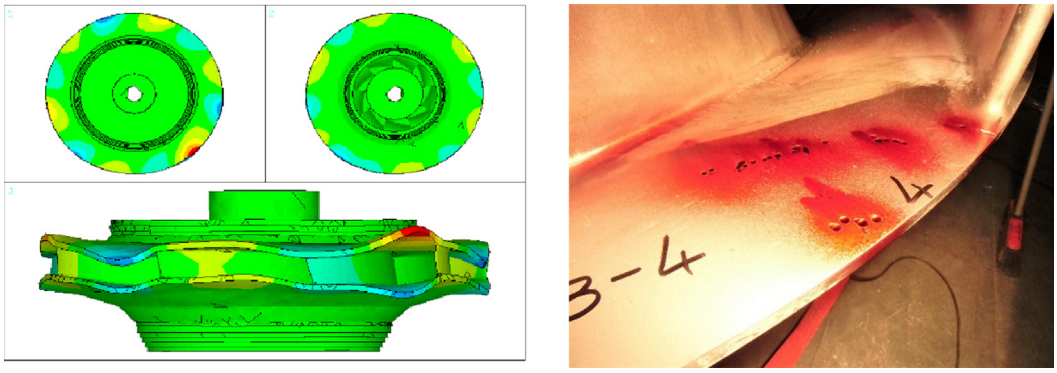

Fig. 16. Left: Deformations in a pump-turbine runner produced by RSI; Right: Cracks in a runner generated by excessive RSI.

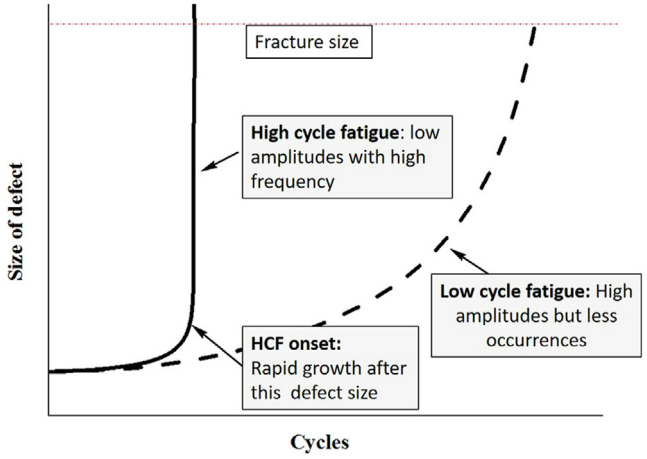

Fig. 17. Typical growth of a crack due to high cycle fatigue [37].

5.3.2. Monitoring of damage

Generally, damage has influences on both the excitations and the dynamic response of the machine. Following the bands levels of specific excitation forces and natural frequencies is useful for improving the accuracy in damage diagnosis. Properly specified spectral alarm bands are probably one of the most efficient ways for detecting potentially serious problems in the machine.

The procedure for specifying meaningful spectral alarm bands comes from the understanding of the excitation forces that occur during machine operation and how they relate to the machine rotating speed. In this paper, the rotating frequency and one of the natural frequencies of the pump-turbine are selected as examples for illustrating the proposed method. The bands to be created and followed are indicated in Fig. 18.

One of the most characteristics is a band around the rotating speed. The rotating frequency of the turbine is constant to keep the frequency and phase of the output stable. Therefore, the spectrum band of rotating frequency can be very narrow. The RMS value of frequency band 8.4375 ± 0.625 Hz is selected as the indicator of rotating frequency B_f. As shown in Fig. 19, the B_f changes significantly with the guide vane opening. The lowest level appears around BEP and then goes up with the increase of the guide vane opening, which is mainly caused by the hydraulic unbalance. There are many typical damages in hydraulic turbines related to the vibration amplitude of rotating frequency, such as runner blockage, broken parts, etc. [1,9]. When related damage emerges, the amplitude of rotating frequency increases [38,39]. Therefore, by setting vibration level thresholds, the type and extent of damage can be detected automatically. In PT, sudden changes in the unbalance force have to be detected as soon as possible because they can be the consequence of fatigue. If unnoticed, they can produce catastrophic damage in a short time.

Other types of damage cause the variation in the structural response of a machine (natural frequencies), which can also be reflected in the vibration signature. For instance, changes in bearing stiffness due to excessive bearing wear or grouting problems can modify the natural frequencies of the rotor. Fig. 19 b represents the band value B_n of one of the rotor natural frequencies. It can be

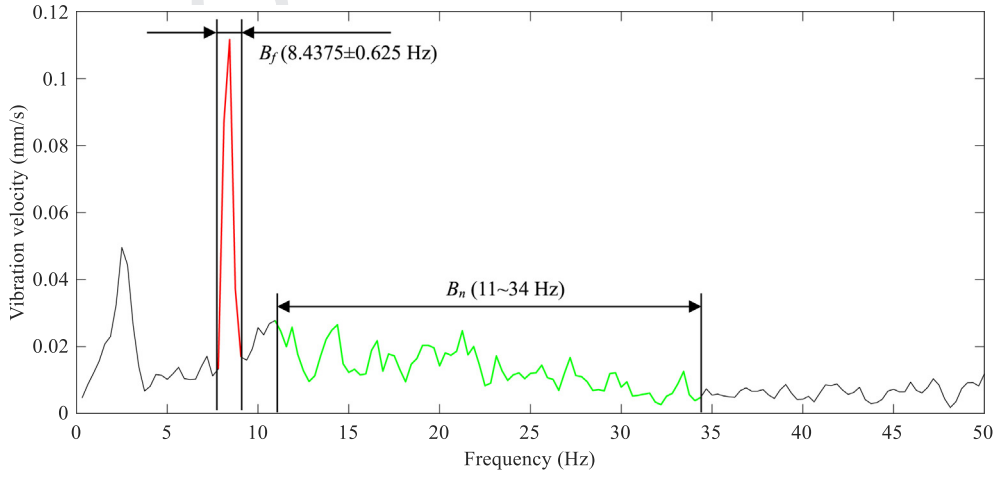

Fig. 18. Band selection of rotating frequency B_f and one of the natural frequencies B_n.

Please cite this article as: W. Zhao, M. Egusquiza, C. Valero et al., On the use of artificial neural networks for condition monitoring of pump-turbines with extended operation, Measurement, https://doi.org/10.1016/j.measurement.2020.107952

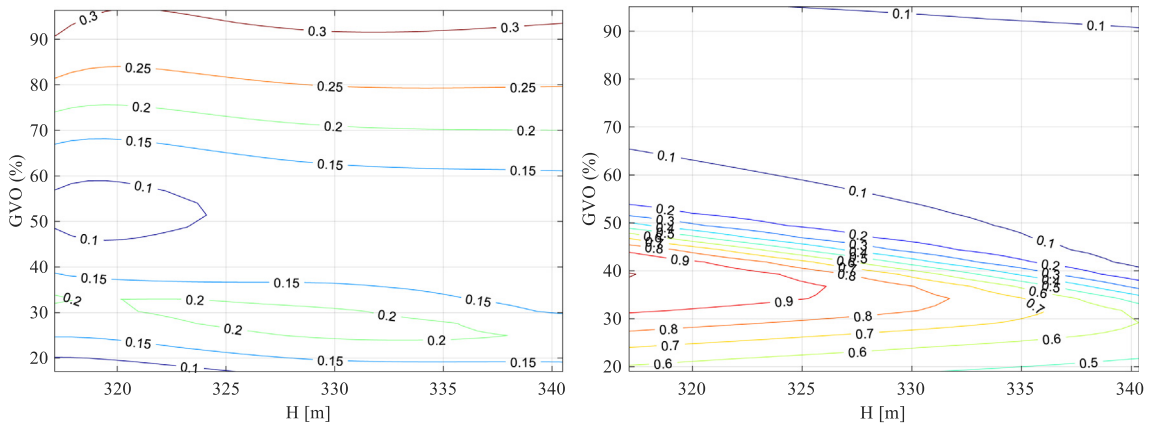

Fig. 19. Mapping of the rotating frequency (left) and one of the natural frequencies of the rotor (right).

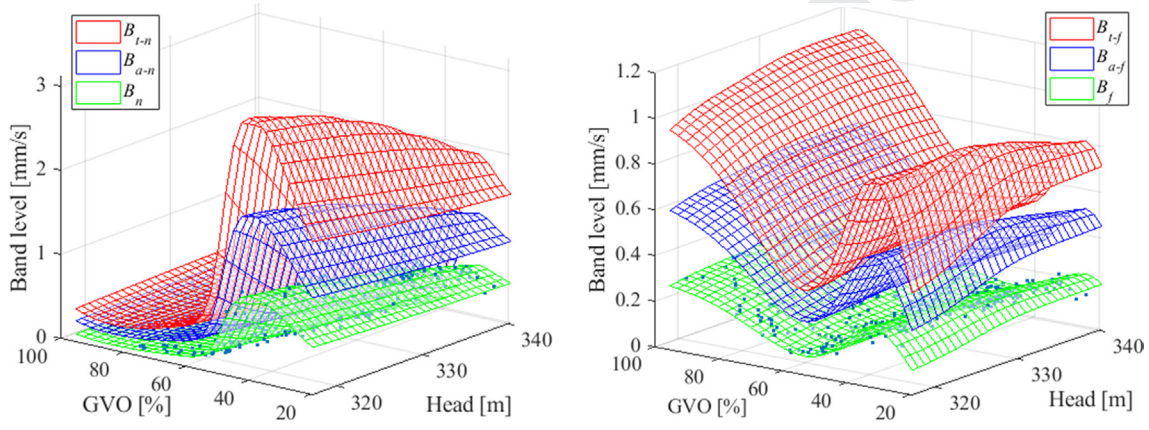

Fig. 20. Alarm and trip thresholds of the rotating speed B_f and natural frequency B_n.

found that B_n has a high value at low load and decreases to almost zero with the load increased to the rated load. This is because natural frequencies are mainly excited by turbulence, which is stronger at low load.

5.3.3. Identification of excessive vibration and damage

For the overall levels, the ISO 20816–5 can be used to select the alarm and trip threshold levels. The Standard recommendations are of 1.9 and 3 mm/s RMS [40]. For the band values, their alarm threshold B_a and trip threshold B_t are defined as:

$$B_a = 1.9 \times (B_i + CI) \quad (5)$$

$$B_t = 3 \times (B_i + CI) \quad (6)$$

where B_a and B_t are the alarm and trip threshold respectively; B_i is the value of the condition indicator under healthy condition; CI is the 95% confidence interval of the measured band values. The two alarm values of B_f and B_n are shown in Fig. 20. Beside these two examples, more vibration indicators like f_b or other natural frequencies can be processed and followed by the proposed method.

6. Conclusions and outlook

In this paper, a monitoring procedure based on the application of Neural Networks (NN) has been developed to deal with the effects of extending the operating conditions of a Pump-turbine (PT).

First, the vibration of the machine was measured from the bearings over a period of time at different operating conditions. The machine worked in pump and in turbine mode for an extended operating range, from 20 to 100% load. Based on the collected data, a single-layer neural network was used to build a mapping of the overall vibration levels of the PT for all the extended operating conditions of the head and discharge. The mapping showed that the vibration of the PT soars when working far from the BEP, especially at low loads. The maximum levels appear at heads lower than 320 m in the opening range 30–40% GVO. Overall values exceed the standard recommendation, so this operating condition should be avoided.

In order to determine how the rise in vibration affects the RUL of the machine components, the main dynamic problems that take place off-design have been listed and their detection from the vibration spectra described. With this information, the frequency bands containing the symptoms of every phenomenon have been defined as condition indicators. Using the same NN procedure, mapping has been created for every indicator over the extended operating range of the PT. Every abnormal operating condition can thus be associated with a range of H and GVO, and the vibration levels can be related to the degradation of certain machine components.

The first indicator was defined to detect the vortex rope. The vortex rope generates large pressure pulsations that can damage the machine and produce power swing. Operation with a strong vortex rope can be considered abnormal because it can impair the operation of the turbine. Although the vibration levels gener-

Please cite this article as: W. Zhao, M. Egusquiza, C. Valero et al., On the use of artificial neural networks for condition monitoring of pump-turbines with extended operation, Measurement, https://doi.org/10.1016/j.measurement.2020.107952

ated by this phenomenon in the bearing are not large, the effects have to be checked with other parameters, like the pressure pulsation and the power swing. The feature selected for the identification of the vortex rope is a frequency band around the precession frequency of 0.25–0.35f_f. In the mapping, the zone between 35 and 45% of the GVO stands out and shows the maximum amplitude at the highest head. Under these conditions, the power swing is excessive.

Another typical problem is cavitation erosion, which increases maintenance works. Erosive cavitation generates high-frequency vibration that is transmitted to the bearings. For its detection, a high-frequency vibration band was selected as an indicator. The operating conditions where erosion occurs are 30–40% GVO and at the lowest head.

Finally, another dangerous situation in PT is produced by strong RSI excitation, which leads to large vibrations in the runner and, therefore, to fatigue problems. In this case, the chosen indicator was the RSI amplitude. The mapping of the RSI excitation shows that the maximum vibration occurs at maximum load and at the highest heads.

Regarding all this information, the worst operating conditions take place at the minimum head with loads of 30–40% and at the maximum head with loads 30–40% and 90–100%. The operation of the machine should be restricted although the effects on the RUL have to be calculated.

About damage detection, the alarm and trip thresholds have to be determined experimentally. Fatigue damage in the runner can produce destruction of one part of the runner what generates an increase in the unbalance force that can be small. Therefore, rapid detection of an increase in f_f can avoid catastrophic damage. Finally, damage can produce a change in amplitude of the natural frequencies of the rotor, therefore the mapping of them is also convenient. For the moment, the monitoring data is based on the steady conditions, the condition monitoring under transient condition would be interesting and might be achieved with the monitoring bigdata accumulation.

Declaration of Competing Interest

The authors declare that they have no known competing financial interests or personal relationships that could have appeared to influence the work reported in this paper.

Acknowledgments

The authors want acknowledge the XFLEX HYDRO project (EU H2020 No. 857832). Weiqiang Zhao would like to acknowledge the China Scholarship Council (CSC) for its grants. Alexandre Presas wants to acknowledge the Serra Hunter program of Generalitat de Catalunya.

References

[1] E. Egusquiza, C. Valero, D. Valentin, A. Presas, C.G. Rodriguez, Condition monitoring of pump-turbines. New challenges, Measurement 67 (2015) 151–163, https://doi.org/10.1016/j.measurement.2015.01.004.
[2] P. Dörfler, M. Sick, A. Coutu, Flow-induced pulsation and vibration in hydroelectric machinery: engineer's guidebook for planning, design and troubleshooting, Springer Science & Business Media, 2012.
[3] M. Nishi, S. Matsunaga, M. Okamoto, K. Takatsu, Wall pressure measurements as a diagnosis of draft tube surge, in: Proc. 15th IAHR Symp. Hydraul. Mach. Cavitation, Belgrade, Serbia, 1990.
[4] F. Avellan, Flow investigation in a Francis draft tube: the FLINDT project, in: Proc. 20th IAHR Symp. Hydraul. Mach. Syst., Charlotte (NC), 2000.
[5] S. Alligné, P. Maruzewski, T. Dinh, B. Wang, A. Fedorov, J. Iosfin, F. Avellan, Prediction of a Francis turbine prototype full load instability from investigations on the reduced scale model, in: IOP Conf. Ser. Earth Environ. Sci., IOP Publishing, 2010, p. 12025.
[6] E. Egusquiza, D. Valentín, A. Presas, C. Valero, Overview of the experimental tests in prototype, in: J. Phys. Conf. Ser., IOP Publishing, 2017, p. 12037.
[7] D. Valentin, A. Presas, M. Egusquiza Montagut, C. Valero, E. Egusquiza, Behavior of Francis turbines at part load. Field assessment in prototype: Effects on power swing, (2019). http://doi.org/10.1088/1755-1315/240/6/062012.
[8] E. Egusquiza, C. Valero, X. Huang, E. Jou, A. Guardo, C. Rodriguez, Failure investigation of a large pump-turbine runner, Eng. Fail. Anal. 23 (2012) 27–34, https://doi.org/10.1016/j.engfailanal.2012.01.012.
[9] E. Egusquiza, C. Valero, A. Estévez, A. Guardo, M. Coussirat, Failures due to ingested bodies in hydraulic turbines, Eng. Fail. Anal. 18 (2011) 464–473, https://doi.org/10.1016/j.engfailanal.2010.09.039.
[10] M. Egusquiza, E. Egusquiza, C. Valero, A. Presas, D. Valentín, M. Bossio, Advanced condition monitoring of Pelton turbines, Measurement 119 (2018) 46–55, https://doi.org/10.1016/j.measurement.2018.01.030.
[11] A. Presas, D. Valentin, M. Egusquiza Montagut, M. Bossio, E. Egusquiza, C. Valero, Optimized Use of Sensors to Detect Critical Full Load Instability in Large Hydraulic, Turbines (2017), https://doi.org/10.3390/proceedings1080822.
[12] M. Schlechtingen, I.F. Santos, S. Achiche, Using data-mining approaches for wind turbine power curve monitoring: a comparative study, IEEE Trans. Sustain. Energy. 4 (2013) 671–679.
[13] M. Schlechtingen, I.F. Santos, Comparative analysis of neural network and regression based condition monitoring approaches for wind turbine fault detection, Mech. Syst. Signal Process. 25 (2011) 1849–1875.
[14] M. Schlechtingen, I.F. Santos, S. Achiche, Wind turbine condition monitoring based on SCADA data using normal behavior models. Part 1: System description, Appl. Soft Comput. 13 (2013) 259–270.
[15] M. Schlechtingen, I.F. Santos, Wind turbine condition monitoring based on SCADA data using normal behavior models. Part 2: Application examples, Appl. Soft Comput. 14 (2014) 447–460.
[16] R.A. Saeed, A.N. Galybin, V. Popov, 3D fluid–structure modelling and vibration analysis for fault diagnosis of Francis turbine using multiple ANN and multiple ANFIS, Mech. Syst. Signal Process. 34 (2013) 259–276, https://doi.org/10.1016/j.ymssp.2012.08.004.
[17] W. Zhao, E. Egusquiza, C. Valero, M. Egusquiza, D. Valentín, A. Presas, A Novel Condition Monitoring Methodology Based on Neural Network of Pump-Turbines with Extended Operating Range, in: 16th IMEKO TC10 Conf., Berlin, 2019, p. 4.
[18] E.E. Estévez, E. UPC, Comportament dinàmic de màquines hidràuliques, Edicions UPC, Barcelona, 2003.
[19] C. Valero, M. Egusquiza, E. Egusquiza, A. Presas, D. Valentin, M. Bossio, Extension of Operating Range in Pump-Turbines. Influence of Head and Load, Energies 10 (2017) 2178.
[20] C.C. Aggarwal, Neural Networks and Deep Learning: A Textbook, Springer International Publishing AG, Yorktown Heights, 2018.
[21] M.Y. Rafiq, G. Bugmann, D.J. Easterbrook, Neural network design for engineering applications, Comput. Struct. 79 (2001) 1541–1552.
[22] A.T. Goh, Some civil engineering applications of neural networks, Proc. Inst. Civ. Eng. - Struct. Build. 104 (1994) 463–469, https://doi.org/10.1680/istbu.1994.27204.
[23] L. Tarassenko, Guide to neural computing applications, Elsevier, 1998.
[24] K.G. Sheela, S.N. Deepa, Review on methods to fix number of hidden neurons in neural networks, Math. Probl. Eng. 2013 (2013).
[25] K. Madsen, H.B. Nielsen, O. Tingleff, Methods for non-linear least squares problems, (1999).
[26] M. Gagnon, S.A. Tahan, P. Bocher, D. Thibault, The role of high cycle fatigue (HCF) onset in Francis runner reliability, in: IOP Conf. Ser. Earth Environ. Sci., IOP Publishing, 2012, p. 22005.
[27] F. Duparchy, A. Favrel, P.Y. Lowys, C. Landry, A. Müller, K. Yamamoto, F. Avellan, Analysis of the part load helical vortex rope of a Francis turbine using on-board sensors, in: J. Phys. Conf. Ser., IOP Publishing, 2015, p. 12061.
[28] D. Valentín, A. Presas, E. Egusquiza, C. Valero, M. Egusquiza, M. Bossio, Power Swing Generated in Francis Turbines by Part Load and Overload Instabilities, Energies 10 (2017) 2124.
[29] X. Escaler, E. Egusquiza, M. Farhat, F. Avellan, M. Coussirat, Detection of cavitation in hydraulic turbines, Mech. Syst. Signal Process. 20 (2006) 983–1007.
[30] A. Presas, Y. Luo, D. Valentin, M. Egusquiza Montagut, Z. Wang, C. Valero, E. Egusquiza, Detection of erosive cavitation on hydraulic turbines through demodulation analysis, (2019). http://doi.org/10.1088/1755-1315/240/6/062048.
[31] D. Valentín, A. Presas, M. Egusquiza, C. Valero, E. Egusquiza, Transmission of High Frequency Vibrations in Rotating Systems. Application to Cavitation Detection in Hydraulic Turbines, Appl. Sci. 8 (2018) 451.
[32] U. Seidel, B. Hübner, J. Löfflad, P. Faigle, Evaluation of RSI-induced stresses in Francis runners, in, IOP Conf. Ser. Earth Environ. Sci., IOP Publishing (2012) 52010.
[33] X. Huang, J. Chamberland-Lauzon, C. Oram, A. Klopfer, N. Ruchonnet, Fatigue analyses of the prototype Francis runners based on site measurements and simulations, IOP Conf. Ser. Earth Environ. Sci. 22 (2014) 12014, https://doi.org/10.1088/1755-1315/22/1/012014.
[34] U. Seidel, C. Mende, B. Hübner, W. Weber, A. Otto, Dynamic loads in Francis runners and their impact on fatigue life, in: IOP Conf. Ser. Earth Environ. Sci., IOP Publishing, 2014, p. 32054.
[35] X. Liu, A. Presas, Y. Luo, Z. Wang, Crack growth analysis and fatigue life estimation in the piston rod of a Kaplan hydro turbine, Fatigue Fract. Eng. Mater. Struct. 41 (2018) 2402–2417.
[36] P. Paris, F. Erdogan, A critical analysis of crack propagation laws, (1963).

Please cite this article as: W. Zhao, M. Egusquiza, C. Valero et al., On the use of artificial neural networks for condition monitoring of pump-turbines with extended operation, Measurement, https://doi.org/10.1016/j.measurement.2020.107952

[37] A. Presas, Y. Luo, Z. Wang, B. Guo, Fatigue life estimation of Francis turbines based on experimental strain measurements: Review of the actual data and future trends, (2019). http://doi.org/10.1016/j.rser.2018.12.001.
[38] M. Zhang, D. Valentín, C. Valero, M. Egusquiza, E. Egusquiza, Failure investigation of a Kaplan turbine blade, Eng. Fail. Anal. (2019), https://doi.org/10.1016/j.engfailanal.2019.01.056.
[39] M. Egusquiza, E. Egusquiza, D. Valentin, C. Valero, A. Presas, Failure investigation of a Pelton turbine runner, Eng. Fail. Anal. 81 (2017) 234–244, https://doi.org/10.1016/j.engfailanal.2017.06.048.
[40] ISO, ISO 20816-5:2018 Mechanical vibration – Measurement and evaluation of machine vibration – Part 5: Machine sets in hydraulic power generating and pump-storage plants, (2018) 60.

Please cite this article as: W. Zhao, M. Egusquiza, C. Valero et al., On the use of artificial neural networks for condition monitoring of pump-turbines with extended operation, Measurement, https://doi.org/10.1016/j.measurement.2020.107952

6.2 Journal paper 2

- W. Zhao, A. Presas, M. Egusquiza, D. Valentín, C. Valero, E. Egusquiza, Increasing the Operating Range and Energy Production in Francis Turbines by An Early Detection of the Overload Instability, Measurement. 181 (2021) 109580. doi: j.measurement.2021.109580.

Measurement 181 (2021) 109580

Contents lists available at ScienceDirect

Measurement

journal homepage: www.elsevier.com/locate/measurement

Increasing the operating range and energy production in Francis turbines by an early detection of the overload instability

Weiqiang Zhao, Alexandre Presas *, Mònica Egusquiza, David Valentín, Eduard Egusquiza, Carme Valero

Centre for Industrial Diagnostics and Fluid Dynamics (CDIF), Polytechnic University of Catalonia (UPC), Barcelona, Spain

ARTICLE INFO

Keywords:
Francis turbine
Overload instability
Data-driven method
PCA
SOM

ABSTRACT

With the increasing entrance of wind and solar power for the generation of electricity, more flexibility is demanded to hydropower plants. More flexibility means that hydro turbines have to increase the operating range between minimum and maximum power. In Francis turbines the maximum power is limited by the appearance of a strong hydraulic excitation called overload instability. When the turbine operates at loads higher than design, the cavitating vortex rope that is generated in the draft tube may become unstable, producing huge pressure fluctuations, vibrations and power swing. Turbines are not allowed to operate under these conditions in order to avoid the destruction of the unit. The overload instability emerges abruptly, even when the machine is operating in a smooth condition. No visible transition can be detected by the monitoring system, so turbine operators have no margin to react. To avoid this phenomenon, operators limit the maximum power much before reaching this condition. By doing that, the maximum power is limited as well as the regulation capacity of the unit. In this paper, the feasibility of detecting the onset of this phenomenon is analyzed. Data-driven methods and artificial intelligence techniques, including principal component analysis, self-organizing map and artificial neural networks, are applied to the data available from experimental tests in a Francis turbine. The signals of vibration, pressure fluctuations and other parameters are combined and studied. The possibilities of a premature detection of the instability before it occurs are discussed. The method could be implemented in the monitoring system of the unit so that the operating range could be safely increased.

1. Introduction

Because of their flexible output power and fast response, hydraulic turbines have been widely used in the last decades to match the generation of energy with the demand of the electricity grid. This task has become more challenging with the massive entrance of new renewable energies, such as wind and solar energies, because of their intermittent and unpredictable nature. For hydraulic turbines, which have to balance this complicated behavior of the electricity grid, this implies working in a wide operating range; far away from its best efficiency point (BEP) and with multiple start and stops. The most common type is the Francis turbine due to its versatility in terms of design head. Francis turbines have been used for more than one century, but due to the relatively new requirements of the electricity market, more dynamic problems and damage have been reported recently. For example, fatigue damage [1,2], resonance problems [3,4] and power swing [5,6] have been reported in the last decade. Minimizing the adverse effects of these phenomena and running the unit safely in an extended operating range is one of the main concerns of turbine operators, manufacturers and researchers.

Regarding Francis turbines, the overload instability is a problem that might be dangerous and hence not part of the operating range of a properly designed runner. This phenomenon was firstly documented in 1940 [7] but it is still one of the main concerns in current operating units [8]. It is known that such phenomenon starts with a stable cavitating vortex rope in the draft tube. Such rope is generally a vertical cavitation column centered in the runner cone [9]. In Fig. 1, the physical parameters' fluctuation of a Francis turbine operating at 96,43% (475 MW) and 98,36% (477 MW) has been represented. The consequences of this vortex rope on the pressure pulsations, vibrations, torque on the shaft and power swing are almost negligible as it can be seen in Fig. 1 left. For certain conditions, which according to the present knowledge are

* Corresponding author.
E-mail address: alexandre.presas@upc.edu (A. Presas).

https://doi.org/10.1016/j.measurement.2021.109580
Received 6 December 2020; Received in revised form 27 April 2021; Accepted 7 May 2021
Available online 18 May 2021

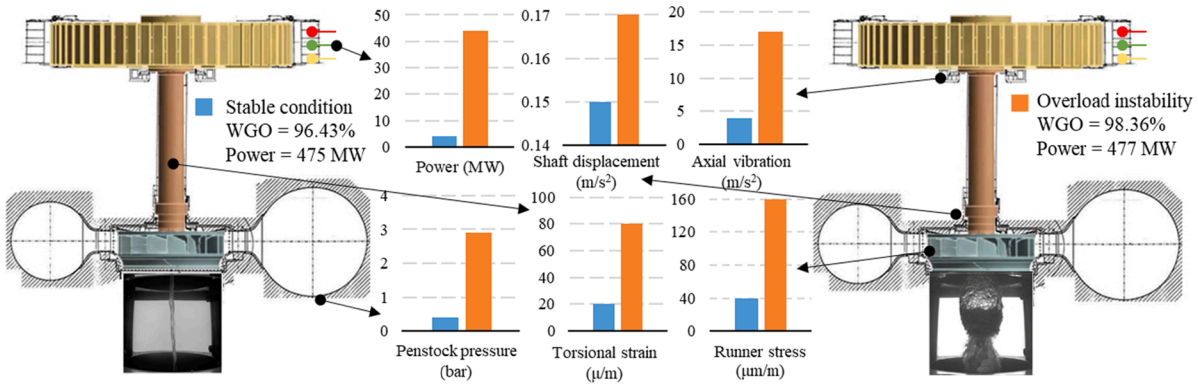

Fig. 1. Example of a Francis turbine with a stable cavitating vortex rope and with an unstable vortex rope. Effects on the fluctuation of the mechanical, hydraulic and electrical system. Vortex rope pictures are taken from [12] and [13]

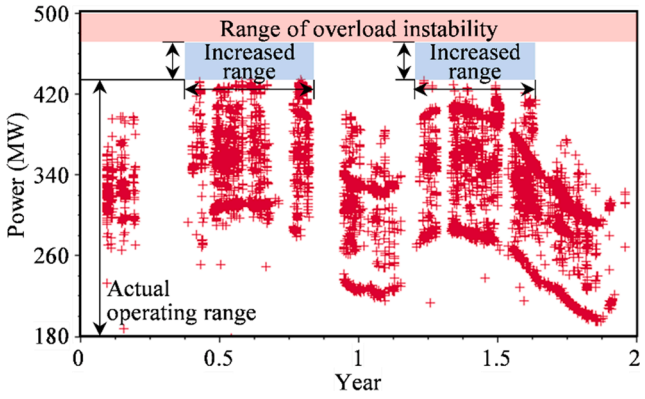

Fig. 2. Actual operating range based on real monitoring data. Estimated possible increased range below the overload instability area.

partially unclear [10], this smooth cavitating column turns suddenly into an important and aggressive cavitating system with huge oscillations of the cavitating volume (Fig. 1 right). Note from the figure, that only a small change in the regulating system (wicket gate opening), and therefore in the output power, triggers this instability. Such instability produces huge pressure oscillations in the hydraulic circuit, torque oscillation in the rotating shaft and finally power swing [8,9,11]. These pressure pulsations can cause damage on the mechanical parts in contact with hydraulic circuits, including pipes, and they compromise the safety of the power station itself [9]. Furthermore, the power swing produced is unacceptable for the stability of the electricity grid.

An early detection of the instability can be a complicated task as the unit normally runs in a stable manner and without any clear symptom before its onset. Nevertheless, the transition to the instability, which entails large pressure, torque and power oscillations, is short [11]. In order to avoid this dangerous situation, some operators choose to work far away from these high loads during the normal operation of the unit [14]. This increases the safety of the system as the risk of instability is decreased but it has the main drawback that the effective operating range of the unit and the amount of energy produced (capacity factor of the unit) is greatly reduced. Real operating data of the analyzed operating unit can be seen in Fig. 2. During approximately half a year, the head of the machine was high and the overload instability may have occurred for full power. Although the unit was able to produce around 490 MW (wicket gate opening of the regulation system at 100%) the operators limited the power of the machine to approximately 440 MW in order to reduce the risk of an overload instability. As seen in Fig. 1 left, the machine could smoothly operate quite close to the instability (around 475 MW), so it can be concluded that with an appropriate monitoring system, the operating range of the machine could be safely increased. In fact, it is roughly estimated that the amount of energy contained in this increased range area (energy that could have been produced with an extended range) is 160 GWh per year.

Therefore, in order to extend the operating range and increase the production of such units in a safe manner, it is of paramount importance to accurately determine the safety operating areas and to quantify the risk or proximity of the instability, even when the machine is running in a smooth condition.

For such purpose, accurate continuous monitoring of the unit is necessary. Condition monitoring systems have been widely used in hydraulic turbines, [14–17] showing relatively good performance in detecting abnormal phenomena and incipient damage. Regarding the overload instability, Presas et al.[18] show that piezoresistive pressure sensors installed on the draft tube and spiral case, which are robust and typically used in monitoring systems, may be the most correlated and sensitive sensors to detect the overload instability phenomenon. Particularly, following the spectral band associated to the frequency of the vortex rope for both sensors, the instability can be easily detected. Nevertheless, that study mainly focuses on the detection of the phenomenon once it has started, leaving a small margin to correct the instability before it is amplified. Therefore, if the objective is an early detection of the instability several seconds before its onset, more refined and advanced data analysis techniques may be necessary.

With the rapid development of computer technology, data driven techniques and artificial intelligence (AI) have attracted considerable attention from researchers all over the world and shown a promising way in machinery condition monitoring applications [19–23]. AI algorithms have been widely applied in condition monitoring, fault diagnosis, prognostics, etc. Generally, an AI diagnosis procedure consists of two steps: feature extraction (data processing) and pattern recognition [24]. During feature extraction, raw data is processed by traditional signal processing methods such as time average, Fourier transform, wavelets and so on. Then the feature matrices are input into AI models for pattern recognition. The aim of pattern recognition is to project the information in feature space into a new recognition space, which involves numerous mathematic tools including mathematical optimization, convex optimization, classification, and probability-based methods [25]. Among them, statistical learning methods and classifiers are the most widely used in machinery engineering applications, including support vector machine (SVM) [26], k-nearest neighbor algorithm (k-NN) [22] and artificial neural network (ANN) [27]. In recent years, deep-learning algorithms like convolutional neural networks (CNN) have also been introduced into fault detection [28,29].

In this paper, we use advanced data driven techniques and AI algorithms to analyze the complex problem of the overload instability in an existing Francis turbine prototype. The main goal is to develop a methodology that is capable of predicting the onset of the instability prematurely. For this purpose, experimental data obtained when the

Table 1
Basic operating parameters of the turbine unit.

Item	Value
Rated output P	444 MW
Rotation speed n	128.4 rpm (2.14 Hz)
Number of runner blades z_b	16
Number of wicket gates	20
Runner diameter D	5.4 m
Rated net head H_n	161.9 m

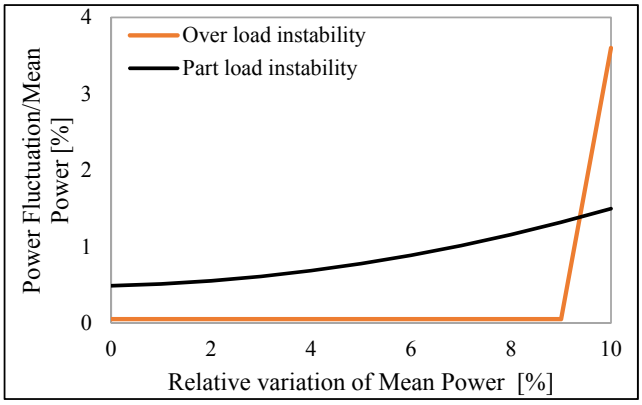

Fig. 3. Relative power fluctuation while entering part load and overload instability [11]

turbine was having strong oscillations at high load have been used. Several signal indicators carefully selected with the accumulated experience analyzing this turbine have been used as inputs of data driven techniques (principal component analysis) and AI algorithms (self-organizing map, artificial neural networks). It has been shown that when such methods are conveniently applied they are perfectly capable of classifying dangerous stable conditions that will lead to instability and to anticipate the onset of the instability several seconds before it occurs. Such methods could be implemented in future advanced monitoring systems.

2. Overload instability in the analyzed unit

2.1. Problem description

The analyzed turbine unit is a large medium-head Francis turbine located in a hydro power plant in Canada, with a rated power of 444 MW. It has a specific speed (n_s) of 46. Other basic parameters are listed in Table 1.

The unit analyzed in this paper presents a clear part load instability [5] and under some circumstances an overload instability with high power fluctuations. These were first analyzed and confirmed by Mueller et al. [9] in a reduced scale model. Later, some works measured and confirmed the existence of power swing in the real prototype [5,11,30,31]. In [5] it was confirmed that the interaction between the planar wave travelling from the draft tube to the penstock and vice versa is able to deform the runner axially and torsionally, producing a fluctuation of the mechanical torque on the shaft which leads to an oscillation in the mechanical and electrical power.

The part load instability can be explained by the precession of the part load vortex rope. The part load vortex rope, which appear always under the Best Efficiency Point (BEP) has a clear precession motion with a frequency of about 0.25–0.35 times the rotating speed of the runner (f_f). When the pressure fluctuations generated by this precession motion coincide with one of the acoustic natural frequencies of the hydraulic circuit, a resonance occurs and the pressure, torque and electrical power fluctuations are greatly amplified. A detailed study of the part load

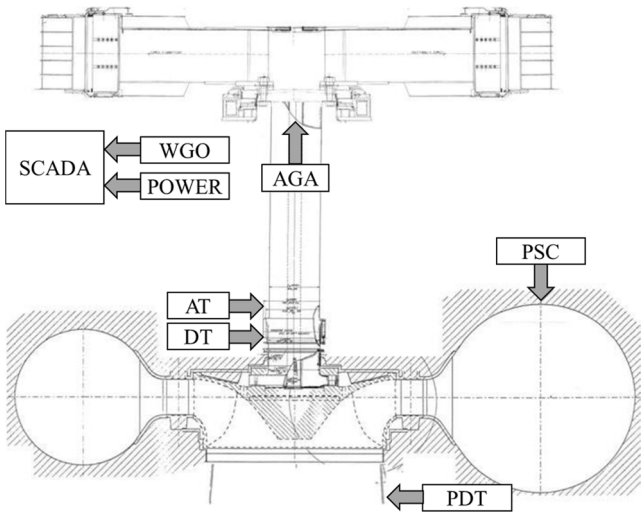

Fig. 4. Sketch of the sensors used (AGA: axial acceleration on generator bearing measured by accelerometer; AT: radial acceleration on turbine bearing measured by accelerometer; DT: displacement on turbine bearing measured by proximity probe; PSC: pressure in the inlet of spiral casing; PDT: pressure in the inlet of draft tube).

instability occurring in this machine can be found in [32].

The overload instability is a much more complex phenomenon, whose causes are not clearly understood at present [10]. Recent studies performed in a reduced scale model [9] point out that such phenomenon can be described as self-excited hydro-mechanical system with positive feedback. Compared to the part load instability, the consequences of the overload instability on the hydraulic, mechanical and electrical system are much more serious due to the self-excited oscillation behavior and because the output power is much larger [33].

In [11] the complexity of an early detection of the overload instability was clearly shown. As it can be observed in Fig. 3, for the part load instability the oscillation amplitude of the power swing increases in a smooth way until the maximum power swing occurs. Therefore, some actions to avoid this operating point can be performed beforehand. For the overload instability, this increase is much more abrupt, showing that this phenomenon cannot be easily detected beforehand and hence it is more dangerous.

This dangerous behavior, when the unit approaches its maximum power, is considered in the general operation of this machine. As shown in Fig. 2, this unit never works with an output power larger than 440 MW in regular operation, even if these conditions are generally stable (band 440 MW-470 MW). Therefore, limiting the output power of the machine reduces the risk of developing the overload instability but the output power and energy produced (capacity factor) by the unit is highly reduced and also the operating range available is narrowed.

2.2. Tests on the overload instability

In the HYPERBOLE project [34], several measurement campaigns were performed in order to measure stresses, vibrations, pressure fluctuations, torque fluctuations and power fluctuations. The data acquired was used to analyze the present unit but also to calibrate numerical, computational and experimental models.

In the present paper we focus on the overload instability and therefore we will analyze the conditions where the wicket gate opening (WGO) was higher than 94% and the output power was close to its maximum for the given net head. In a normal operation, such situation is generally avoided in order to prevent the overload instability. Nevertheless, during the tests such conditions were reached in a safe way, where the output power was manually adjusted. In this way, if the operators thought that the existing power fluctuation and pressure

Table 2
Operation parameters of the overload instability datasets.

Overload test	Net head (m)	WGO (%)	Power (MW)	Peak to peak value of power (MW)	Instability
*S-U*1	176.0	98.2	477.8	42.0	Yes
*S-U*2	175.8	99.0	477.1	47.0	Yes
*S-U*3	173.5	102.6	465.1	35.1	Yes
*S-S*1	178.7	94.0	474.1	3.0	No
*S-S*2	162.9	99.4	400.2	2.4	No

fluctuation was too high, the power of the unit was slightly reduced by closing the wicket gates and the machine turned back to a stable condition.

The sensors and signals used for the present study are schematized in Fig. 4: two pressure sensors on the draft tube (PDT) and spiral case (PSC) respectively, an axial (AGA) and radial accelerometer (AT) on the generator and turbine bearing respectively, a displacement sensor on the shaft (DT) and the SCADA operating signals of the WGO and Power (POW). The sampling frequency of the acquisition system was set at 4096 Hz. All the signals were simultaneously acquired by a B&K LAN XI module. More details on the experimental set-up can be found in [11]. The selected sensors for this study are robust and have also been used for long term condition monitoring [14] and therefore their signals can be used in advanced monitoring systems that could continuously control the risk of instability.

Five situations where the WGO reached a value higher than 94%: *S-S*1, *S-S*2, *S-U*1, *S-U*2 and *S-U*3 have been chosen. *S-S* represents a stable condition that remains stable when the maximum possible WGO is reached, while *S-U* refers to the stable condition leading to an overload instability. Table 2 shows the main operating parameters during these operating conditions. In *S-U*1 and *S-U*2, the head was relatively high and the instability appeared as seen in Fig. 5b and Fig. 5c. It can be appreciated that the overload instability appears suddenly and the power oscillation increases fast from 3 MW to 4 MW to approximately 30 MW-50 MW. Nevertheless, in a similar operating condition *S-S*1 (Fig. 5a), the instability was not developed even though the output power (mean value) was less than 1% lower than in *S-U*1 and *S-U*2. Comparing *S-S*1, *S-U*1 and *S-U*2, one could think that a larger WGO is the main cause for the instability development but in *S-S*2 (Fig. 5d) no instability appeared even with 100% of WGO. In this situation the head was low and the output power was also lower than in the other conditions. In *S-U*3 (Fig. 5e) the instability also appeared with a WGO around 100% but with less head and output power than for the stable condition *S-S*1. For the conditions tested, no clear relationship was observed with the submergence level of the runner.

Regarding the time scale in Fig. 5, for *S-U* conditions $t = 0\ s$ is defined for the inflection point where the power fluctuation starts to increase. For *S-S* conditions, where no instability has been developed, we consider $t = 0$ s as the operating point where the maximum WGO is achieved.

Two things can be concluded from this preliminary analysis. First, power oscillations produced by the overload instability are unacceptable for the safety of the electrical grid. These can also be dangerous for the pow er station itself. As a reference, IEC 60041 defines a stable condition when the oscillation of the power (peak-peak) is less than 3% and in this

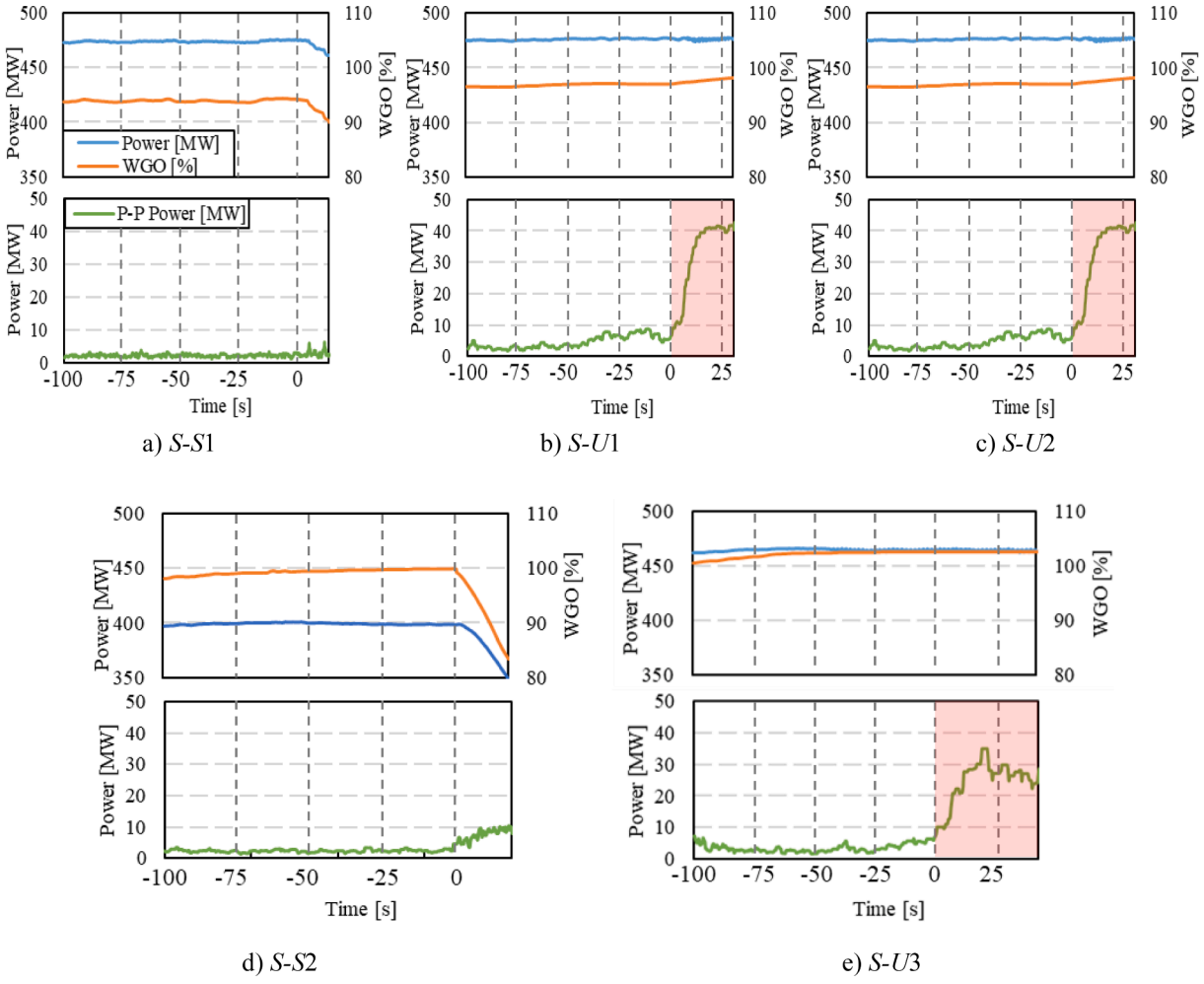

Fig. 5. Variation of power, WGO and peak to peak value of power during the overload instability tests (Instabilities are marked with red background).

Table 3
Condition indicator definition.

Nomenclature	Description
RMS	Root mean square value of the time signal
P2P	Peak to peak value of the time signal
P2P/RMS	P2P to RMS ratio
MEAN	Mean value of the time signal
f_{vr}	Vortex rope band value of the envelope curve
f_{vr}	RMS value of the vortex rope band
f_b	RMS value of the blade passing frequency band

Table 4
Used indicators.

	PSC10	PDT10	AGA12	AT9	DT9	POW	WGO
RMS	1	8	15	21			
P2P	2	9	16	22	27	31	
P2P/RMS	3	10	17	23			
MEAN	4	11					32
f_{vr}	5	12	18	24	28		
f_{vr}	6	13	19	25	29		
f_b	7	14	20	26	30		

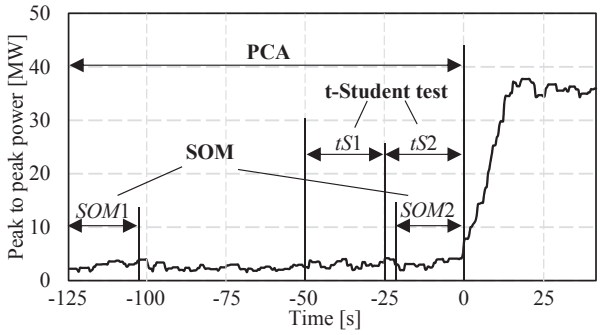

Fig. 6. Timeframes used for every method.

case such value has reached 10%. Second, this phenomenon cannot be foreseen from the monitoring data and thus its early detection and prevention is a challenging task. Its appearance cannot be explained only by a single operating parameter such as the WGO or the output power.

2.3. Data set and indicators used for the analyses

In order to analyse the instability, different time signals measured are windowed with a 4 s-window and a set of indicators is obtained. Then the window is shifted 0.25 s and a new set of indicators is calculated. Two main types of indicators have been obtained for every window. The first type of indicators is calculated in the time domain. These are the RMS value, the mean value and the peak-peak value of the signal part. The second type of indicators correspond to frequency bands obtained after performing the Fast Fourier Transform (FFT). The main spectral bands have been selected according to the excitation forces of the machine. In this case a band around the main excitation frequency of the vortex rope ($f_{vr} \approx 0.8$ Hz, around 35% of the rotating speed) has been selected. Also, an indicator for the same frequency band of the envelope of the time signal has been calculated (f_{vr}). Finally, a band around the blade passing frequency has been also obtained ($f_b \approx 34.28$ Hz). The list of indicators calculated for every sensor is shown in Table 3. Similar indicators have been previously used for the analysis of instabilities in Francis turbines [5,11,15,30], showing the effectivity of them to detect the unstable behavior and to analyze the dynamic behavior of the machine.

Table 5
Results of the t-Student test for the indicators. In bold potential indicators for an early detection of the overload instability.

Indicator	*S-S1*	*S-U1*	Indicator	*S-S1*	*S-U1*	Indicator	*S-S1*	*S-U1*
PSC-RMS	✓	✓	PDT-f_{vr}	×	✓	AT-P2P/RMS	×	×
PSC-P2P	×	✓	PDT- f_{vr}	×	✓	AT-f_{vr}	✓	×
PSC-P2P/RMS	×	✓	PDT- f_b	✓	×	AT- f_{vr}	×	×
PSC-MEAN	✓	✓	AGA-RMS	×	✓	AT- f_b	✓	×
PSC-f_{vr}	×	✓	AGA-P2P	×	✓	**DT9-P2P**	✓	✓
PSC- f_{vr}	×	✓	AGA-P2P/RMS	×	✓	**DT9-f_{vr}**	✓	✓
PSC- f_b	✓	✓	AGA-f_{vr}	✓	×	**DT9- f_{vr}**	✓	✓
PDT-RMS	×	✓	AGA- f_{vr}	×	×	DT9- f_b	×	×
PDT-P2P	×	✓	**AGA- f_b**	✓	✓	POW-P2P	×	×
PDT-P2P/RMS	×	✓	AT-RMS	×	✓	WGO-MEAN	×	✓
PDT-MEAN	×	✓	AT-P2P	✓	×			

The final list of selected indicators is shown in Table 4 (32 indicators). Some indicators are not considered as they don't have a physical meaning due to the sensor characteristics. For example, the mean value for an IEPE accelerometer is always filtered. For the displacement sensor the mean value is arbitrary depending on the distance sensor-shaft.

These indicators, which are obtained every 0.25 s for the five conditions tested in Fig. 5, is the whole dataset used in this paper. Depending on the analysis performed, different timeframes of the data will be used. For convenience of the readers, Fig. 6 includes the timeframes used for every method.

3. Analysis of the data during the stable condition

The early detection of the overload instability of a Francis turbine is necessary if the unit has to work close to this condition. In classical condition monitoring, signal indicators conveniently selected are trended and compared with reference levels in order to detect abnormal phenomena. In this section, besides this method, we also use PCA (Principal Component Analysis) and SOM (Self-Organizing Map) as alternative methods to detect changes in the high dimension data that could indicate the onset of the instability.

3.1. Data analysis by single indicators

By means of statistical tests (Independent two sample t-Student test) the data from −50 s to −25 s (*tS1* in Fig. 6) is compared with the data from −25 s to 0 s (*tS2* in Fig. 6). Both datasets have 100 samples (4 samples per second for 25 s). As both datasets (*tS1* and *tS2*) have the same number of samples and assuming equal population variance for both groups, the *t* statistic can be calculated as [35]:

$$t = \frac{\overline{X}_{ts1} - \overline{X}_{ts2}}{s_p \sqrt{\frac{1}{n_{ts1}} + \frac{1}{n_{ts2}}}} \tag{1}$$

With

$$s_p = \sqrt{\frac{(n_{ts1}-1)s^2_{ts1} - (n_{ts2}-1)s^2_{ts2}}{n_{ts1} + n_{ts2} - 2}} \tag{2}$$

Where, $\overline{X}_{ts}, s^2{}_{ts}, n_{ts}$ are the sample mean, sample variance and number of samples for each group. The *p-value* is obtained according to the corresponding t-Student distribution (two-tail test) and compared with a

Table 6
Selected indicators for all the conditions tested.

	Stable conditions		Unstable conditions		
	*S-S*2	*S-S*1	*S-U*1	*S-U*2	*S-U*3
PSC-RMS	✓	✓	✓	×	×
PSC-MEAN	✓	✓	✓	×	×
AGA- f_b	✓	✓	✓	×	×
PSC- f_b	✓	✓	✓	×	×
DT9-P2P	✓	✓	✓	✓	×
DT9-f_{vr}	✓	✓	✓	×	×
DT9- f_{vr}	✓	✓	✓	×	×

significance level $\alpha = 0.05$ [35]. If the obtained *p-value* is less than the significance level it may be concluded that there is a statistical difference between both groups.

A robust indicator for an early detection of the instability should have a statistical change for *S-U* conditions (*p-value* $< \alpha$) and no significant statistical change for *S-S* conditions (*p-value* $\geq \alpha$). A first list of potential indicators is obtained by comparing the condition *S-S*1 and the condition *S-U*1.Table 5 shows the results of the decision tests for the indicators analyzed. For the stable condition *S-S*1, ✓ means that the indicator has not a significant change (*p-value* $\geq \alpha$) while × means that there is statistical difference between them (*p-value* $< \alpha$). For the stable condition that leads to instability *S-U*1, the meaning of ✓ and × is the opposite as we should expect a significant change in the indicator, when the instability is about to appear.

Only a few indicators have the desired behavior for both situations, which are marked in bold font. Nevertheless, when using the rest of analyzed unstable and stable conditions available, there is no indicator which behaves as desired (Table 6). From this section, we conclude that for an early detection of the instability, the trend of a single indicator is not significant enough and that more refined techniques are necessary.

3.2. Data clustering by PCA (3-dimensional space)

Principal component analysis (PCA) is a widely used method for multivariable data processing [36]. By the decomposition of the correlation or covariance matrix, this method can transform the original multidimensional data to a new space which has less dimensions than the original one, while preserving most of its information [37]. Assume the feature pattern $X_{m\times n}$ is a matrix with n indicators and m samples. The feature matrix can be projected to a new space by a transform matrix T:

$$Y = TX \tag{3}$$

The transform matrix T can be obtained by either eigen decomposition (ED) or singular vector decomposition (SVD), but SVD is preferred for large scale data since SVD requires less operations [38]:

$$XX^T = U\Lambda U^T \tag{4}$$

As XX^T is a symmetric matrix, according to SVD, U is an orthogonal matrix with all the vectors orthogonal with each other. The singular values $\{v_1, v_2, \ldots, v_n\}$ are sorted from largest to smallest on the diagonal of matrix Λ. T is built by the first d columns of U. The number d can be determined by the eigenvalues:

$$\frac{\sum_{i=1}^{d} v_i}{\sum v_i} \times 100\% > p\%\# \tag{5}$$

Therefore, the first d principal components (PCs) contain more than p % of the information of X.

From the original set of indicators, we don't use the mean value of the power as it can differ a lot between different conditions. For example, the maximum power is 400 MW and 490 MW in *S-S*2 and *S-U* respectively while both situations could potentially develop overload instability. As a consequence, two sets of data with different mean power would appear in two separated clusters, hiding relevant information.

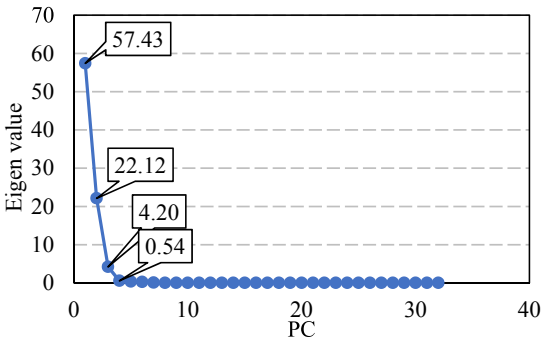

Fig. 7. Eigenvalues obtained from one (*S-U*1) of the correlation matrices of test data.

The measured signals before the instability in each condition are used as the feature pattern, which is a 500 × 32 matrix. As the samples are obtained every 0.25 s, this means that for all the conditions the corresponding data is taken from −125 s to 0 s according to Fig. 6. The matrix is processed by Equation (4) and the eigenvalues and loading matrix are obtained. To decide which of the eigenvectors gives maximum variance in the data, a score test is carried out in Fig. 7 (scree plot). It can be seen that except the first three values, the others are much lower than 1.0. Therefore, according to Kaiser's principle [38], the first 3 dimensions of the projection space are sufficient for retaining most of the original data.

The score tests for the rest of analyzed conditions have been carried out and the intrinsic dimensionality is also 3 and therefore the data is generally well described in the three-dimensional space. The representation of the data on the different operating conditions in its first three principal components (PCs) is shown in Fig. 8.

It can be seen in the figure that the data related to *S-U* conditions are close to each other (Fig. 9b) while the *S-S* clusters are well separated. This clustering by PCA allows a much clearer view than the analysis performed in the previous section. It has to be noticed again that all this data corresponds to stable conditions (with almost no power swing), from which some finally developed into unstable conditions (*S-U*1, *S-U*2 and *S-U*3). The interpretation of this figure may be summarized as follows: when the unit works in a stable condition and the PCA components of the indicators selected fall inside the critical area, the overload instability will soon appear. These borders can be further refined with more measured data for the machine working in mid heads. In terms of physical interpretation of the operation of the unit, this figure can be interpreted as follows: when increasing the WGO of the machine, the cluster of the data moves in the vertical direction (PC3) into a more unstable condition. This condition is reached earlier when the mean power (also net head) is large. For low head conditions (*S-S*2), even when working at the maximum design opening (100% of WGO), the cluster does not fall inside the unstable area. Therefore, the instability does not occur.

Although this method could be used to separate and classify both types of stable conditions (*S-S* and *S-U*) a further analysis of the cluster does not show or explain the proximity of the onset of the instability. This is shown in Fig. 9. PCA analysis is applied to the data shown in Fig. 9 a, corresponding to *S-U*1 condition. Fig. 9 b shows that the stable and unstable parts have formed well separated clusters with a very short transition from one cluster to the other. A detailed analysis of the stable part cluster (Fig. 9 c) shows that there is not a clear trend of the points of the cluster when the instability is about to occur, i.e., red colored points are randomly located in the cluster. This might be because the information neglected in the other components are critical for the evolution of the signal before the instabilities. It could be possible to visualize a trend on the data considering the components neglected in a higher dimension space. Nevertheless, this cannot be visualized directly.

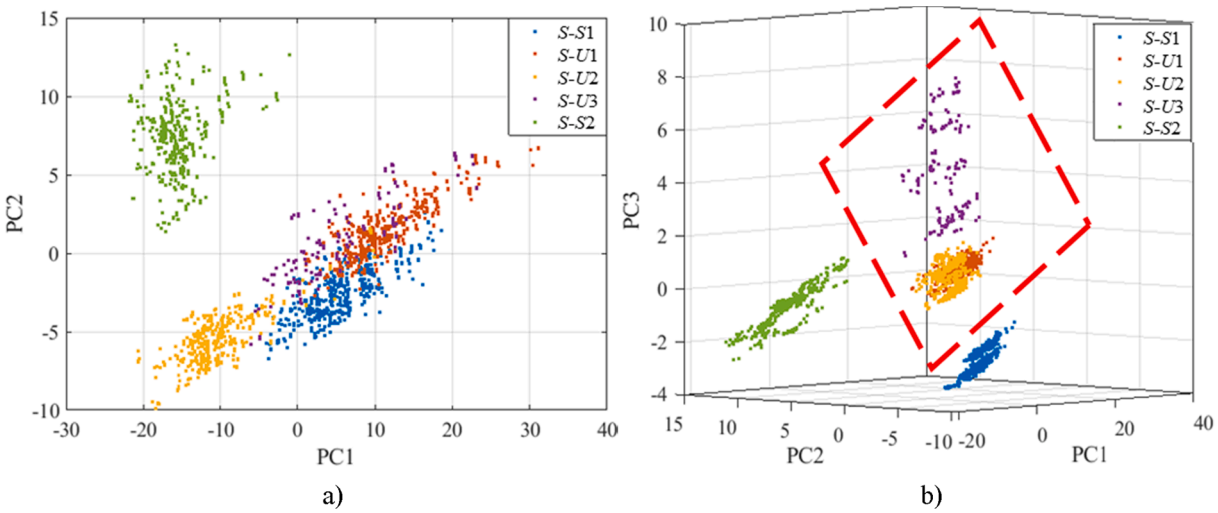

Fig. 8. PCs constructed from the data before instabilities (only *S-U*1, *S-U*2 and *S-U*3 lead finally to the overload instability): a) first 2 PCs; b) first 3 PCs. Red line encloses the *S-U* conditions.

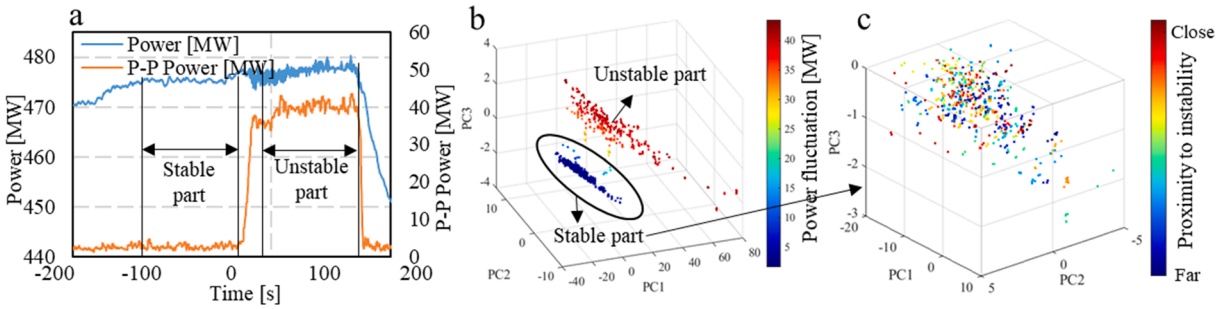

Fig. 9. a) Time data analyzed for *S-U*1 condition. Stable and unstable part. b) PCA of the data. Clusters of the stable and unstable part. Colors according to Power swing. c) Detailed analysis of the stable cluster. Colors according to the proximity of the instability.

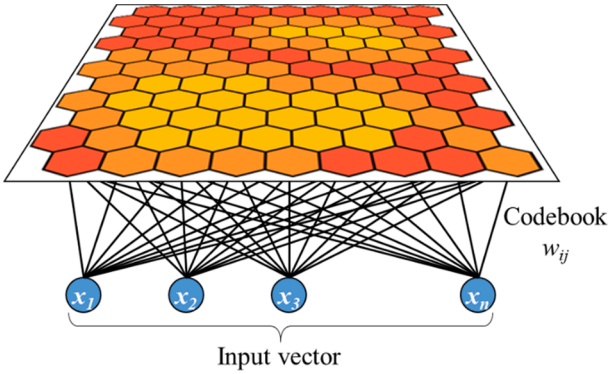

Fig. 10. SOM model.

To summarize, PCA is able to classify and separate both types of stable conditions (*S-S* and *S-U*). Nevertheless, during this stable phase there is no clear trend of the cluster moving towards the instability and the distance between the two clusters is not reduced, when considering the three-dimensional space of PC1, PC2 and PC3. In order to see if it is possible to detect some trends of the data during the stable part, further clustering methods are explored.

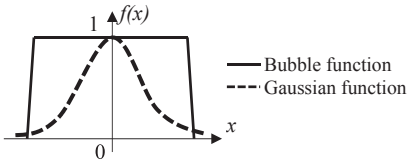

Fig. 11. Neighborhood function.

3.3. Data clustering by SOM (higher dimensional space)

The self-organizing map (SOM) is an algorithm that implements a characteristic nonlinear projection from the high-dimensional space of data onto a low-dimensional array of clusters [39]. Being firstly proposed in 1990 [40], it has been proven useful in many applications [41]. As shown in Fig. 10, a SOM network is composed of 2 layers: input layer and competitive layer (output layer). A typical training process of SOM is shown below:

Initialization. A typical self-organizing map is a two-dimensional array of neurons as shown in Equation (6), where p and q are the size of the output pattern. One neuron m_i is a vector called the codebook vector with the same dimension as the input vectors, as shown in Equation (7), where n is the dimension of the input pattern. During map initialization, random values are assigned to codebook vectors.

$$M = \{m_1, m_2, \cdots, m_{p\times q}\} \tag{6}$$

$$m_i = \{m_{i1},\ m_{i2}, \ldots,\ m_{in}\} \tag{7}$$

Training. A similarity measure (e.g., Euclidean distance) is performed between the input vector and all the codebook vectors [42]. The codebook vector with greatest similarity with the input sample is chosen to be the best-matching unit (BMU) [43], noted as m_c. After m_c is found,

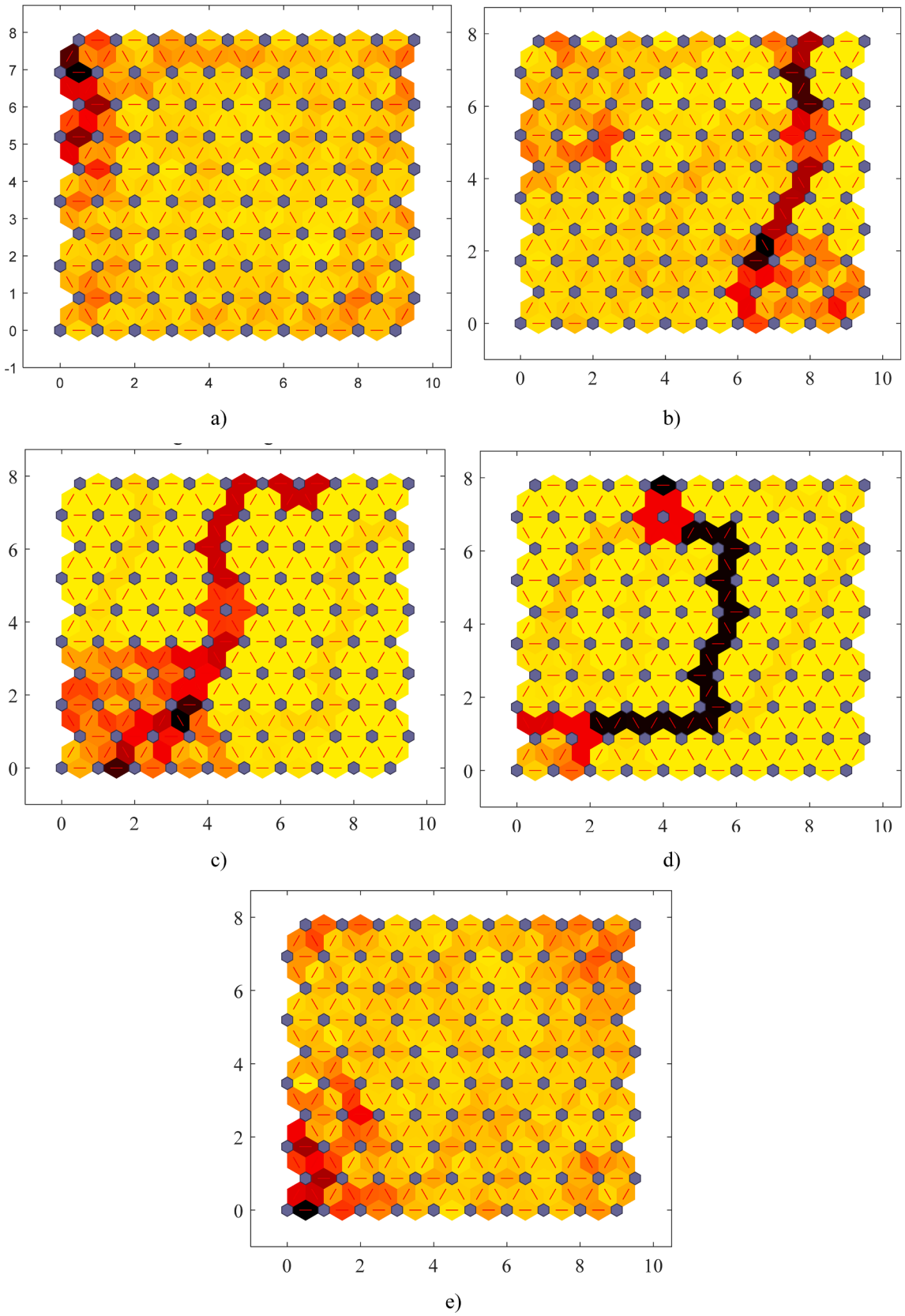

Fig. 12. SOM neighbor distances for a) *S-S*1, b) *S-U*1, c) *S-U*2, d) *S-U*3 and e) *S-S*2. In *S-S*1 and *S-S*2 the instability did not occur, while in *S-U*1, *S-U*2 and *S-U*3 the instability appeared few seconds after.

the topological neighbors of m_c are modified in different degrees which is determined by a neighborhood function. The neighborhood function is usually a bubble function (Fig. 11) which is similar to Gaussian function but easier for the computer to calculate.

$$\|x - m_c\| = \min_i \{\|x - m_i\|\} \tag{8}$$

Visualization. One of the most typical visualization methods of the training result of SOM is a unified distance matrix (U-matrix) [42]. A U-matrix visualizes the distances between the neurons, which are represented with different colors in a heatmap. Dark coloring between two neurons corresponds to a wide distance while light coloring implies the codebook vectors are close to each other, so that the light area can be regarded as a cluster center of the input pattern.

For a 2-D map space in the competitive layer, the visible nodes are arranged in regular hexagonal or rectangular grid and map units (or neurons) usually form a 2-D lattice, thus the high dimensional space can be mapped into a plane. The unsupervised learning algorithm allows SOM to cluster data without knowing the class memberships of the input data so that it can be used to detect features inherent problems. In our case, beyond the "stable" time signal before instabilities occurrence, the combination of the indicators may have changed in a higher dimension space which might be reflected by changes in SOM model.

In this case, the data used is the stable part used for PCA (Fig. 9 a) but only 17% data from the two ends *SOM*1 (from −125 s to −104 s) and *SOM*2 (from −21 s to 0 s) are extracted (see Fig. 6). For the data of *S-S*1, the start and end part of the signal include 84 samples respectively, so that the input pattern of *S-S*1 is a 168*32 matrix. Accordingly, the size of competition layer is set as 10*10 to visualize the map. The codebook values in the neurons are initialized randomly before training. The update range of bubble function is 3, which means the nearest 3 nodes of the winner will be updated.

The SOM neighbor distances of each condition are shown in Fig. 12. There are 100 nodes connected in hexagonal topology in each map. The color between two adjacent nodes represents the distance between them. Apparently, the distances map of *S-S* condition and *S-U* condition are quite different. Despite some dark colors on the edge, the colors in *S-S*1 map are uniform, indicating that the distances between different nodes are similar. This means it is difficult to find any clear trend among all of the samples in this data set. A similar result is generated by SOM model in the data of *S-S*2.

For the stable conditions that lead to an instability (*S-U*1, *S-U*2 and *S-U*3) the color distribution is completely different: a line of dark points splits the color map into two parts or clusters. In one cluster, all nodes are closely connected with the adjacent nodes (light color). The dark color in the maps, indicates that a long distance between the two clusters exists.

4. Early detection of the overload instability by artificial neural network

The objective of the previous section was to see if some trends or features of the data during the stable conditions could indicate the onset of the instability. As a conclusion, none of the single indicators was able to explain the difference between the stable condition that leads to instabilities (*S-U* conditions) from those which do not (*S-S* conditions). PCA could separate the *S-S* conditions and *S-U* conditions in a 3-dimensional space but it did not show a clear trend of the data towards the instability. With SOM, the data corresponding to the stable part was clearly separated in two groups for the *S-U* conditions and therefore a high risk of developing the instability when the data cluster "crossed" the dark line in Fig. 12. After having confirmed this, in this section we propose training an artificial neural network in order to quantify the proximity of the instability beforehand, which is the final goal of the paper.

In order to do that, an artificial unstable index (*AUI*) has been

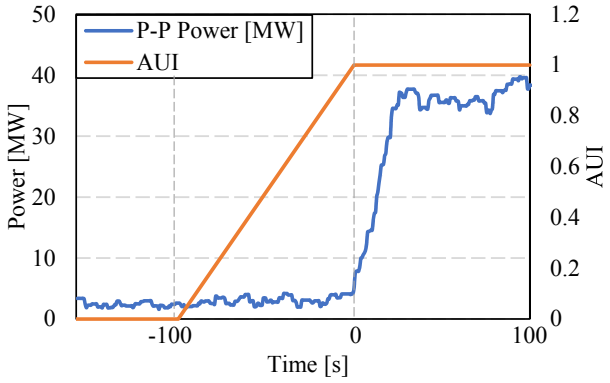

Fig. 13. Definition of artificial unstable index in the transition to an unstable condition (*S-U*1).

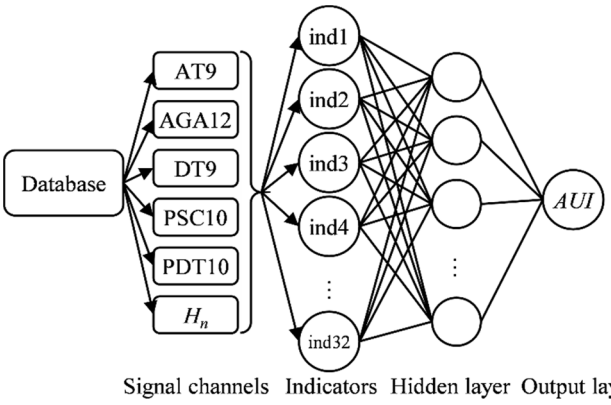

Fig. 14. Architecture of the used ANN.

defined. According to the result obtained by SOM, a significant change between the data *SOM*1 and *SOM*2 (Fig. 6) was observed for the *S-U* conditions. As the dataset *SOM*1 ends at t = -104 s, the *AUI* is 0 until t = -100 s (few seconds after *SOM*1 data ends) and increases linearly to 1 exactly at the critical point (t = 0 s) (Fig. 13). For a stable condition outside this range this index is constantly set at 0. Although this definition is totally arbitrary, it has been proved to give good results for the rest of the conditions tested. If a similar methodology was applied in other Francis turbine, slightly different criteria for the definition of the *AUI* could be used depending on the behavior of the machine.

For the ANN (Fig. 14), the inputs are the 32 indicators and the output the *AUI*. The optimum number of neurons in the hidden layer is set as 30 after several trials in which the number of layers and perceptrons in the hidden layers were changed [44]. Levenberg-Marquardt (LM) back-propagation function is chosen as the training algorithm. This training method has a faster convergence speed on training process of middle-sized feedforward networks [45]. In present study, a conventional multilayer perceptron has been used, which has shown a good performance for the existing data. As the inputs have a time order, a time convolutional neural network could be used in future works [46].

The training conditions are the conditions *S-U*1, *S-U*2 and the totally stable condition *S-S*1. For validation, the condition *S-U*3 and condition *S-S*2 have been considered. Fig. 15 shows the results of the trained NN applied into the validation conditions. A moving average of 5 samples has been calculated in order to damp the oscillations of the data. The *AUI* for condition *S-U*3 (Fig. 15 a) increases from 0 to 1 in a relatively smooth way before the instability appears. It also shows the same trend as for the trained conditions, which have a linear variation. For the stable condition *S-S*2 (Fig. 15 b), the *AUI* shows a constant trend near zero. These results show that the trained ANN is capable of correctly

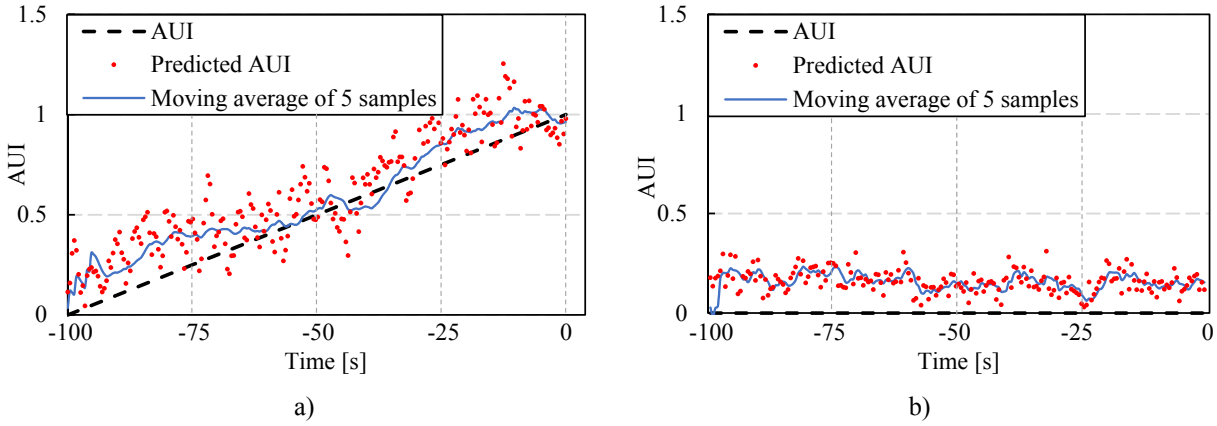

Fig. 15. *AUI* prediction result by ANN: a) *S-U*3 (before instability); b) *S-S*2 (no instability occurred).

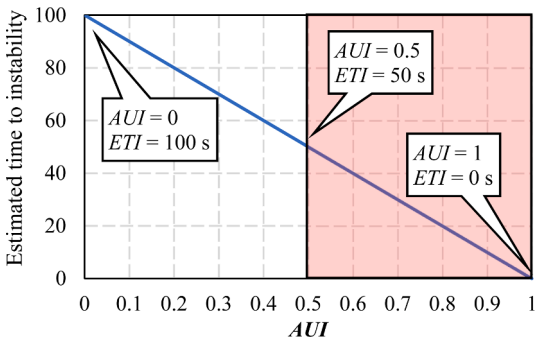

Fig. 16. Relationship between *AUI* and estimated time to instability.

predicting the trend and classifying an *S-U* and *S-S* condition. With more training data, based on stable and unstable conditions, we expect having more precise trends around the defined *AUI*.

Finally, we can relate the *AUI* with the estimated time to instability (*ETI*) as it is a more intuitive parameter. A larger *ETI* means more margin to do some corrections in the unit before the instability really occurs. As shown in Fig. 16, for *AUI* equals to 1 *ETI* is 0 and for *AUI* equals to 0 *ETI* is set to 100 s, as defined in the training conditions. An *AUI* close to 0 is not significant and can correspond to any operating condition of the machine. Therefore, it is necessary to set an alarm threshold (for example $AUI = 0.5$ as shown in Fig. 16) which will correspond to the remaining time until instability. A suitable threshold can decrease false alarms significantly while keeping sufficient time margin for regulation.

To summarize, with the indicators selected and an appropriate definition of the *AUI* and by training the ANN during different overload instability tests (*S-S* and *S-U* conditions), it is shown that an early detection of the overload instability is possible. With more data available it is expected that the trend of the predicted *AUI* for new conditions would be closer to the ideal *AUI*.

5. Conclusions

The overload instability in a Francis turbine is a dangerous phenomenon that produces undesired power swings in the electrical grid and can also compromise the safety of the power station. This phenomenon is particularly challenging to detect and to anticipate, as the transition from a stable condition to an unstable condition happens in a short time. In order to avoid risks, some operators avoid using the machine at high loads. As a consequence, the capacity factors and operating ranges of such power plants are drastically reduced.

This paper explores the feasibility of using data-driven methods for an early detection of the overload instability in a Francis turbine prototype. It has been shown that with AI techniques the instability can be successfully predicted several seconds before it occurs. The implementation of these methods in advanced monitoring systems would be beneficial for the operators as the operating range and capacity factor of the power station could be safely extended. For the analyzed unit, implementing such method to the current monitoring strategy could safely increase the output power by 35 MW (8% of the rated power), which roughly represents 160 GWh every year.

The unit was monitored with many sensors during stable operating conditions finally leading to an overload instability. A set of signal indicators based on previous analyses of the machine and on the monitored data for more than one year have been obtained. These include time indicators and spectral bands.

A first analysis of the indicators during the stable conditions preceding the instabilities has led to the following conclusions. Statistical hypothesis testing of the indicators during the stable conditions preceding the instability have demonstrated that there is not a single indicator that can clearly predict the onset of the instability. With principal component analysis (PCA) the data of the stable conditions preceding the instability can be clearly clustered. The stable operating conditions that finally lead to an overload instability can be classified and separated from those which did not. The self-organizing map (SOM) has been used as an alternative method for clustering. It has been shown that SOM is able to detect changes in the data set before the instability occurs. Nevertheless, this method is not able to quantify the proximity of the instability onset.

Therefore, artificial neural networks (ANN) have been used to predict and to quantify the risk of overload instability before occurrence. An artificial unstable index (*AUI*), which increases when the instability is about to occur, has been used to train the neural network. It has been proved that the trained ANN is able to quantify the risk of instability several seconds beforehand and, therefore, that an early detection of the overload instability is possible.

CRediT authorship contribution statement

Weiqiang Zhao: Conceptualization, Formal analysis, Investigation, Methodology, Visualization. **Alexandre Presas:** Data curation, Writing - review & editing. **Mònica Egusquiza:** Validation. **David Valentín:** Software. **Carme Valero:** Project administration. **Eduard Egusquiza:** Supervision.

Declaration of Competing Interest

The authors declare that they have no known competing financial interests or personal relationships that could have appeared to influence the work reported in this paper.

Acknowledgements

The authors want acknowledge the XFLEX HYDRO project (EU H2020 No. 857832). Weiqiang Zhao would like to acknowledge the China Scholarship Council (CSC) for its grants. Alexandre Presas and David Valentin wants to acknowledge the Serra Hunter program of Generalitat de Catalunya.

References

[1] A. Presas, Y. Luo, Z. Wang, B. Guo, Fatigue life estimation of Francis turbines based on experimental strain measurements: Review of the actual data and future trends, Renew. Sustain. Energy Rev. 102 (2019) 96–110, https://doi.org/10.1016/j.rser.2018.12.001.
[2] X. Liu, Y. Luo, Z. Wang, A review on fatigue damage mechanism in hydro turbines, Renew. Sustain. Energy Rev. 54 (2016) 1–14, https://doi.org/10.1016/j.rser.2015.09.025.
[3] D. Valentín, A. Presas, E. Egusquiza, C. Valero, M. Bossio, Dynamic response of the MICA runner. Experiment and simulation, J. Phys. Conf. Ser. 813 (2017) 12036, https://doi.org/10.1088/1742-6596/813/1/012036.
[4] L.Y. He, Z.W. Wang, S. Kurosawa, Y. Nakahara, Resonance investigation of pump-turbine during startup process, in: IOP Conf. Ser. Earth Environ. Sci., IOP Publishing, 2014: p. 32024.
[5] D. Valentín, A. Presas, E. Egusquiza, C. Valero, M. Egusquiza, M. Bossio, Power Swing Generated in Francis Turbines by Part Load and Overload Instabilities, Energies. 10 (2017) 2124.
[6] D. Valentín, A. Presas, M. Egusquiza, C. Valero, E. Egusquiza, Behavior of Francis turbines at part load. Field assessment in prototype: Effects on power swing, IOP Conf. Ser. Earth, Environ. Sci. 240 (2019), 062012, https://doi.org/10.1088/1755-1315/240/6/062012.
[7] W.J. Rheingans, Power swings in hydroelectric power plants, Trans. ASME. 62 (1940) 171–184.
[8] D. Valentín, A. Presas, C. Valero, M. Egusquiza, E. Egusquiza, Detection of Hydraulic Phenomena in Francis Turbines with Different Sensors, Sensors. 19 (2019) 4053.
[9] A. Müller, A. Favrel, C. Landry, F. Avellan, Fluid–structure interaction mechanisms leading to dangerous power swings in Francis turbines at full load, J. Fluids Struct. 69 (2017) 56–71, https://doi.org/10.1016/j.jfluidstructs.2016.11.018.
[10] P.K. Dörfler, On the High-partial-load Pulsation in Francis Turbines, Int. J. Fluid Mach. Syst. 12 (2019) 200–216.
[11] A. Presas, D. Valentin, M. Egusquiza, C. Valero, E. Egusquiza, Sensor-Based Optimized Control of the Full Load Instability in Large Hydraulic Turbines, Sensors. 18 (2018) 1038.
[12] A. Müller, A. Favrel, C. Landry, K. Yamamoto, F. Avellan, Experimental Hydro-Mechanical Characterization of Full Load Pressure Surge in Francis Turbines, in, J. Phys. Conf. Ser. (2017) 12018.
[13] A. Müller, M. Dreyer, N. Andreini, F. Avellan, Draft tube discharge fluctuation during self-sustained pressure surge: fluorescent particle image velocimetry in two-phase flow, Exp. Fluids. 54 (2013) 1514.
[14] C. Valero, E. Egusquiza, A. Presas, D. Valentin, M. Egusquiza, M. Bossio, Condition monitoring of a prototype turbine. Description of the system and main results, in, J. Phys. Conf. Ser., IOP Publishing (2017) 12041.
[15] E. Egusquiza, C. Valero, D. Valentin, A. Presas, C.G. Rodriguez, Condition monitoring of pump-turbines, New challenges, Measurement. 67 (2015) 151–163, https://doi.org/10.1016/j.measurement.2015.01.004.
[16] M. Egusquiza, E. Egusquiza, C. Valero, A. Presas, D. Valentín, M. Bossio, Advanced condition monitoring of Pelton turbines, Measurement. 119 (2018) 46–55, https://doi.org/10.1016/j.measurement.2018.01.030.
[17] C. Valero, M. Egusquiza, E. Egusquiza, A. Presas, D. Valentin, M. Bossio, Extension of Operating Range in Pump-Turbines, Influence of Head and Load, Energies. 10 (2017) 2178, https://doi.org/10.3390/en10122178.
[18] A. Presas, E. Egusquiza, C. Valero, D. Valentin, U. Seidel, Feasibility of using PZT actuators to study the dynamic behavior of a rotating disk due to rotor-stator interaction, Sensors (Basel). 14 (2014) 11919–11942, https://doi.org/10.3390/s140711919.
[19] W. Zhao, M. Egusquiza, C. Valero, D. Valentín, A. Presas, E. Egusquiza, On the Use of Artificial Neural Networks for Condition Monitoring of Pump-Turbines with Extended Operation, Measurement. 163 (2020), 107952, https://doi.org/10.1016/j.measurement.2020.107952.
[20] M.C. Garcia, M.A. Sanz-Bobi, J. Del Pico, SIMAP: Intelligent System for Predictive Maintenance: Application to the health condition monitoring of a windturbine gearbox, Comput. Ind. 57 (2006) 552–568.
[21] M. Schlechtingen, I.F. Santos, S. Achiche, Using data-mining approaches for wind turbine power curve monitoring: a comparative study, IEEE Trans. Sustain. Energy. 4 (2013) 671–679.
[22] M. Schlechtingen, I.F. Santos, Comparative analysis of neural network and regression based condition monitoring approaches for wind turbine fault detection, Mech. Syst. Signal Process. 25 (2011) 1849–1875.
[23] W. Zhao, M. Egusquiza, A. Estevez, A. Presas, C. Valero, D. Valentín, E. Egusquiza, Improved damage detection in Pelton turbines using optimized condition indicators and data-driven techniques, Struct. Heal. Monit. (2021) 147592172098183. doi:10.1177/1475921720981839.
[24] A.K.S. Jardine, D. Lin, D. Banjevic, A review on machinery diagnostics and prognostics implementing condition-based maintenance, Mech. Syst. Signal Process. 20 (2006) 1483–1510.
[25] R. Liu, B. Yang, E. Zio, X. Chen, Artificial intelligence for fault diagnosis of rotating machinery: A review, Mech. Syst. Signal Process. 108 (2018) 33–47.
[26] R. Zhao, R. Yan, Z. Chen, K. Mao, P. Wang, R.X. Gao, Deep learning and its applications to machine health monitoring, Mech. Syst. Signal Process. 115 (2019) 213–237.
[27] R.A. Saeed, A.N. Galybin, V. Popov, 3D fluid–structure modelling and vibration analysis for fault diagnosis of Francis turbine using multiple ANN and multiple ANFIS, Mech. Syst. Signal Process. 34 (2013) 259–276, https://doi.org/10.1016/j.ymssp.2012.08.004.
[28] L. Jing, M. Zhao, P. Li, X. Xu, A convolutional neural network based feature learning and fault diagnosis method for the condition monitoring of gearbox, Measurement. 111 (2017) 1–10.
[29] A. Severyn, A. Moschitti, Unitn: Training deep convolutional neural network for twitter sentiment classification, in: Proc. 9th Int. Work. Semant. Eval. (SemEval 2015), 2015: pp. 464–469.
[30] A. Presas, D. Valentin, E. Egusquiza, C. Valero, Detection and analysis of part load and full load instabilities in a real Francis turbine prototype, HYdropower Plants Perform, Flex. Oper. Towar. Lean Integr. New Renew. Energies Symp. HYPERBOLE 2017 (813) (2017) 12038, https://doi.org/10.1088/1742-6596/813/1/012038.
[31] E. Egusquiza, D. Valentín, A. Presas, C. Valero, Overview of the experimental tests in prototype, J. Phys. Conf. Ser. 813 (2017), 012037, https://doi.org/10.1088/1742-6596/813/1/012037.
[32] A. Favrel, A. Müller, C. Landry, K. Yamamoto, F. Avellan, LDV survey of cavitation and resonance effect on the precessing vortex rope dynamics in the draft tube of Francis turbines, Exp. Fluids. 57 (2016) 168.
[33] A. Favrel, A. Müller, C. Landry, K. Yamamoto, F. Avellan, Study of the vortex-induced pressure excitation source in a Francis turbine draft tube by particle image velocimetry, Exp. Fluids. 56 (2015) 215.
[34] EPFL, HYdropower Plants PERformance and flexiBle Operation towards Lean Integration of New Renewable Energies, EPFL. (2017). https://hyperbole.epfl.ch/SitePages/Hyperbole.aspx.
[35] E.L. Lehmann, J.P. Romano, Testing statistical hypotheses, Springer Science & Business Media, 2006.
[36] K.L. Sainani, Introduction to principal components analysis, PM R. 6 (2014) 275–278, https://doi.org/10.1016/j.pmrj.2014.02.001.
[37] A. Bellino, A. Fasana, L. Garibaldi, S. Marchesiello, PCA-based detection of damage in time-varying systems, Mech. Syst. Signal Process. 24 (2010) 2250–2260.
[38] I. Jolliffe, Principal component analysis, in: Int. Encycl. Stat. Sci., Springer, 2011: pp. 1094–1096.
[39] T. Kohonen, E. Oja, O. Simula, A. Visa, J. Kangas, Engineering applications of the self-organizing map, Proc. IEEE. 84 (1996) 1358–1384.
[40] J. Kangas, T. Kohonen, J. Laaksonen, Variants of self-organizing maps, IEEE Trans. Neural Networks. 1 (1990) 93–99.
[41] J. Baglin, Improving your exploratory factor analysis for ordinal data: A demonstration using FACTOR, Pract. Assessment, Res. Eval. 19 (2014) 2.
[42] J. Hollmën, V. Tresp, O. Simula, A self-organizing map for clustering probabilistic models, (1999).
[43] J. Hollmën, Process modeling using the self-organizing map, (1996).
[44] L. Tarassenko, Guide to neural computing applications, Elsevier, 1998.
[45] W. Zhao, E. Egusquiza, C. Valero, M. Egusquiza, D. Valentín, A. Presas, A Novel Condition Monitoring Methodology Based on Neural Network of Pump-Turbines with Extended Operating Range, in: 16th IMEKO TC10 Conf., Berlin, 2019: p. 4. https://www.imeko.org/publications/tc10-2019/IMEKO-TC10-2019-024.pdf.
[46] S. Bai, J.Z. Kolter, V. Koltun, An empirical evaluation of generic convolutional and recurrent networks for sequence modeling, ArXiv Prepr, ArXiv1803.01271. (2018).

6.3 Journal paper 3

- W. Zhao, M. Egusquiza, A. Estevez, A. Presas, C. Valero, D. Valentín, E. Egusquiza, Improved damage detection in Pelton turbines using optimized condition indicators and data-driven techniques, Struct. Heal. Monit. (2021) 147592172098183. doi: 10.1177/1475921720981839.

UNIVERSITAT POLITÈCNICA DE CATALUNYA BARCELONATECH

Weiqiang Zhao <weiqiang.zhao@upc.edu>

Structural Health Monitoring - Decision on Manuscript ID SHM-20-0369.R2

3 messages

Structural Health Monitoring <onbehalfof@manuscriptcentral.com> Sun, Nov 29, 2020 at 6:44 PM
Reply-To: mdtodd@ucsd.edu
To: weiqiang.zhao@upc.edu

29-Nov-2020

Dear Mr. Zhao:

It is a pleasure to accept your manuscript entitled "Improved Damage Detection in Pelton Turbines Using Optimized Condition Indicators and Data-driven Techniques" in its current form for publication in Structural Health Monitoring. The comments of the reviewer(s) who reviewed your manuscript are included at the foot of this letter.

If you would like your article to be freely available online immediately upon publication (as some funding bodies now require), you can opt for it to be published under the SAGE Choice Scheme on payment of a publication fee. Please simply follow the link to the Contributor Agreement form in the next email and you will be able to access instructions and further information about this option within the online form.

Thank you for your fine contribution. On behalf of the Editors of Structural Health Monitoring, we look forward to your continued contributions to the Journal.

Sincerely,
Prof. Michael Todd
Editor in Chief, Structural Health Monitoring
mdtodd@ucsd.edu

Reviewer(s)' Comments to Author:

Reviewer: 1

Comments to the Author
The authors have clarified the confusion clearly. I am happy to recommend to accept this paper for publication in the Journal SHM.

Associate Editor's Comments to Author:

Associate Editor
Comments to the Author:
The paper is recommended for publication.

Improved Damage Detection in Pelton Turbines Using Optimized Condition Indicators and Data-driven Techniques

Weiqiang Zhao[1], Mònica Egusquiza[1], Aida Estevez[2], Alexandre Presas[1], Carme Valero[1], David Valentín[1], Eduard Egusquiza[1]

[1] Centre for Industrial Diagnostics and Fluid Dynamics (CDIF), Polytechnic University of Catalonia (UPC), Barcelona, Spain, weiqiang.zhao@upc.edu, +34 657080743
[2] Dpto. Ingeniería mecánica y fabricación. Escuela Técnica Superior de Ingeniería, Universidad de Sevilla, Sevilla, Spain

Abstract

The health condition of hydraulic turbines is one of the most critical factors for the operation safety and financial benefits of a hydro power plant. After the massive entrance of intermittent renewable energies, hydropower units have to regulate their output much more frequently for the balancing of the power grid. Under these conditions, the components of the machine have to withstand harsher excitation forces, which are more likely to produce damage and eventual failure in the turbines. To ensure the reliability of these machines, improved condition monitoring techniques are increasingly demanded.

In this paper, the feasibility of upgrading condition monitoring of Pelton turbines using novel vibration indicators and data-driven techniques is discussed. The new indicators are selected after performing a detailed analysis of the dynamic behavior of the turbine using numerical models and field measurements. After that, Factor Analysis (FA) is carried out in order to assess which are the most informative indicators and to reduce the dimension of the input data.

For the validation of the proposed method, monitoring data from an actual Pelton turbine that suffered from an important fatigue failure due to a crack propagation on the buckets have been used. The novel condition indicators as well as classical indicators based on the spectrum and harmonics levels have been obtained while the machine was in good operation, during different stages of damage and after repair. All of these have been used to train an Artificial Neural Network (ANN) model in order to predict the evolution of the crack until failure occurs. The results show that using the improved monitoring methodology enhances the ability to predict the appearance of damage in comparison to typical condition indicators.

Keywords: condition monitoring; Pelton turbine; damage detection; condition indicator; Factor Analysis (FA); Principal Component Analysis (PCA).

1. Introduction

Hydropower is one of the most important renewable energies, which converts the potential energy of water into electric energy. After its development since more than one century ago, hydropower has become a reliable energy resource. Over the last years, with the entrance of new renewable energies like solar photovoltaics and wind energy, whose output is random and hard to regulate, hydropower has become extremely significant for balancing the generation and consumption of electricity. Over the last decade, the installed capacity of wind and solar energy has increased from 13.2% and 2.1% to 24.0% and 20.7%, respectively [1]. This new scenario requires hydropower units to regulate their output much more frequently for the balancing of the power grid. Therefore, more flexibility is demanded and turbines have to operate many hours off-design. Due to the more severe operating conditions, components from Pelton turbine are more prone to suffer damage and/or failure [2–4]. Unexpected failures of the turbine may result in substantial economic losses, not only due to the costs related to the repair or replacement of the component but also to the downtime and production loss thus caused.

As the most common action-type turbine, Pelton turbines are widely used in high-head hydropower plants. In the turbine, the high pressure of the water at the entrance is converted into a high velocity jet using a nozzle. The jet impinges the runner as shown in Figure 1, converting the kinetic energy of the water into mechanical energy that is converted into electricity by the generator. During operation, strong pulsating forces are produced on the runner. The buckets that receive directly the high speed jet of water resemble a cantilever beam and have to transmit the torque to the wheel. For this reason, the fatigue of the material on the bucket area is one of the most common causes of failure in this type of turbines.

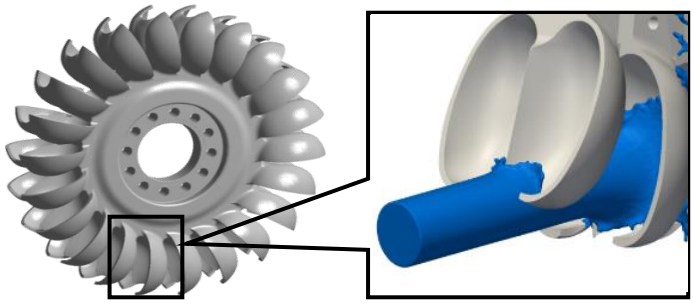

Figure 1 Schematic of the operation of the Pelton turbine bucket[5]

In order to ensure the availability of the machine, effective strategies such as periodic inspections and condition monitoring have been applied for protecting the machine and preventing serious failure [6]. Usually, sensors are installed on bearings where the vibrations generated by the turbine and the generator are transmitted. Vibration signals, as well as the operating parameters, are recorded by an acquisition system to be analyzed for diagnosis. From vibration signals condition indicators can be calculated, which should be effective to detect

damage. These indicators are trended and compared to some alarm and trip levels.

Nowadays, remote online monitoring systems have been applied on hydropower plants so that it is possible to monitor the turbine in a diagnostics center far away from the power plant [7]. Accelerometers located in bearings are the sensors currently used to measure machine vibrations. Other types of sensors like acoustic emission sensors, strain gauges and microphones have also been tested to monitor the condition of hydraulic turbines[8–10].

Selecting alarm and trip levels able to identify incipient damage in the runner is a complex task[6]. First, the levels of each indicator must be mapped for all operating conditions with the machine in good condition. Second, a mapping of the evolution of these condition indicators under a damage situation should also be represented. Machine learning techniques can be used for such purpose[11], but they need large amounts of historic data that encompass the evolution of the machine vibration from good condition to failure. Since turbines are never allowed to operate until the end of their useful life, one of the limitations in condition monitoring of hydropower plants is the lack of data. These shortcomings can be partially overcome with the use of sophisticated numerical simulation models where synthetic damage can be simulated[12].

Being different from the general machinery, the main components of hydro turbine units such as the runner and the generator are tailor-made pieces. The layout of turbine units also varies from one machine to another, which leads to different structural responses. Because of the above reasons, the diagnosis of a hydraulic turbine depends much on expertise and historical data. Some typical types of damage can be detected but many of them, especially the ones taking place in the runner, are not detectable before failure occurs[13]. This happens because the runner vibrations can hardly be detected by monitoring vibrations in the bearing; natural frequencies of the runner do not produce important deformations in the rotor[14].

In recent years, significant efforts have been made in application of data-driven and artificial intelligence (AI) for structural damage detection. Several researchers have applied Artificial Neural Network (ANN) on the vibration pattern for damage diagnosis or fault detection on various types of machines including helicopter pump [15], wind turbine [16], railway wheel [17], etc. However, there are a few studies on the implementation of AI on the experimental data of hydraulic turbines. With the development of computer techniques, more simulation data on hydraulic turbines are available for the training of ANN: R.A. Saeed et al. [18] used Principal Component Analysis (PCA) to extract features from the frequency response function (FRF) obtained from the simulation of a hydro turbine runner. The FRF features were used for training ANN in order to predict the crack length on the blade. With the years of accumulation of on-line condition monitoring data, it would become possible the application and optimization of data-driven and AI techniques for the monitoring of hydraulic turbines.

Although AI has been proven to be an effective tool for vibration-based structural damage diagnosis in several studies, there remains a very common hurdle in most of the studies: the size of the input data, which is determined by the resolution of the spectrum. A higher resolution provides more details about the dynamic response of the structure but the amount of data is too large for the neural networks' applications on engineering problems. A general way to deal with this problem is to use principal component analysis (PCA) to reduce the size of the input pattern[13]. However, the calculation of one principal component (PC) depends on every input variable, which means the PCs will change with the increase of the samples. In addition, there is no real meaning in the extracted principal components [14]. To address this problem, factor analysis is proposed. It describes variables in terms of a lower number of factors that have different loading values regarding the input variables and also tries to find out one or more latent variables (factors) that exert causal influence (loadings) on these observed variables [15]. It was firstly proposed in 1904 for the explanation of psychological theories [16]. During its development of more than one century, many researchers have contributed to its theory including the number of factors to retain [17], factor extraction algorithms [18] and so on. Nowadays, factor analysis has been applied into engineering applications: Mansi Tripathi and Sunil Kumar Singal introduced factor analysis into weight determination to develop a novel water quality analysis[19]. Reenu Maskey et al. provided explicit information on the appropriate application of exploratory factor analysis on engineering problem[20]. The development of factor analysis has made possible to optimize monitoring by compressing the monitoring indicators into interpretable factors.

In this paper, a novel condition monitoring method for Pelton turbines is introduced and discussed. The first step consists in defining optimized condition monitoring indicators based on an extensive analysis of the dynamic behavior of a Pelton turbine. The main advantage of these new condition indicators is the ability of detecting runner vibrations and its variation with abnormal operation and damage. The second step consists in applying FA in order to optimize the new indicators and reduce their dimension.

To validate this new procedure, monitoring data from an existing Pelton turbine has been used. The machine suffered a catastrophic failure in which one of the buckets broke off during operation. The inspection of the machine later revealed the failure was due to a deviated jet, which caused several cracks to appear and propagate on different buckets. To check the ability of the new methodology to predict the propagation of the cracks, the novel condition indicators have been extracted from the available data and used to define an Artificial Damage Index (*ADI*) based on the typical crack propagation behavior. These have been used in an ANN model in order to predict the *ADI* until failure occurs. The same process has been followed for the typical condition indicators used normally in condition monitoring of Pelton turbines in order to compare the results with the new method.

The paper is organized as follows: Section 2 introduces the novel condition indicators and the FA algorithm, Section 3 presents the application of the proposed method and two comparative methods on the real case, in Section 4 the failure prediction performance of the proposed indicators is compared with the conventional methods and Section 5 provides the concluding remarks.

2. Methodology for improved monitoring of Pelton turbines

2.1. Definition of new condition indicators based on dynamic analysis

Typical vibration condition indicators are effective for detecting some types of damage, but in many cases the symptoms are only perceptible when damage is at an advanced stage [2,29,30]. It is thus of high interest to upgrade the current monitoring procedures so that any variation in the behavior of the turbine is rapidly detected by the system and the potential effects on the lifetime of the structure assessed. In Figure 2, a sketch of a typical Pelton turbine has been represented. The excitation force is applied to the runner and vibrations are measured in the bearings with accelerometers.

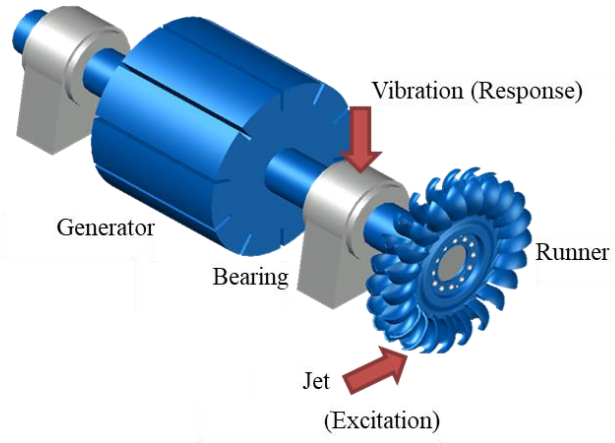

Figure 2 Pelton sketch showing the excitation and the monitoring position

As indicated above, the jet impinges directly on the runner buckets generating strong vibrations that depend on the turbine structural response. In this type of turbine, the natural frequencies more prone to be excited are the ones of the runner. One of the issues, as in many hydraulic turbines, is that runner vibrations can hardly be detected by monitoring vibrations in the bearing because natural frequencies of the runner do not produce important deformations on the rotor. In Figure 3, the deformations in a runner and rotor when excited by the jet have been represented. The numerical simulation was done with Finite Element Method (FEM) and checked experimentally. It can be observed that while the runner has large deformations, the rotor is barely affected. In case of damage or abnormal operation, the runner dynamics varies and these changes have to be detected by the monitoring system.

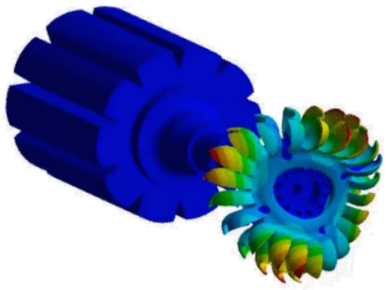

Figure 3 Deformations of a Pelton runner

A more detailed dynamic analysis of Pelton runners [31] indicate that the runner response is quite complicated, with many natural frequencies and mode-shapes (tangential, axial and radial). They are close to each other with high modal density and covering a high frequency range well above the rotor natural frequencies. In Figure 4, the first natural frequencies of a Pelton runner and associated mode-shapes detected during the start-up transient are indicated.

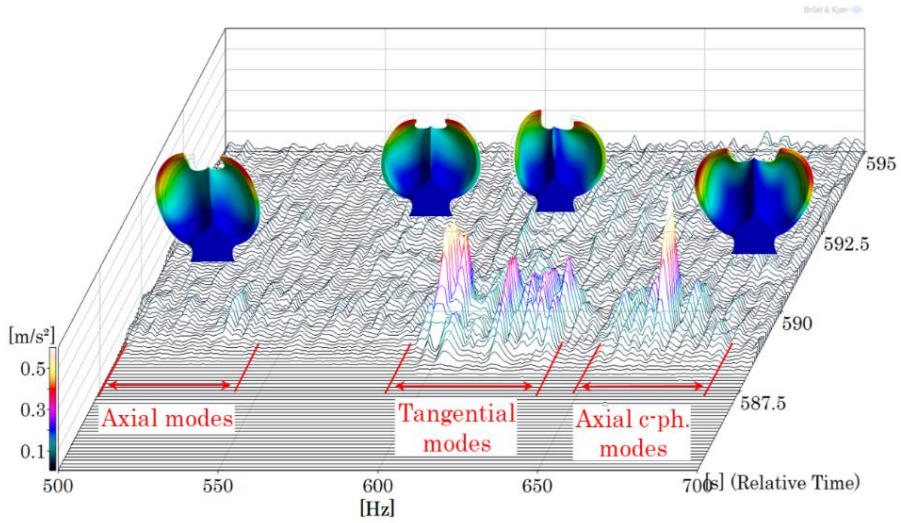

Figure 4 Excitation of the first runner natural frequencies during start-up of a Pelton turbine

The main forces affecting a Pelton turbine during operation are of mechanical, hydraulic and electromagnetic origin. The main hydraulic force comes from the impingement of the water jet on the buckets. Every time a bucket is in front of an injector, the runner receives a strong impact. During the impact, runner natural frequencies are excited. In normal operating conditions the tangential modes are basically the ones to be excited (jets hit the runner tangentially), but with abnormal operation or incipient damage other types of natural frequencies are excited too. The emergence of incipient damage in a structure may lead to a change in its dynamic response, which subsequently can be reflected in the vibration behavior [13,32]. The point is to

detect the change in the runner vibrations and associate them to abnormal operation and damage.

For improving the condition monitoring the natural frequencies of the rotor and of the runner have to be monitored. In the new condition indicators, besides the typical synchronous bands for unbalance, misalignment and bucket passing frequencies, other bands related to the natural frequencies of the structure have been considered.

2.2. Dimension reduction of indicators based on Factor Analysis and Principal Component Analysis

In this paper two different methods are used to reduce the dimension of the indicators sets. These methods are the so-called Principal Component Analysis (PCA) and Factor Analysis (FA).

The procedure of PCA is shown in Figure 5. By PCA, an indicator matrix is rotated into a new projection matrix. The projection vectors (each being a linear combination of the variables) are an uncorrelated orthogonal basis set. The first PC has the largest possible variance, and each succeeding component in turn has the highest variance possible under the constraint that it is orthogonal to the preceding components. Only the components with highest eigenvalues are retained for the analysis[22].

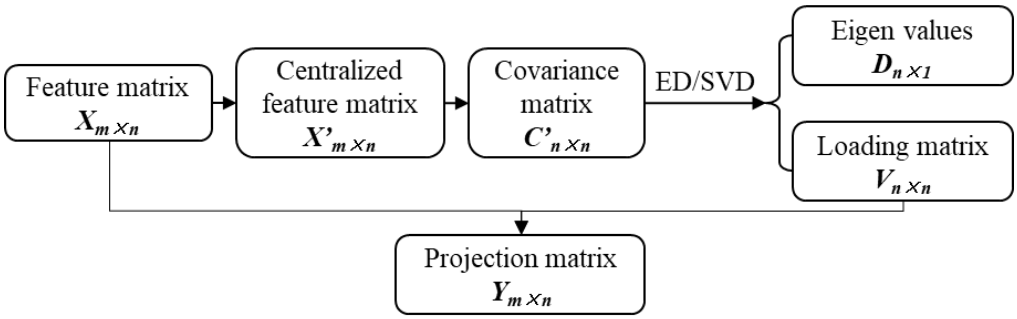

Figure 5 Procedure of PCA

In a FA model, each condition indicator can be represented as a linear combination of the common factors and specific factors[33]:

$$X_{d\times n} = \mu_{d\times n} + \Lambda_{d\times M} F_{M\times n} + E_{d\times n} \quad (1)$$

Where X is the indicator matrix with n indicators (n dimension) and d samples, μ is the mean value of each column of X and Λ is a constant d-by-M matrix of factor loadings. The $(i,j)^{th}$ element of the d-by-M matrix Λ is the coefficient, or loading, of the j^{th} factor for the i^{th} variable. F is a matrix of M common factors of the indicator matrix, and E is a vector of independent specific factors which represents the portion that cannot be explained by the common factors. In the indicator matrix, all of the indicators share these M common factors and each can be represented as a linear function of common factors and its specific factor:

$$X_i = \mu_i + a_{i1}F_1 + a_{i2}F_2 + \cdots + a_{iM}F_M + \varepsilon_i, (i = 1,2, \ldots d) \quad (2)$$

The indicators are related to the common factors by the factor loadings and can be classified into different common factors according to the loadings. Moreover, each common factor usually has a physical explanation regarding the dynamic behavior of the machine, which is an important advance compared to PCA. The main steps of FA are the following:

1) Calculating the eigenvalue of the covariance matrix of the input samples. The eigenvalues are the key for deciding the number of the common factors. According to the literature reviewed, a scree test is the most common and accurate criterion [34]: retaining all the factors above (i.e., to the left of) the inflection point of the scree plot of the eigenvalues.

2) Loading matrix calculation. With damage, some condition indicators severely change their values, especially when the machine approaches failure. Therefore, principal factor analysis is applied in the proposed method, which is suitable for corrupt data[23]. According to principal component method, the loading matrix Λ is computed by the following equation:

$$\Lambda_{d\times M} = \left(\sqrt{\lambda_1}\eta_1, \sqrt{\lambda_2}\eta_2, \cdots, \sqrt{\lambda_M}\eta_M\right) \quad (3)$$

Where $\lambda_1 \geq \lambda_2 \geq \ldots \geq \lambda_M$ are the m largest eigenvalues of the correlation coefficient matrix of X and η_1, η_2, …, η_M are the corresponding orthonormalized eigenvectors of the eigenvalues.

3) Factor rotation. The idea of factor rotation is to transform the loading matrix into a structure where each of the retained factors are ideally loaded on fewer variables, i.e. to make sure the projection of each variable on the rotated factor axis is the largest (or the lowest). By factor rotation, the new factor loading matrix can be simplified and the factors have more physical meaning or interpretability.

2.3. Failure prediction by ANN regression

As one of the most common regression tools, a supervised ANN is developed in order to build up the relation between condition indicators and damage. Since a single hidden layer ANN with sufficient number of neurons will be suitable to fit any continuous function[35], a feed-forward neural network with one hidden layer as shown in Figure 6 has been used. The input layer consists of neurons for the normalized monitoring indicators, and the neurons in the hidden layer are defined as sigmoid activation functions. The output layer contains one neuron which equals to a parameter related to a specific damage such as crack length.

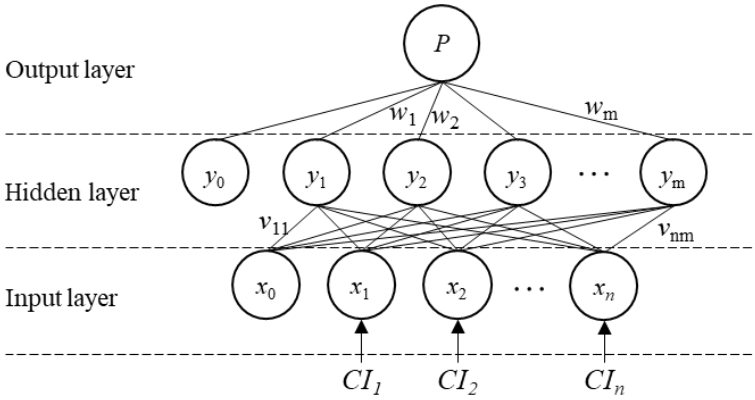

Figure 6 Architecture of the ANN model

The LM (Levenberg-Marquardt) backpropagation function is applied as the update function:

$$\Delta w = [J^T J + \lambda I]^{-1} J^T e \tag{4}$$

Where J is the Jacobian matrix of the partial derivative of E with respect to v or w. I and e represent an identity matrix and output error vector respectively. λ is large in the beginning of the learning phase, which increases the convergence speed and then decreases in order to make the approximation more accurate. The ANN model will be trained by the indicators and be used for damage detection.

3. Study on an actual Pelton turbine

3.1. Case description

An existing Pelton turbine prototype has been investigated to verify the proposed method. It is a horizontal shaft machine consisting of two runners, one shaft and a generator. The structure is supported by two bearings, located between each one of the runners and the generator. Both runners have 22 buckets and each one of them is operated by one jet. The main characteristics of the machine are listed in Table 1.

Table 1 Basic operation parameters of the turbine unit

Parameter	Value
Rated head	770 m
Maximum power	34 MW
Rotating speed f_f	600 rpm (10Hz)
Number of buckets Z_b	22
Bucket passing frequency f_b	220 Hz

The researched turbine had been monitored by a monitoring system for 13 years. A total of 5 accelerometers were installed on both bearings in the radial and axial directions, as seen in Figure 7.

Accelerometers A11 and A31 were installed horizontally in the same direction in which the jet impinges the runner. A14, A34 and A35 were installed in the vertical and axial directions, respectively. The data was collected when the machine was operating at 40% and 100% of the rated output. Therefore, the measurement points are named after sensor and output (e.g. A14-04 and A14-10 represent measurement point A14 at 40% and 100% rated output respectively).

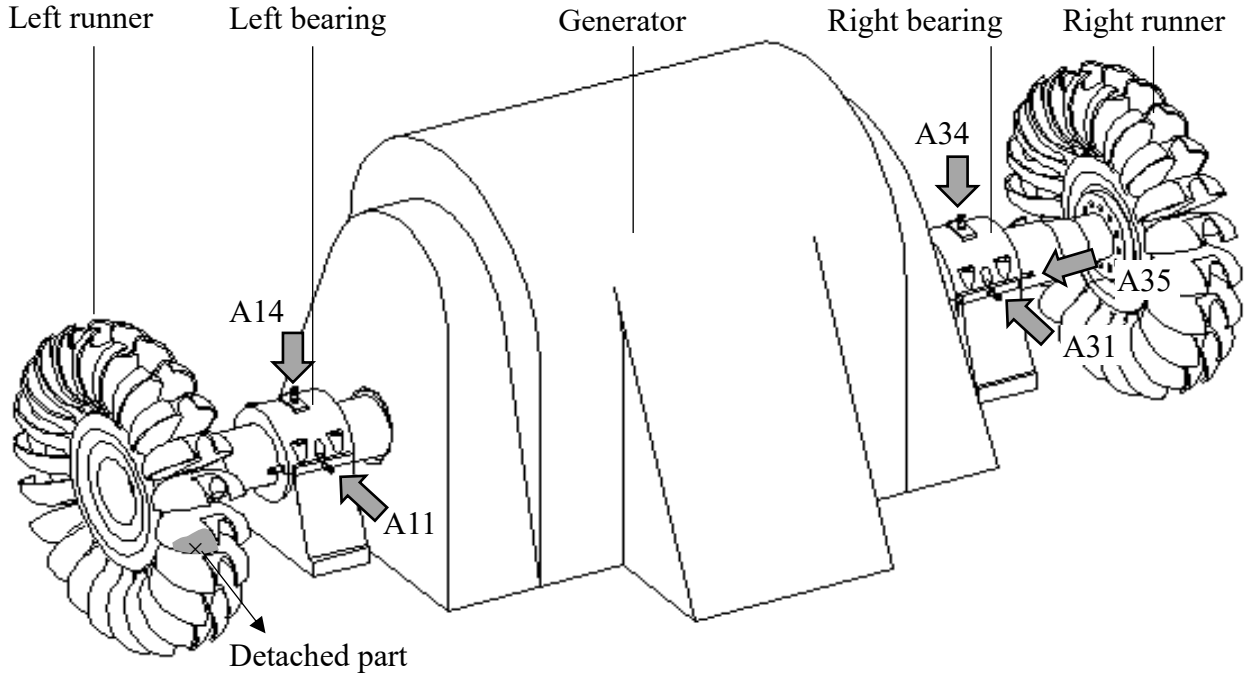

Figure 7 Sketch of the Pelton turbine and layout of the vibration sensors

For the analysis, a history case has been selected. On the 29th of August, 2011, the system detected an abnormal root mean square (RMS) vibration value surpassing the alarm threshold and the machine was stopped. The following inspection revealed the cause of the increased vibration: a piece of one bucket broke off while in operation and, in addition, cracks were present in the same area of several buckets (Figure 8). The inspection of the runner indicated that the incident took place due to the fatigue of the material, for which it was assumed that the machine had not been operating properly for some time. Machine vibrations in all the monitoring locations were available with the machine in good condition, with incipient damage and with severe damage [36,37]. After that, the machine was repaired and put again into service.

Figure 8 Damage in a bucket

3.2. New condition monitoring method

In order to implement the new condition indicators on the monitoring system, an extensive analysis of the dynamic behavior of the turbine was carried out [31,39]. First, the natural frequencies of the machine were determined by means of numerical and experimental analysis on the prototype. After that, the response (i.e., vibration) of the machine under the dynamic loading of the water jets was studied. These investigations provided a deeper understanding of the operation of the Pelton turbine and allowed defining new frequency bands related to the most excitable modes of the runner. Besides the typical synchronous bands for unbalance, misalignment and bucket passing frequencies, other bands related to the natural frequencies of the structure were devised. The latter is divided into two main groups, the ones corresponding to the rotor's natural frequencies and the ones belonging to the runner.

The rotor modes involve the deformation of the whole turbine and are found at frequencies below 300 Hz. The runner modes are found over 500 Hz and only involve the deformation of the runner and/or the buckets. Only the most relevant harmonic bands are selected according to the main excitation forces on the Pelton turbine (f_f,$2f_f$, $3f_f$, f_b, $2f_b$ and $3f_b$) (Figure 9). The proposed new condition indicators are listed in Table 2. For each measuring position, 12 spectral bands are selected as damage indicators.

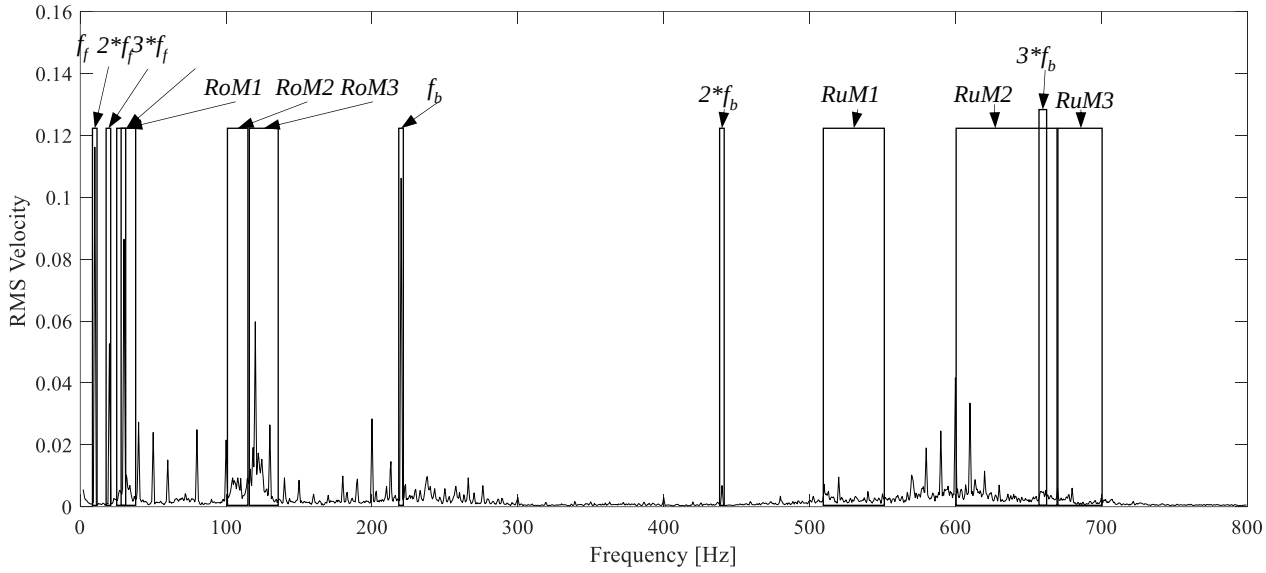

Figure 9 Vibration spectrum of the Pelton turbine and spectral bands

Table 2 The frequency ranges of the spectral bands

Mode/ frequency	Mode description	Abbreviation	Frequency range
f_f and harmonics	f_f	f_f	9-11Hz
	2*f_f	2f_f	19-21Hz
	3*f_f	3f_f	29-31Hz
Rotor modes	Rotor mode 1	*RoM*1	25-38Hz
	Rotor mode 2	*RoM*2	102-115Hz
	Rotor mode 3	*RoM*3	115-134Hz
f_b and harmonics	f_b	f_b	219-221Hz
	2*f_b	2f_b	439-441Hz
	3*f_b	3f_b	659-661Hz
Runner modes	Axial runner mode	*RuM*1	510-550Hz
	Tangential runner mode	*RuM*2	600-670Hz
	Rim runner mode	*RuM*3	670-700Hz

After extracting the new condition indicators based on the dynamics of the turbine, FA technique is used to reduce the dimension of the database and select the most relevant indicators. FA is preferred over PCA for dimension reduction as the physical meaning of the indicators is retained. The measurement point A34-10 is taken as an example to describe the process.

First, the number of common factors is determined by scree test[26]. The relative eigenvalues, as well as their cumulative percentages, are displayed in Figure 10. From the scree plot it can be seen that the inflection point is the third one, which indicates that three common factors are sufficient for retaining most of the information of the indicator matrix.

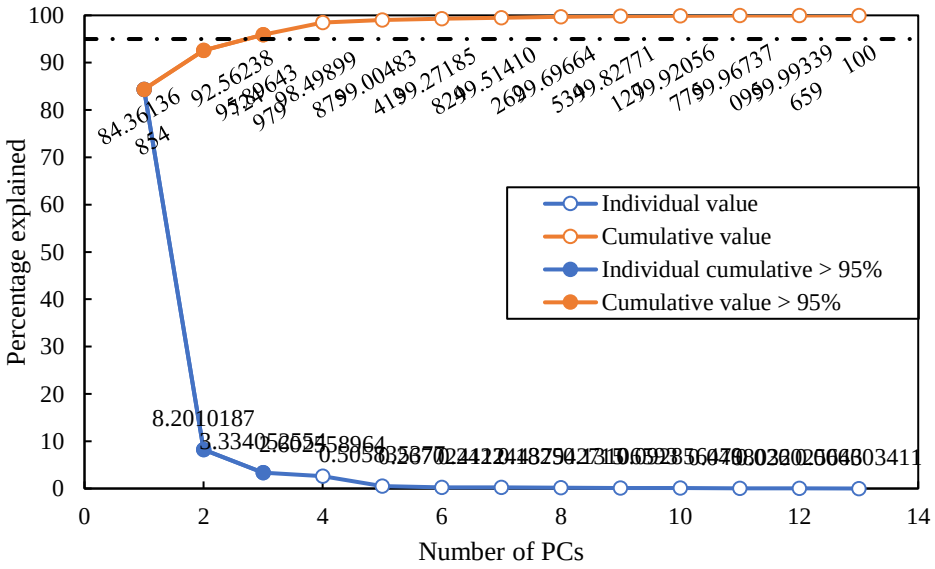

Figure 10 Scree plot of the PCA result of point A34-10

After the retained number has been determined, FA is conducted on the indicator matrix. The loading matrix is calculated according to Equation 3. The loadings of each indicator on the 3 common factors are listed in Table 3, as well as the module of each indicator, which is the Euclidean norm of the loadings.

Table 3 Loading factor of each damage indicator of point A34-10

Indicator	Factor1	Factor2	Factor3	Module
f_f	-0.4337	0.1769	0.3147	0.5643
2*f_f	0.0387	-0.0440	-0.8386	0.8406
3*f_f	-0.3144	0.8485	0.3779	0.9806
Rotor mode 1	-0.2751	0.9032	0.3218	0.9975
Rotor mode 2	0.0368	0.4883	0.0200	0.4901
Rotor mode 3	-0.4351	0.2472	0.3843	0.6310
f_b	-0.0392	0.1362	0.2187	0.2606
2*f_b	-0.4199	0.5066	0.7337	0.9855
3*f_b	0.9085	0.0224	-0.0414	0.9097
Runner mode 1	-0.4024	0.6606	0.5677	0.9595
Runner mode 2	0.8938	-0.1856	-0.2492	0.9463
Runner mode 3	0.8416	-0.1578	-0.0389	0.8571

Taking advantage of 3 loading factors, the loading matrix of point A34-10 can be represented in a 3D plot, which is helpful for visualizing and comparing the loadings of the indicators. The loading vectors are shown in Figure 11. Thus, the direction and length (module) of each vector indicate its relevancy with the common factors. For example, there are 4 indicators with negative loadings on the first common factor and 7 with positive loadings. The indicator 3*f_b has the smallest angle with the axis and largest loading value, which indicates 3*f_b has the greatest dependency with the first common factor. On the contrary, the length of vector

f_b is 0.2606, which is too small to represent any common factor.

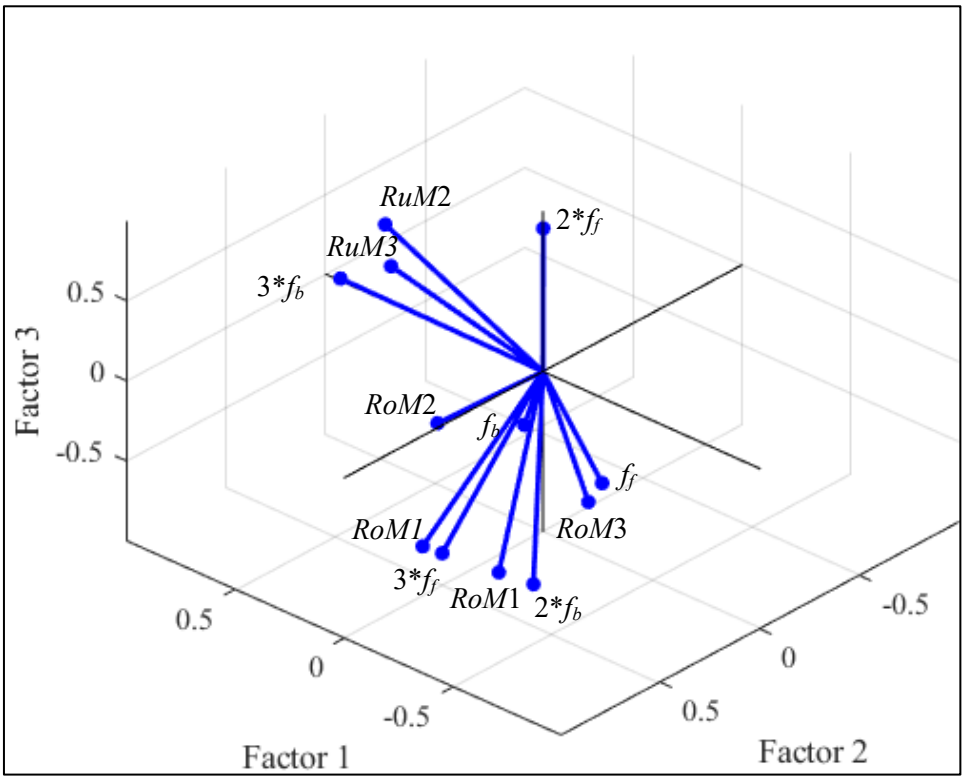

Figure 11 Loading factors of each new indicator on the three common factors

The three common factors are calculated and displayed in Figure 12, as well as their corresponding indicators. The data before and after repair is separated by a dash line. According to Table 3 and Figure 11, the indicators 3f_b and *RuM*2 and *RuM*3 have the highest loading value on the common factor 1, which means they have a similar trend with each other before and after failure. The evolution of these three indicators as well as the corresponding factor are shown in Figure 11 a. Before the failure their values grow gradually and after repair they increase dramatically. In the whole range, their values are higher after repair than before failure. However, factor 2 (Figure 11 b) shows an inverse trend to factor 1 since the value plummets after repair. Being Similarly, it shows a slight increase before failure, as factor 1. The indicators 3f_f, *RoM*1 and *RoM*2 have a high relevancy with this common factor. As for factor 3 (Figure 11 c), the value is higher in good condition than damage condition. However, there's no significant trend during failure.

The FA can be regarded as a modal decomposition process: the vibration behavior of the structure is a superposition of different modes. Therefore, the indicators with high loading on the common factors are the most significant indicators and the indicators which have low loading on every factor are regarded as redundant components. For the measurement points, the indicators with loading module larger than 0.5 are selected as the most significant indicators. The same process has been carried out on the indicators of every measurement

point and the modules have been listed in Table 4. The indicators with modules lower than 0.5 (marked in red) were eliminated from the indicator matrix. In this way, the dimension of the indicator set is reduced.

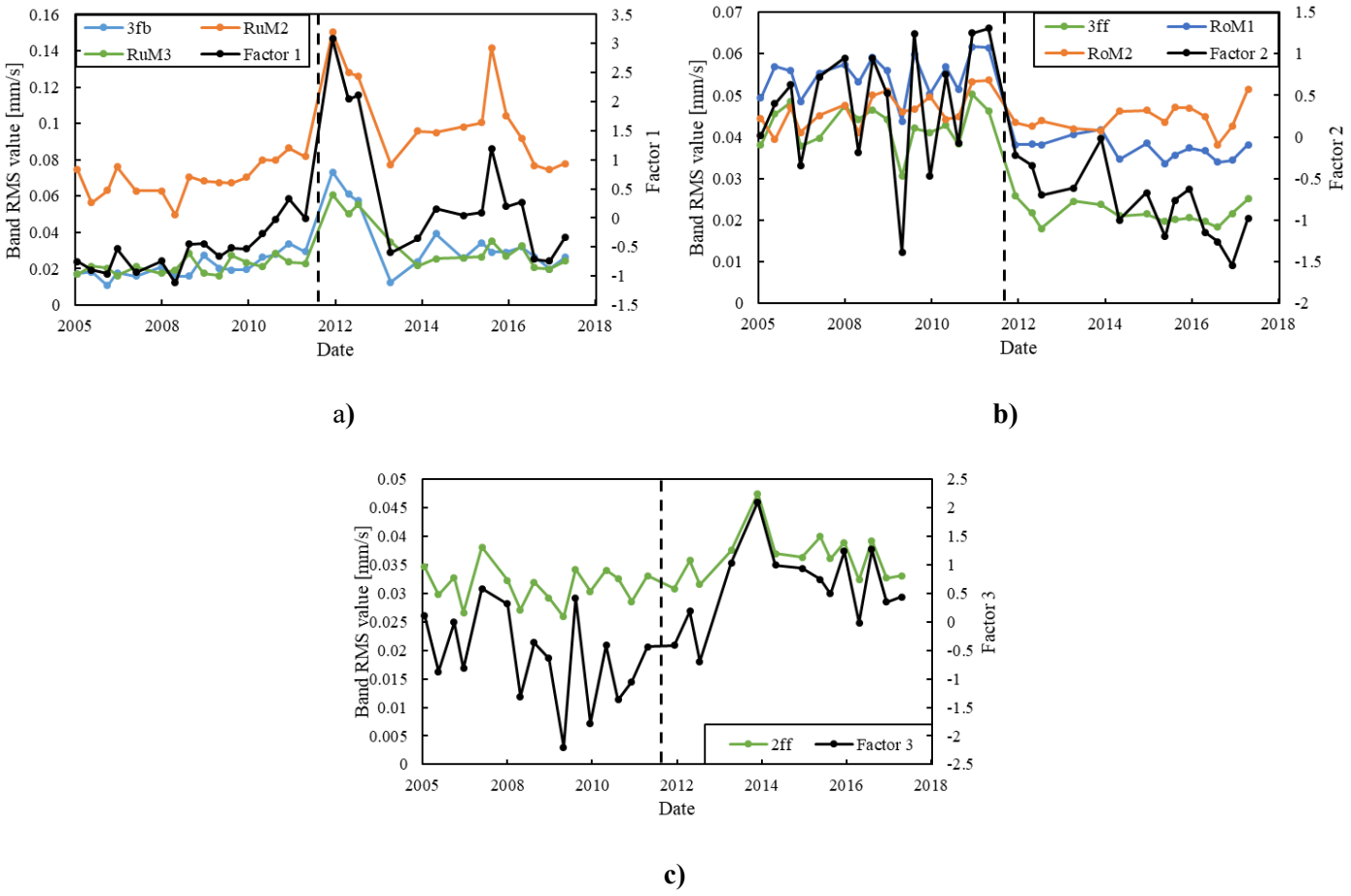

Figure 12 Common factors and the corresponding damage indicators

Table 4 Loading factor modules

Indicator	A11-04	A11-10	A14-04	A14-10	A31-04	A31-10	A34-04	A34-10	A35-04	A35-10
f_f	0.89	0.92	**0.45**	**0.37**	0.65	0.75	0.61	0.56	0.79	0.87
$2f_f$	**0.21**	0.91	0.53	0.86	0.86	0.93	0.62	0.84	0.53	0.87
$3f_f$	0.76	0.99	1.00	1.00	1.00	1.00	0.99	0.98	0.97	1.00
*RoM*1	0.77	0.96	0.91	0.89	1.00	1.00	1.00	1.00	1.00	0.99
*RoM*2	0.96	0.92	0.92	0.89	0.74	0.51	0.74	**0.49**	0.80	**0.22**
*RoM*3	0.78	0.93	0.91	0.95	0.95	**0.22**	0.92	0.63	0.94	0.54
f_b	0.69	0.69	0.75	0.87	0.90	0.77	0.61	**0.26**	**0.43**	**0.44**
$2f_b$	0.59	0.51	**0.48**	0.84	0.75	0.58	0.82	0.99	**0.33**	0.80
$3f_b$	**0.42**	**0.23**	**0.09**	0.54	0.97	0.61	1.00	0.91	0.88	0.84
*RuM*1	0.97	0.96	0.94	0.98	0.86	0.94	0.91	0.96	0.91	0.93
*RuM*2	0.99	0.93	0.80	0.89	0.58	1.00	0.77	0.95	0.94	0.97
*RuM*3	0.70	**0.44**	0.67	0.52	0.98	0.92	0.97	0.86	1.00	0.95

3.3. Comparative condition indicators (conventional indicators)

Two comparative sets of indicators are extracted from the raw signal and used for training the ANNs to compare their respective damage detection performance with the newly proposed method. In these two cases, the selection of condition indicators (spectral bands) has been performed without taking into account the specific dynamic characteristics of the Pelton turbine studied, but the typical bands used for this type of machinery.

The first condition indicator is the spectrum level of the turbine. The whole vibration spectrum (magnitude of the spectrum after applying the Fast Fourier Transform) is considered in order to build this set of indicators. According to the configuration of our monitoring system, the frequency range is 3-800 Hz with a resolution of 0.5 Hz, so there are 1595 lines in each spectrum. For each measuring point, the input pattern contains 1595 columns.

The second set encompasses the harmonics levels of the spectrum. The spectral bands of the rotating speed and its harmonics are excited by unbalance or misalignment of the rotor. Different types of damage can be reflected by changes in the harmonics of f_f [15,30,40]. The energy of a spectral band with a width of 2Hz and containing each harmonic is calculated according to Equation 2. Since the range of the spectrum is 3~800 Hz, 78 indicators are extracted from the raw data. Therefore, for one measurement point, the input contains 78 columns.

Traditional data-driven methods usually operate on the indicators without physical meaning. Generally, the routine process consists in extracting indicators and then reducing the dimension of the indicators' set by PCA [18,41]. Therefore, for the "spectrum level" and the "harmonic level" sets, which contain a lot of indicators with no clear physical meaning, the PCA technique is used to reduce the dimension.

Figure 13 shows the PCA result of the spectrum and harmonics indicators on measuring point A31-04. From the scree plot it can be seen that the first 18 components are able to explain more than 95% of the whole data contained in the "spectrum level" set of A31-04. Therefore, only these components are retained for this indicators' set. Similarly, 13 PCs are retained for "harmonic level" set of A31-04. The numbers of retained indicators of all measurement points using these two indicators' set are listed in Table 5.

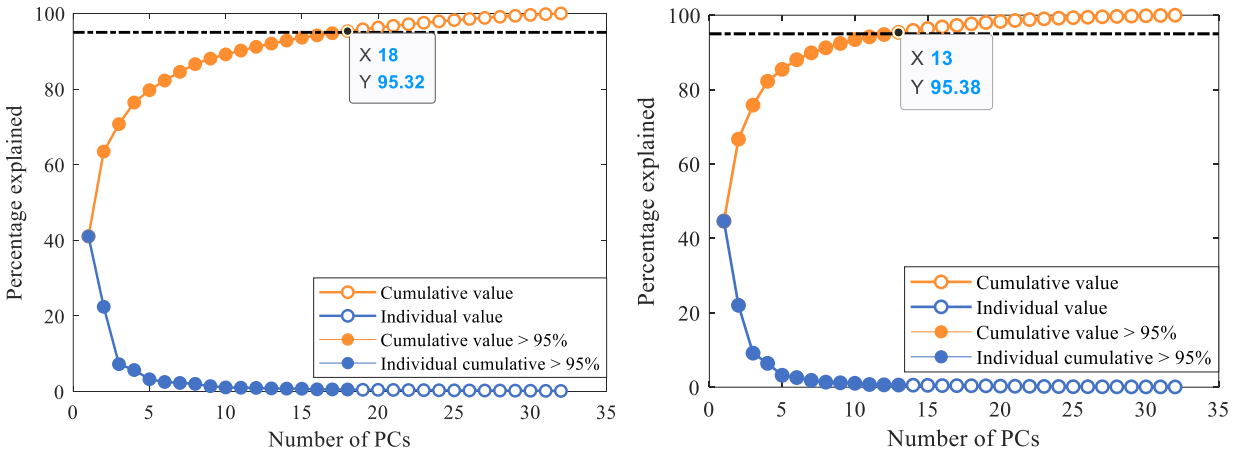

Figure 13 PCA scree plot of the "spectrum level" and "harmonic level" indicators' sets on point A31-04

Table 5 Numbers of retained indicators for each measurement point

Point	A11-04	A11-10	A14-04	A14-10	A31-04	A31-10	A34-04	A34-10	A35-04	A35-10
Spectrum level	15	17	15	12	18	21	16	17	17	18
Harmonics level	14	13	13	12	13	14	12	12	14	11

3.4. Definition of Artificial Damage Index (ADI)

The typical growth of a crack due to fatigue cycles is represented in Figure 14. According to [38], the growth of a defect is slow during the first stage and develops very rapidly after "High cycle fatigue onset". The development of the crack is divided into three stages: good condition, incipient damage and developed damage. This kind of evolution makes the detection of the incipient damage even more challenging as the crack size rapidly increases just before failure occurs. To evaluate the prediction performance of the different combinations of damage indicators, an Artificial Damage Index (*ADI*) is introduced. For the evolution of the *ADI* a power function, which is more progressive than the crack size evolution, is selected so that the sensitivity of the ANN for damage detection is increased. In equation 5, t is the normalized time with a range of 0 to 1, where t=0 is the moment when the machine starts the operation without any damage and t=1 is the time when failure occurs.

$$ADI = t^{1.85}, (t \in [0,1]) \quad (5)$$

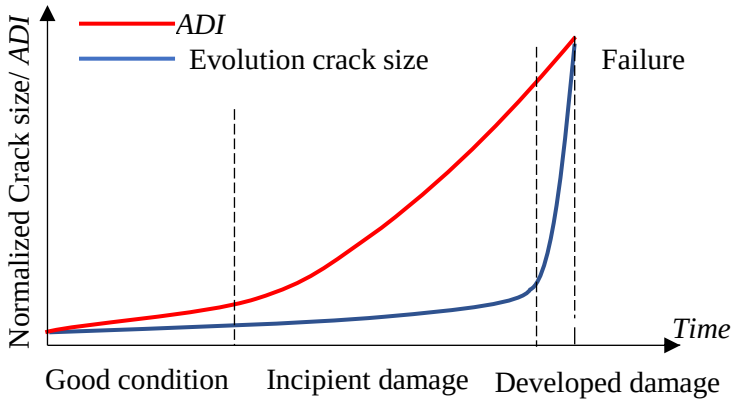

Figure 14 The curve of real crack size and the Artificial Damage Index

4. Results

The final set of indicators after applying the dimension reduction techniques (FA and PCA) are used to train the back-propagation neural networks (BPNN), whose output is the *ADI*. For each measuring point, the best perceptron number of the ANNs is optimized. Given there are only 33 samples (<50) in the database, leave-one-out cross validation (LOOCV) is applied to evaluate the prediction performance of different data sets. In LOOCV, each sample in turn is removed and the model is refitted using the remaining observations. The process is repeated again and again until every observation is predicted and predicted only once. The Root-Mean-Square Error (RMSE) of the prediction residuals are compared.

$$RMSE = \sqrt{\frac{1}{n}\sum_{1}^{n}\left(ADI_p - ADI_0\right)^2} \tag{6}$$

Where ADI_p is the predicted damage index in each round of LOOCV and n equals to the total number of observations, which is 33 in our case. For each point, 50 trials have been carried out on the 3 groups of indicators respectively. Their *RMSE* have been calculated and are shown in Figure 15.

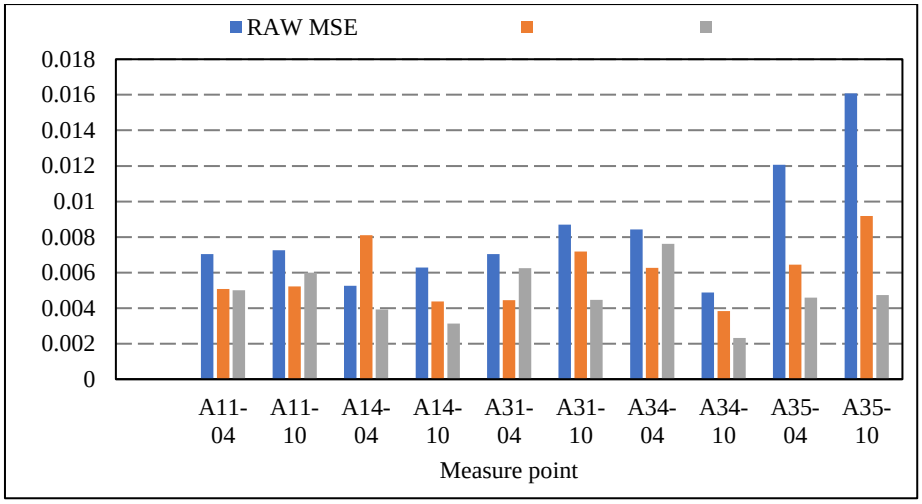

Figure 15 Prediction performance of the three indicators' set for each measurement point and averaged performance

It can be observed from the chart that the prediction result of the "spectrum level" set has the largest error in every point and the proposed set of indicators has the lowest error in most of the measurement points. The mean *RMSE* in the rightmost item in the chart indicates that the proposed condition indicators have the lowest error among the three data sets. Compared to the "spectrum level" and "harmonic level" indicators, the prediction error of new condition indicators has been decreased by 23.62% and 10.88% respectively. The most accurate point for the damage detection is the vertical position when the machine is working at 100% load (A34-10) and when the data set containing the new condition indicators is used. It can be concluded that the new condition indicators have a better correlation with the *ADI* for almost all the sensors analyzed (minimum RMSE). The reason lies in the characteristics of the especially selected spectral bands in the proposed set of indicators, which are more correlated to both the dynamic response of the structure and excitation forces. Thus, these indicators are more sensitive to detect the onset of an incipient damage.

Sensor A31 is located on the same bearing as A34, measuring vibrations in the horizontal direction. However, the prediction error is much higher than A34. This can be explained by the dynamic response of the structure: the weight of the runner makes the oil film thinner in the journal bearing, which makes the coherence between the bearing and the shaft higher on the vertical direction than in the horizontal direction. Another reason lies in the direction of the horizontal water jet, which causes too much noise on the measurement.

To assess the influence of dimension reduction by FA, the whole indicators in A34-10 before FA and after FA are used for predicting the *ADI*. Results are shown in Figure 16. It can be seen that the dimension reduction did not affect the *ADI* prediction and therefore the less important indicators according to FA technique could be removed.

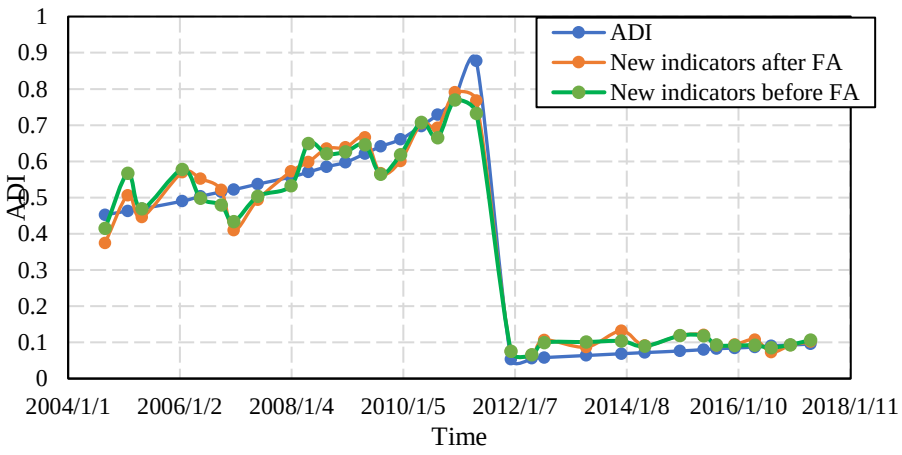

Figure 16 Predicted ADI by indicators before and after FA in point A34-10

5. Conclusions

In this paper, a new method to detect incipient damage in Pelton turbines has been presented. This has been attained by combining the expertise on the dynamic behavior of the machine with data-driven techniques including FA and ANN. The first step consists in extracting the new condition indicators from the vibration monitoring data according to the main excitations and the natural frequencies of the machine. After that, FA is carried out on the indicators: the ability of each indicator to take the damage information is quantified and the indicators which have low loading values to all of the common factors are eliminated from the data matrices. Finally, the selected indictors are used for training neural networks to form a damage detection model.

To verify the performance of the proposed method, an actual case of a Pelton turbine was studied. The studied machine suffered a failure where one bucket of the runner broke off during operation due to a deviated jet. The vibration data was recorded during normal operation, before and after failure took place and after the runner was repaired. An artificial damage index was defined according to the monitoring data and used as the output for the networks' training. As comparative groups, two traditional indicators' sets were introduced: a set containing the whole spectrum and a set containing the harmonics of the rotational speed. The dimensions of the comparative damage indicators were reduced by PCA.

The mean squared errors of each indicators' set show that the proposed new condition indicators' set have the best damage detection performance. For this new condition indicators' set the prediction error is decreased by 23.62% and 10.88% compared to the spectrum and harmonics indicators respectively. The measurement point A34 for the machine working at 100% rated output is selected as the best monitoring position. The indicators related to the rotor modes, runner modes, bucket passing frequency and rotating frequency have been determined by FA as the most important indicators for predicting the damage on the runner, which justify

the proposed new condition indicators adopted in this paper. In conclusion, the final set of proposed indicators contains more relevant information and has a smaller dimension compared to the previous ones.

Acknowledgments

The authors want to acknowledge the XFLEX HYDRO project (EU H2020 No. 857832). Weiqiang Zhao would like to acknowledge the China Scholarship Council (CSC) for its grants. Alexandre Presas and David Valentin wants to acknowledge the Serra Hunter Program of Generalitat de Catalunya. The authors are grateful to the reviewers for their insightful comments and suggestions.

References

[1] A. Whiteman, J. Esparrago, S. Rueda, S. Elsayed, I. Arkhipova, RENEWABLE CAPACITY STATISTICS 2019, Abu Dhabi, 2019. www.irena.org/Publications.

[2] M. Egusquiza, E. Egusquiza, D. Valentin, C. Valero, A. Presas, Failure investigation of a Pelton turbine runner, Eng. Fail. Anal. 81 (2017) 234–244. doi:10.1016/j.engfailanal.2017.06.048.

[3] D. Ferreño, J.A. Álvarez, E. Ruiz, D. Méndez, L. Rodríguez, D. Hernández, Failure analysis of a Pelton turbine manufactured in soft martensitic stainless steel casting, Eng. Fail. Anal. 18 (2011) 256–270.

[4] J.C. Chávez, J.A. Valencia, G.A. Jaramillo, J.J. Coronado, S.A. Rodríguez, Failure analysis of a Pelton impeller, Eng. Fail. Anal. 48 (2015) 297–307.

[5] C. Vessaz, E. Jahanbakhsh, F. Avellan, Flow simulation of a Pelton bucket using finite volume particle method, in: IOP Conf. Ser. Earth Environ. Sci., IOP Publishing, 2014: p. 12003. doi:10.1088/1755-1315/22/1/012003.

[6] E. Egusquiza, C. Valero, D. Valentin, A. Presas, C.G. Rodriguez, Condition monitoring of pump-turbines. New challenges, Measurement. 67 (2015) 151–163. doi:10.1016/j.measurement.2015.01.004.

[7] ISO, ISO 20816-5:2018 Mechanical vibration -- Measurement and evaluation of machine vibration -- Part 5: Machine sets in hydraulic power generating and pump-storage plants, (2018) 60.

[8] D. Valentín, A. Presas, M. Egusquiza, C. Valero, E. Egusquiza, Transmission of High Frequency Vibrations in Rotating Systems. Application to Cavitation Detection in Hydraulic Turbines, Appl. Sci. 8 (2018) 451.

[9] D. Valentín, A. Presas, M. Bossio, M. Egusquiza, E. Egusquiza, C. Valero, Feasibility of Detecting Natural Frequencies of Hydraulic Turbines While in Operation, Using Strain Gauges, Sensors. 18 (2018) 174.

[10] D. Valentín, A. Presas, C. Valero, M. Egusquiza, E. Egusquiza, Detection of Hydraulic Phenomena in Francis Turbines with Different Sensors, Sensors. 19 (2019) 4053.

[11] W. Zhao, M. Egusquiza, C. Valero, D. Valentín, A. Presas, E. Egusquiza, On the Use of Artificial Neural Networks for Condition Monitoring of Pump-Turbines with Extended Operation, Measurement. (2020) 107952.

[12] M. Egusquiza, E. Egusquiza, C. Valero, A. Presas, D. Valentín, M. Bossio, Advanced condition monitoring of Pelton turbines, Measurement. 119 (2018) 46–55. doi:https://doi.org/10.1016/j.measurement.2018.01.030.

[13] A. Presas, Y. Luo, Z. Wang, B. Guo, Fatigue life estimation of Francis turbines based on experimental strain measurements: Review of the actual data and future trends, Renew. Sustain. Energy Rev. 102 (2019) 96–110. doi:10.1016/j.rser.2018.12.001.

[14] E. Egusquiza, C. Valero, A. Presas, X. Huang, A. Guardo, U. Seidel, Analysis of the dynamic response of pump-turbine impellers. Influence of the rotor, Mech. Syst. Signal Process. 68–69 (2016) 330–341. doi:https://doi.org/10.1016/j.ymssp.2015.05.034.
[15] G.P. Succi, H. Chin, Helicopter Hydraulic Pump Condition Monitoring Using Neural Net Analysis of the Vibration Signature, SAE Technical Paper, 1996.
[16] M. Schlechtingen, I.F. Santos, Comparative analysis of neural network and regression based condition monitoring approaches for wind turbine fault detection, Mech. Syst. Signal Process. 25 (2011) 1849–1875.
[17] C. Zang, M. Imregun, Structural damage detection using artificial neural networks and measured FRF data reduced via principal component projection, J. Sound Vib. 242 (2001) 813–827.
[18] R.A. Saeed, A.N. Galybin, V. Popov, 3D fluid–structure modelling and vibration analysis for fault diagnosis of Francis turbine using multiple ANN and multiple ANFIS, Mech. Syst. Signal Process. 34 (2013) 259–276. doi:https://doi.org/10.1016/j.ymssp.2012.08.004.
[19] D.D. Kosambi, Statistics in function space, in: DD Kosambi, Springer, 2016: pp. 115–123.
[20] K. Pearson, On lines and planes of closest fit to systems of points in space (1901), Cited On. (1975) 26.
[21] H. Hotelling, Analysis of a complex of statistical variables into principal components., J. Educ. Psychol. 24 (1933) 417.
[22] I. Jolliffe, Principal component analysis, in: Int. Encycl. Stat. Sci., Springer, 2011: pp. 1094–1096.
[23] L.R. Fabrigar, D.T. Wegener, R.C. MacCallum, E.J. Strahan, Evaluating the use of exploratory factor analysis in psychological research., Psychol. Methods. 4 (1999) 272.
[24] C. Spearman, " General Intelligence" Objectively Determined and Measured., (1961).
[25] J.C. Watson, Establishing evidence for internal structure using exploratory factor analysis, Meas. Eval. Couns. Dev. 50 (2017) 232–238.
[26] J. Baglin, Improving your exploratory factor analysis for ordinal data: A demonstration using FACTOR, Pract. Assessment, Res. Eval. 19 (2014) 2.
[27] M. Tripathi, S.K. Singal, Allocation of weights using factor analysis for development of a novel water quality index, Ecotoxicol. Environ. Saf. 183 (2019) 109510.
[28] R. Maskey, J. Fei, H.-O. Nguyen, Use of exploratory factor analysis in maritime research, Asian J. Shipp. Logist. 34 (2018) 91–111.
[29] E. Egusquiza, C. Valero, X. Huang, E. Jou, A. Guardo, C. Rodriguez, Failure investigation of a large pump-turbine runner, Eng. Fail. Anal. 23 (2012) 27–34. doi:10.1016/j.engfailanal.2012.01.012.
[30] E. Egusquiza, C. Valero, A. Estévez, A. Guardo, M. Coussirat, Failures due to ingested bodies in hydraulic turbines, Eng. Fail. Anal. 18 (2011) 464–473. doi:https://doi.org/10.1016/j.engfailanal.2010.09.039.
[31] M. Egusquiza Montagut, Study of the dynamic behavior of Pelton Turbines, Universitat Politècnica de Catalunya, 2020.
[32] M. Zhang, D. Valentin, C. Valero, M. Egusquiza, W. Zhao, Numerical Study on the Dynamic Behavior of a Francis Turbine Runner Model with a Crack, Energies. 11 (2018) 1630.
[33] H.H. Harman, Modern factor analysis, University of Chicago press, 1976.
[34] A.B. Costello, J. Osborne, Best practices in exploratory factor analysis: Four recommendations for getting the most from your analysis, Pract. Assessment, Res. Eval. 10 (2005) 7.
[35] C.C. Aggarwal, Neural Networks and Deep Learning: A Textbook, Springer International Publishing AG, Yorktown Heights, 2018.
[36] M. Gagnon, S.A. Tahan, P. Bocher, D. Thibault, The role of high cycle fatigue (HCF) onset in Francis runner reliability, in: IOP Conf. Ser. Earth Environ. Sci., IOP Publishing, 2012: p. 22005.
[37] X. Liu, A. Presas, Y. Luo, Z. Wang, Crack growth analysis and fatigue life estimation in the piston rod of a Kaplan hydro turbine, Fatigue Fract. Eng. Mater. Struct. 41 (2018) 2402–2417.
[38] A. Presas, Y. Luo, Z. Wang, B. Guo, Fatigue life estimation of Francis turbines based on experimental strain measurements: Review of the actual data and future trends, Renew. Sustain. Energy Rev. 102

(2019) 96–110.
[39] M. Egusquiza, C. Valero, D. Valentín, A. Presas, E. Egusquiza, Dynamic response of Pelton runners: Numerical and experimental analysis in prototypes, Renew. Energy. (2020).
[40] E.E. Estévez, E. UPC, Comportament dinàmic de màquines hidràuliques, Edicions UPC, Barcelona, 2003. http://hdl.handle.net/2099.3/36745.
[41] M. Ahmed, M. Baqqar, F. Gu, A.D. Ball, Fault detection and diagnosis using Principal Component Analysis of vibration data from a reciprocating compressor, in: Proc. 2012 UKACC Int. Conf. Control, IEEE, 2012: pp. 461–466.

REFERENCES

[1] International Hydropower Association (IHA), 2020 Hydropower Status Report, London, 2020.

[2] International Energy Agency, World Energy Outlook 2020, Paris, 2020. https://www.iea.org/reports/world-energy-outlook-2020.

[3] B. Looney, Statistical Review of World Energy, 2020, (2020) 65. www.bp.com.

[4] I.R.E. Agency, (IRENA), Renewable capacity statistics 2021, Abu Dhabi, 2021.

[5] International Energy Agency, Global Energy Review 2020, Paris, 2020. https://www.iea.org/reports/global-energy-review-2020.

[6] P. Denholm, M. O'Connell, G. Brinkman, J. Jorgenson, Overgeneration from solar energy in california. a field guide to the duck chart, National Renewable Energy Lab.(NREL), Golden, CO (United States), 2015.

[7] IEA, More of a good thing – is surplus renewable electricity an opportunity for early decarbonisation?, IEA. (2019) 1. https://www.iea.org/commentaries/more-of-a-good-thing-is-surplus-renewable-electricity-an-opportunity-for-early-decarbonisation.

[8] F. Paraschiv, D. Erni, R. Pietsch, The impact of renewable energies on EEX day-ahead electricity prices, Energy Policy. 73 (2014) 196–210.

[9] W. Zhao, M. Egusquiza, C. Valero, D. Valentín, A. Presas, E. Egusquiza, On the Use of Artificial Neural Networks for Condition Monitoring of Pump-Turbines with Extended Operation, Measurement. 163 (2020) 107952. doi:10.1016/j.measurement.2020.107952.

[10] E. Egusquiza, C. Valero, X. Huang, E. Jou, A. Guardo, C. Rodriguez, Failure investigation of a large pump-turbine runner, Eng. Fail. Anal. 23 (2012) 27–34.

[11] C. Valero, E. Egusquiza, A. Presas, D. Valentin, M. Egusquiza, M. Bossio, Condition monitoring of a prototype turbine. Description of the system and main results, in: J. Phys. Conf. Ser., IOP Publishing, 2017: p. 12041.

[12] E. Egusquiza, C. Valero, D. Valentin, A. Presas, C.G. Rodriguez, Condition monitoring of pump-turbines. New challenges, Measurement. 67 (2015) 151–163. doi:10.1016/j.measurement.2015.01.004.

[13] M. Egusquiza, E. Egusquiza, C. Valero, A. Presas, D. Valentín, M. Bossio, Advanced condition monitoring of Pelton turbines, Measurement. 119 (2018) 46–55. doi:https://doi.org/10.1016/j.measurement.2018.01.030.

[14] J. MacIntyre, J. Tait, S. Kendal, P. Smith, Neural networks applications in condition

monitoring, WIT Trans. Inf. Commun. Technol. 6 (1970).
[15] M. Bossio, D. Valentín, A. Presas, D.R. Martin, E. Egusquiza, C. Valero, M. Egusquiza, Numerical study on the influence of acoustic natural frequencies on the dynamic behaviour of submerged and confined disk-like structures, J. Fluids Struct. 73 (2017) 53–69. doi:10.1016/j.jfluidstructs.2017.05.008.
[16] E. Egusquiza, C. Valero, A. Presas, X. Huang, A. Guardo, U. Seidel, Analysis of the dynamic response of pump-turbine impellers. Influence of the rotor, Mech. Syst. Signal Process. 68–69 (2016) 330–341. doi:https://doi.org/10.1016/j.ymssp.2015.05.034.
[17] A. Presas, D. Valentin, E. Egusquiza, C. Valero, U. Seidel, Dynamic response of a rotating disk submerged and confined. Influence of the axial gap, J. Fluids Struct. 62 (2016) 332–349.
[18] A. Presas, D. Valentin, E. Egusquiza, C. Valero, U. Seidel, Influence of the rotation on the natural frequencies of a submerged-confined disk in water, J. Sound Vib. 337 (2015) 161–180. doi:10.1016/j.jsv.2014.10.032.
[19] D. Valentín Ruiz, D. Ramos Martín, M. Bossio, A. Presas Batlló, E. Egusquiza Estévez, M. del C. Valero Ferrando, Influence of the boundary conditions on the natural frequencies of a Francis turbine, in: 2016.
[20] M. Zhang, On the changes in dynamic behavior produced by the hydraulic turbine runner damage, Universitat Politècnica de Catalunya, 2019.
[21] M. Egusquiza, E. Egusquiza, D. Valentin, C. Valero, A. Presas, Failure investigation of a Pelton turbine runner, Eng. Fail. Anal. 81 (2017) 234–244. doi:10.1016/j.engfailanal.2017.06.048.
[22] E. Egusquiza, C. Valero, A. Estévez, A. Guardo, M. Coussirat, Failures due to ingested bodies in hydraulic turbines, Eng. Fail. Anal. 18 (2011) 464–473. doi:https://doi.org/10.1016/j.engfailanal.2010.09.039.
[23] E. Egusquiza, C. Valero, X. Huang, E. Jou, A. Guardo, C. Rodriguez, Failure investigation of a large pump-turbine runner, Eng. Fail. Anal. 23 (2012) 27–34. doi:10.1016/j.engfailanal.2012.01.012.
[24] M. Zhang, D. Valentín, C. Valero, M. Egusquiza, E. Egusquiza, Failure investigation of a Kaplan turbine blade, Eng. Fail. Anal. (2019). doi:https://doi.org/10.1016/j.engfailanal.2019.01.056.
[25] C.G. Rodriguez, B. Mateos-Prieto, E. Egusquiza, Monitoring of rotor-stator interaction in pump-turbine using vibrations measured with on-board sensors rotating with shaft, Shock Vib. 2014 (2014).
[26] C.G. Rodriguez, E. Egusquiza, F. Santos Ilmar, Frequencies in the Vibration Induced by the Rotor Stator Interaction in a Centrifugal Pump Turbine, J. Fluids Eng. 129 (2007) 1428–1435. doi:10.1115/1.2786489.
[27] ISO, ISO 20816-5:2018 Mechanical vibration -- Measurement and evaluation of machine vibration -- Part 5: Machine sets in hydraulic power generating and pump-storage plants, (2018) 60.

[28] J. Moor, The Dartmouth College artificial intelligence conference: The next fifty years, Ai Mag. 27 (2006) 87.
[29] F. Rosenblatt, Principles of neurodynamics. perceptrons and the theory of brain mechanisms, Cornell Aeronautical Lab Inc Buffalo NY, 1961.
[30] F. Rosenblatt, The perceptron: a probabilistic model for information storage and organization in the brain., Psychol. Rev. 65 (1958) 386.
[31] B. Widrow, M.E. Hoff, Adaptive switching circuits, Stanford Univ Ca Stanford Electronics Labs, 1960.
[32] M. Minsky, S.A. Papert, Perceptrons: An introduction to computational geometry, MIT press, 2017.
[33] N.M. Nasrabadi, Pattern recognition and machine learning, J. Electron. Imaging. 16 (2007) 49901.
[34] P.J. Werbos, Backpropagation through time: what it does and how to do it, Proc. IEEE. 78 (1990) 1550–1560.
[35] J.J. Hopfield, Neural networks and physical systems with emergent collective computational abilities, Proc. Natl. Acad. Sci. 79 (1982) 2554–2558.
[36] D.E. Rumelhart, J.L. McClelland, P.D.P.R. Group, Parallel distributed processing, IEEE Massachusetts, 1988.
[37] M.I. Jordan, Serial order: A parallel distributed processing approach, in: Adv. Psychol., Elsevier, 1997: pp. 471–495.
[38] Y. LeCun, L.D. Jackel, L. Bottou, A. Brunot, C. Cortes, J.S. Denker, H. Drucker, I. Guyon, U.A. Muller, E. Sackinger, Comparison of learning algorithms for handwritten digit recognition, in: Int. Conf. Artif. Neural Networks, Perth, Australia, 1995: pp. 53–60.
[39] I.J. Goodfellow, J. Pouget-Abadie, M. Mirza, B. Xu, D. Warde-Farley, S. Ozair, A. Courville, Y. Bengio, Generative adversarial networks, ArXiv Prepr. ArXiv1406.2661. (2014).
[40] J.L. McClelland, D.E. Rumelhart, P.D.P.R. Group, Parallel distributed processing, MIT press Cambridge, MA, 1986.
[41] S.W. Doebling, C.R. Farrar, M.B. Prime, D.W. Shevitz, Damage identification and health monitoring of structural and mechanical systems from changes in their vibration characteristics: a literature review, (1996).
[42] J.N. Kudva, N. Munir, P.W. Tan, Damage detection in smart structures using neural networks and finite-element analyses, Smart Mater. Struct. 1 (1992) 108.
[43] J. Rhim, S.W. Lee, A neural network approach for damage detection and identification of structures, Comput. Mech. 16 (1995) 437–443.
[44] J.E. Stephens, R.D. VanLuchene, Integrated assessment of seismic damage in structures, Comput. Civ. Infrastruct. Eng. 9 (1994) 119–128.
[45] C. Povich, T. Lim, An artificial neural network approach to structural damage detection using frequency response functions, in: Adapt. Struct. Forum, 1994: p. 1751.
[46] G.P. Succi, H. Chin, Helicopter Hydraulic Pump Condition Monitoring Using Neural Net Analysis of the Vibration Signature, SAE Technical Paper, 1996.

[47] M.C. Garcia, M.A. Sanz-Bobi, J. Del Pico, SIMAP: Intelligent System for Predictive Maintenance: Application to the health condition monitoring of a windturbine gearbox, Comput. Ind. 57 (2006) 552–568.
[48] M. Schlechtingen, I.F. Santos, Comparative analysis of neural network and regression based condition monitoring approaches for wind turbine fault detection, Mech. Syst. Signal Process. 25 (2011) 1849–1875.
[49] S.C. Miao, J.H. Yang, X.H. Wang, J.C. Li, T.L. Li, Blade pattern optimization of the hydraulic turbine based on neural network and genetic algorithm, J. Aerosp. Power. 30 (2015) 1918–1925.
[50] B. Daniel Marjavaara, T. Staffan Lundström, T. Goel, Y. Mack, W. Shyy, Hydraulic turbine diffuser shape optimization by multiple surrogate model approximations of Pareto fronts, (2007).
[51] P. Zhang, G. Chen, X. Zhang, Application of BP neural network and RBF neural network in extending hydraulic turbine combined characteristic curve, China Rural Water Hydropower. 11 (2012) 125–131.
[52] A. Presas, D. Valentin, W. Zhao, M. Egusquiza, C. Valero, E. Egusquiza, On the use of neural networks for dynamic stress prediction in Francis turbines by means of stationary sensors, Renew. Energy. 170 (2021) 652–660. doi:10.1016/j.renene.2021.02.013.
[53] A. Presas, D. Valentin, W. Zhao, C. Valero, M. Egusquiza Montagut, E. Egusquiza, Strain prediction in Francis runners by means of stationary sensors, in: 30th Symp. Hydraul. Mach. Syst., Lausanne, 2020: p. 4.
[54] C. Zang, M. Imregun, Structural damage detection using artificial neural networks and measured FRF data reduced via principal component projection, J. Sound Vib. 242 (2001) 813–827.
[55] R.A. Saeed, A.N. Galybin, V. Popov, 3D fluid–structure modelling and vibration analysis for fault diagnosis of Francis turbine using multiple ANN and multiple ANFIS, Mech. Syst. Signal Process. 34 (2013) 259–276. doi:https://doi.org/10.1016/j.ymssp.2012.08.004.
[56] I. Jolliffe, Principal component analysis, in: Int. Encycl. Stat. Sci., Springer, 2011: pp. 1094–1096.
[57] L.R. Fabrigar, D.T. Wegener, R.C. MacCallum, E.J. Strahan, Evaluating the use of exploratory factor analysis in psychological research., Psychol. Methods. 4 (1999) 272.
[58] M. Tripathi, S.K. Singal, Allocation of weights using factor analysis for development of a novel water quality index, Ecotoxicol. Environ. Saf. 183 (2019) 109510.
[59] R. Maskey, J. Fei, H.-O. Nguyen, Use of exploratory factor analysis in maritime research, Asian J. Shipp. Logist. 34 (2018) 91–111.
[60] W. Zhao, E. Egusquiza, C. Valero, M. Egusquiza, D. Valentín, A. Presas, A Novel Condition Monitoring Methodology Based on Neural Network of Pump-Turbines with Extended Operating Range, in: 16th IMEKO TC10 Conf., Berlin, 2019: p. 4. https://www.imeko.org/publications/tc10-2019/IMEKO-TC10-2019-024.pdf.
[61] W. Zhao, M. Egusquiza, A. Estevez, A. Presas, C. Valero, D. Valentín, E. Egusquiza,

Improved damage detection in Pelton turbines using optimized condition indicators and data-driven techniques, Struct. Heal. Monit. (2021) 147592172098183. doi:10.1177/1475921720981839.
[62] W. Zhao, A. Presas, M. Egusquiza, D. Valentín, C. Valero, E. Egusquiza, Increasing the Operating Range and Energy Production in Francis Turbines by An Early Detection of the Overload Instability, Measurement. 181 (2021) 109580. doi:j.measurement.2021.109580.
[63] M. Zhang, D. Valentin, C. Valero, M. Egusquiza, W. Zhao, Numerical Study on the Dynamic Behavior of a Francis Turbine Runner Model with a Crack, Energies. 11 (2018) 1630. doi:10.3390/en11071630.
[64] M.Y. Rafiq, G. Bugmann, D.J. Easterbrook, Neural network design for engineering applications, Comput. Struct. 79 (2001) 1541–1552.
[65] D. Valentín, A. Presas, E. Egusquiza, C. Valero, M. Egusquiza, M. Bossio, Power Swing Generated in Francis Turbines by Part Load and Overload Instabilities, Energies. 10 (2017) 2124.
[66] W.J. Rheingans, Power swings in hydroelectric power plants, Trans. ASME. 62 (1940) 171–184.
[67] D. Valentín, A. Presas, C. Valero, M. Egusquiza, E. Egusquiza, Detection of Hydraulic Phenomena in Francis Turbines with Different Sensors, Sensors. 19 (2019) 4053.
[68] A. Müller, A. Favrel, C. Landry, F. Avellan, Fluid–structure interaction mechanisms leading to dangerous power swings in Francis turbines at full load, J. Fluids Struct. 69 (2017) 56–71. doi:https://doi.org/10.1016/j.jfluidstructs.2016.11.018.
[69] E. Egusquiza, D. Valentín, A. Presas, C. Valero, Overview of the experimental tests in prototype, J. Phys. Conf. Ser. 813 (2017) 012037. doi:10.1088/1742-6596/813/1/012037.
[70] A. Presas, D. Valentin, E. Egusquiza, C. Valero, Detection and analysis of part load and full load instabilities in a real Francis turbine prototype, HYdropower Plants Perform. Flex. Oper. Towar. Lean Integr. New Renew. Energies Symp. HYPERBOLE 2017. 813 (2017) 12038. doi:10.1088/1742-6596/813/1/012038.
[71] A. Presas, D. Valentin, M. Egusquiza Montagut, M. Bossio, E. Egusquiza, C. Valero, Optimized Use of Sensors to Detect Critical Full Load Instability in Large Hydraulic Turbines, Proceedings. 1 (2017) 822. doi:10.3390/proceedings1080822.
[72] A. Presas, D. Valentin, M. Egusquiza, C. Valero, E. Egusquiza, Sensor-Based Optimized Control of the Full Load Instability in Large Hydraulic Turbines, Sensors. 18 (2018) 1038.
[73] M. Egusquiza, C. Valero, D. Valentín, A. Presas, E. Egusquiza, Dynamic response of Pelton runners: Numerical and experimental analysis in prototypes, Renew. Energy. (2020).
[74] M. Egusquiza Montagut, Study of the dynamic behavior of Pelton Turbines, Universitat Politècnica de Catalunya, 2020.